



# A65 – Detect and Avoid Risk Ratio Validation Final Report

7/31/2024 Updated 16 Oct 2025



## **NOTICE**

This document is disseminated under the sponsorship of the U.S. Department of Transportation in the interest of information exchange. The U.S. Government assumes no liability for the contents or use thereof. The U.S. Government does not endorse products or manufacturers. Trade or manufacturers' names appear herein solely because they are considered essential to the objective of this report. The findings and conclusions in this report are those of the author(s) and do not necessarily represent the views of the funding agency. This document does not constitute FAA policy. Consult the FAA sponsoring organization listed on the Technical Documentation page as to its use.



### **Legal Disclaimer**

The information provided herein may include content supplied by third parties. Although the data and information contained herein has been produced or processed from sources believed to be reliable, the Federal Aviation Administration makes no warranty, expressed or implied, regarding the accuracy, adequacy, completeness, legality, reliability or usefulness of any information, conclusions or recommendations provided herein. Distribution of the information contained herein does not constitute an endorsement or warranty of the data or information provided herein by the Federal Aviation Administration or the U.S. Department of Transportation. Neither the Federal Aviation Administration nor the U.S. Department of Transportation shall be held liable for any improper or incorrect use of the information contained herein and assumes no responsibility for anyone's use of the information. The Federal Aviation Administration and U.S. Department of Transportation shall not be liable for any claim for any loss, harm, or other damages arising from access to or use of data or information, including without limitation any direct, indirect, incidental, exemplary, special or consequential damages, even if advised of the possibility of such damages. The Federal Aviation Administration shall not be liable to anyone for any decision made or action taken, or not taken, in reliance on the information contained herein.



## TECHNICAL REPORT DOCUMENTATION PAGE

1. Report No. A11L.UAS.105	2. Government Acco		3. Recipient's Cata	log No.
4. Title and Subtitle	1		5. Report Date	
ASSURE A65 – Risk Ratio Validation			12 July 2024	
ASSURE AUS – RISK Ratio Validation			6. Performing Orga	anization Code
7. Author(s)			8. Performing Orga	anization Report No.
Dylan Amerson ORCID - Amerson				•
Kyle Ryker ORCID - Ryker				
Christopher White				
Chris Goodin, Ph.D.				
Lalitha Dabbiru, Ph.D.				
Kari Babski-Reeves, Ph.D.				
Seunghan Lee, Ph.D. <u>ORCID - Lee</u>				
Seth Gibson-Todd				
Aaron LeGrand				
Rahul Sah  9. Performing Organization Name and Address			40	(777 + 76)
9. Performing Organization Name and Address Mississippi State University			10. Work Unit No.	(TRAIS)
Raspet Flight Research Laboratory				
114 Airport Road				
Starkville, MS 39759				
Starkvine, wis 37/37			11. Contract or Gr	ant No
			15-C-UAS-MSU-07	
12. Sponsoring Agency Name and Add	ress			and Period Covered
U.S. Department of Transportation			Final Report	
Federal Aviation Administration			1 October 2022 – 31	October 2024
Washington, DC 20591				
			14. Sponsoring Ago 5401	ency Code
15. Supplementary Notes			3401	
This document serves as the final report for flight testing information and data analysi in the National Airspace System (NAS). I they are implemented into the NAS.	s from a series of tests	to evaluate human pilo	t ability to see other air	rcraft while operating
17. Key Words		18. Distribution Sta	ntement	
See and Avoid		This document is available to the U.S. public through the		
Detect and Avoid			Information Service	
Risk Ratios			document is also avail	· / 1 0
Visual Detection			tion William J. Hughe	
Industry Standards		actlibrary.tc.faa.gov.		
UAS			A4 37 A5	
19. Security Classif. (of this report)	20. Security Classif	. (of this page)	21. No. of Pages	22. Price
Unclassified	Unclassified		145	



## TABLE OF CONTENTS

T	ECHNICAL REPORT DOCUMENTATION PAGE	IV
Т.	ABLE OF CONTENTS	V
Τ.	ABLE OF FIGURES	VII
т	ABLE OF TABLES	IX
		X
	ABLE OF ACRONYMS	
Τ.	ABLE OF SYMBOLS	XI
E	XECUTIVE SUMMARY	2
1	INTRODUCTION & BACKGROUND	3
	PURPOSE 3 RESEARCH QUESTIONS	4
2	EXPERIMENTAL PLANNING	4
	PERSONNEL	4
	EQUIPMENT	5
	TEST AIRCRAFT	
	TESTING LOCATION AND FLIGHT PATHS	
	Crewed Fixed Wing Overtake Geometry	
	Rotorcraft Crossing and Head On Geometry	
	Rotorcraft Overtake Geometry	
	UAS Overtake Geometry	
	FLIGHT TEST PROCEDURE	18
	Preflight 18	
	Inflight 19 Postflight	10
	<i>i</i> C	
	DATA MANAGEMENT	
3		22
	PARTICIPANT DEMOGRAPHICS	
	SURVEY AND INTERVIEW ANALYSIS	
	FLIGHT TESTING ENVIRONMENT	27
4		31
	TOBII EYE TRACKING DATA STRUCTURE	
	SEQUENCE ANALYSIS	
	RESEARCH HYPOTHESIS 1: THE EYE SCANNING PATTERNS OF PILOTS DIFFER SIGNIFICANTLY BETWEEN VARIOUM MISSION STAGES OF A FLIGHT.	
	RESEARCH HYPOTHESIS 2: THE EYE SCANNING PATTERNS OF PILOTS, AS INDICATED BY AVERAGE RELATIVE	
	FREQUENCY OF GAZE POINTS, DO NOT SHOW SIGNIFICANT DIFFERENCES ACROSS DIFFERENT AIRCRA TYPES	
	RESEARCH HYPOTHESIS 3: PILOTS EXHIBIT SIGNIFICANT DIFFERENCES IN EYE SCANNING PATTERNS DURING H	
	ON VERSUS OVERTAKING ENCOUNTERS IN FLIGHT.	
	RESEARCH HYPOTHESIS 4: EXPERIENCED PILOTS EXHIBIT MORE DIVERSE AND COMPREHENSIVE EYE SCANNIN	
	PATTERNS COMPARED TO NOVICE PILOTS DURING STANDARD FLIGHT OPERATIONS	
	RESEARCH HYPOTHESIS 5: INCREASED PILOT ENGINE HOURS LEAD TO WIDER SCANNING BEHAVIOR, REGARDI	
	OF THE TYPE OF INTRUDERS (BOTH IN UAS AND ROTORCRAFT OVERTAKES) AND THE MISSIONS (BOT	
	OVERTAKES AND HEAD-ON/CROSSING).	
	SCANNING BEHAVIORS AND COGNITION AWARENESS BASED ON FLIGHT/PILOT CONFIGURATION	
	ENCOUNTER SET	
	Fixed Wing Encounters	43



	Rotorcraft Encounters	47
	Rotorcraft EncountersUAS Encounters	54
5	MODELING AND SIMULATION	58
	ENCOUNTER SIMULATIONS	
	HARDWARE IN THE LOOP SIMULATION DEVELOPMENT	68
6	CONCLUSION	70
7	APPENDIX	72
	SUBJECT PILOT BRIEFING SCRIPT	
	DEMOGRAPHICS AND SITUATIONAL AWARENESS SURVEY / SEMI-STRUCTURED INTERVIEW	73
	SUBJECT PILOT DATABASE (REMOVED)	
	A65 ENCOUNTER DATA	75
	A23 ENCOUNTER DATA	82
	ADDITIONAL HAZARD IDENTIFICATION FORMS	91
	TEST AIRCRAFT CHARACTERISTICS	94
	RISK RATIO VALUES	1
8	REFERENCES	10



## **TABLE OF FIGURES**

Figure 1. Tobii Pro Glasses 3, recording unit, and Glasses 3 application (Tobii, n.d.).	6
Figure 2. Sentry ADS-B receiver unit and Sony PX-470 audio recorder.	7
Figure 3. DSU's Cessna 172P (Left) and Cessna 172R (Right) (FlightAware, n.d.).	7
Figure 4. DSU's Cirrus SR20 (Duff, 2023).	8
Figure 5. Provine Helicopters' Bell 206B.	8
Figure 6. RFRL's Hempel 60% Clipped Wing Cub.	9
Figure 7. Sectional chart for KRNV (marked by red rectangle) and surrounding area.	9
Figure 8. Aerial view of KRNV.	10
Figure 9. Triangle flight path for fixed wing intruder.	10
Figure 10. Triangle flight path for ownship aircraft.	11
Figure 11. Hourglass flight path overlaid on sectional.	11
Figure 12. Ownship hourglass flight path, in orange, and its direction, shown in blue.	12
Figure 13. Intruder hourglass flight path, in orange, and its direction, shown in red.	12
Figure 14. Diamond flight path for overtake encounters. Ownship shown in green and intruder in red.	13
Figure 15. Ownship's diamond shaped flight path for overtake encounters.	14
Figure 16. Intruder's diamond shaped flight path for overtake encounters.	14
Figure 17. Ownship UAS-Overtake Flight Path 1	15
Figure 18. Site 1 UAS Intruder Flight Path 1	16
Figure 19. Site 2 UAS Intruder Flight Path 1	16
Figure 20. Ownship UAS-Overtake Flight Path 2	17
Figure 21. Site 1 UAS Intruder Flight Path 2	18
Figure 22. Hazard identification form for a collision hazard.	21
Figure 23. Years of experience as a pilot for each Subject pilot tested.	23
Figure 24. Subject Pilot's familiarity with aircraft flown.	23
Figure 25. Subject Pilot's attention paid to scanning for traffic.	24
Figure 26. Subject Pilot's attention paid to weather conditions during flight.	28
Figure 27. Subject Pilot's gaze point on left and pupil diameter on right.	31
Figure 28. Correlation matrix heatmap for relationship between eye tracking parameters.	32
Figure 29. Eye movement sequence of a pilot during two phases of flight.	33
Figure 30. Scan pattern in C172 on left and Cirrus SR20 on right.	34
Figure 31. Scan pattern in a head-on encounter on left and overtake encounter on right.	35
Figure 32. Scan pattern based on engine hours with 150hrs on left and 750hrs on right.	36
Figure 33. Experience impacts on scan pattern for pilots with less than 120 single engine hours.	37
Figure 34. Experience impacts on scan pattern for pilots with more than 120 single engine hours.	38
Figure 35. Typical Subject Pilot scan patterns in rotorcraft encounters.	39
Figure 36. Typical Subject Pilot scan patterns in UAS encounters.	39
Figure 37. Relationship between engine hours and eye fixation.	40
Figure 38. Relationship between experience level and pupil diameter and saccades.	41
Figure 39. Effects of landmark reliance on pupil diameter and time to fixation.	42
Figure 40. Effects of sunglasses on saccades and time to fixation.	43
Figure 41. Detection distances of the fixed wing intruder during overtake encounters.	44
Figure 42. Probability of detection of the fixed wing intruder aircraft in overtake geometry.	44
Figure 43. Closest point of approach between the ownship and fixed wing intruder.	45
Figure 44. Closest point of approach between the ownship and fixed wing intruder separated by detect	
status.	46
Figure 45. Closing rate between ownship and fixed wing intruder.	47
Figure 46. Detection distances of the rotorcraft intruder in all encounter geometries.	48
Figure 47. Detection distances of the rotorcraft intruder in head-on encounter geometries.	48
Figure 48. Detection distances of the rotorcraft intruder in overtake encounter geometries.	49
Figure 49. Detection distances of the rotorcraft intruder in crossing encounter geometries.	49



Figure 50. Probability of detection of the rotorcraft intruder aircraft all encounter geometries.	50
Figure 51. Probability of detection of the rotorcraft intruder in overtake geometry.	50
Figure 52. Probability of detection of the rotorcraft intruder in head on geometry.	51
Figure 53. Probability of detection of the rotorcraft intruder in crossing geometry.	52
Figure 54. Closest point of approach between the ownship and rotorcraft intruder.	52
Figure 55. Closest point of approach between the ownship and rotorcraft intruder separated by dete	ection
status.	53
Figure 56. Closing rate between ownship and rotorcraft intruder.	53
Figure 57. Closing rate between ownship and rotorcraft intruder sorted by detection status.	54
Figure 58. Probability of detection of UAS intruder in overtake geometry	55
Figure 59. Detection distances of the UAS intruder during overtake encounters.	56
Figure 60. Closest point of approach between ownship and UAS intruder for all overtake encounters	
Figure 61. Closest point of approach between the ownship and UAS intruder separated by detection s	tatus.
	57
Figure 62. Closing rate between ownship and UAS intruder sorted by detection status.	58
Figure 63. Different standards for ownship Field-of-View.	59
Figure 64. Comparison of results for different encounter datasets.	61
Figure 65. Fitting result for fixed wing overtake encounters.	62
Figure 66. Fitting result for rotorcraft encounters.	62
Figure 67. Fitting of combined dataset with A23 results included.	63
Figure 68. Risk Ratio vs $\beta$ for one and two Cessna aircraft maneuvering after a detection in the "Stan	dard"
case (Turn Rate = standard turn, delay = 12 sec).	65
Figure 69. Risk ratio for both aircraft performing detect and avoid, versus only one aircraft, for a rar	ige of
values of beta	67
Figure 70. Simulation development setup.	68
Figure 71. Simulated head-on encounter (front and tail views with HUD).	69



## **TABLE OF TABLES**

Table 1. DSU's student pilot flight windows.	18
Table 2. Data and metrics recorded during flight testing.	20
Table 3. Demographics overview of test participants.	22
Table 4. Ratings overview of test participants.	22
Table 5. Factors that made acquisition easier for fixed wing intruder.	24
Table 6. Factors that made acquisition easier for rotorcraft intruder.	25
Table 7. Factors that made acquisition easier for UAS intruder	25
Table 8. Factors that made acquisition harder for fixed wing intruder.	26
Table 9. Factors that made acquisition harder for rotorcraft intruder.	26
Table 10. Factors that made acquisition harder for UAS intruder	27
Table 11. Weather conditions during testing.	29
Table 12. Correlation between eye tracking variables.	33
Table 13. Types and number of encounters generated in flight testing.	43
Table 14. Summary of encounters with rotorcraft intruder.	47
Table 15. Beta values for each encounter set.	60
Table 16. Encounter simulation results for $\beta$ =2859.	65



#### TABLE OF ACRONYMS

**Acronym** Meaning

ADS-B Automatic Dependent Surveillance System Broadcast

AGL Above Ground Level
AOI Area of Interest
ASO Aviation Safety Officer

ASSURE Alliance for System Safety of UAS through Research Excellence

ASTM American Society of Testing and Materials

CFR Code of Federal Regulations
CPA Closest Point of Approach
CTMC Continuous Time Markov Chain

DAA Detect and Avoid
DSU Delta State University

FAA Federal Aviation Administration

FDM Flight Dynamics Model

FOV Field of View
GA General Aviation
GCS Ground Control Station
GPS Global Positioning System
HITL Hardware-in-the-Loop
HUD Heads Up Display
IRB Institutional Review Board

IRB Institutional Review Board KRNV Cleveland Municipal Airport

MIT-LL Massachusetts Institute of Technology – Lincoln Laboratory

MSU Mississippi State University
NAS National Airspace System
NMAC Near Mid Air Collision
PIC Pilot in Command

RFRL Raspet Flight Research Laboratory

SAA See-and-Avoid SSD Solid-State Drive

sUAS Small Uncrewed Aircraft System
TAA Technically Advanced Aircraft
UAS Unmanned Aircraft System(s)

UE Unreal Engine
VFR Visual Flight Rules
WCV Well Clear Volume

WP Waypoint





## TABLE OF SYMBOLS

Symbol	Meaning
$\overline{A}$	Visual cross section of the intruder
β	Pilot attentiveness factor
λ	Visual acquisition rate
φ	Azimuth Angle
P	"Instantaneous" probability of visual acquisition of a target
Q	Opportunity integral
R	Visibility factor
r	Range between ownship and intruder



#### **EXECUTIVE SUMMARY**

The Federal Aviation Administration (FAA), funding the Alliance for System Safety of UAS through Research Excellence (ASSURE) Center of Excellence, seeks to better understand the effectiveness of the current General Aviation (GA) pilot's role in seeing aircraft which may pose a collision risk and avoiding potential mid-air collisions. Various previous studies have developed data-based models which provide a mathematical approach to crediting the pilot's ability to visually acquire an intruding aircraft. These efforts, although credible in approach and research findings, require modernization given the quickly evolving airspace, changes to pilot training, and technological advancements to cockpit situational awareness instruments. Through this effort, titled A65 Detect and Avoid Risk Ratio Validation, researchers at Mississippi State University's (MSU) Raspet Flight Research Laboratory (RFRL), Department of Industrial and Systems Engineering, and Center for Advanced Vehicular Systems have both validated past efforts and demonstrated new modelling techniques to supply the sponsor with a 21st century take on GA pilot Seeand-Avoid (SAA) performance. By collecting human factors data through an extensive flight test campaign with Delta State University's (DSU) Department of Commercial Aviation, MSU researchers suggest the actual visual acquisition performance for GA pilots, of varying skill levels and experience, flying in cruise flight with the opportunity to spot various types of aircraft. Through eye tracking technology, researchers found that pilot experience with the aircraft they are flying, and overall flight hours had a positive effect on scanning behavior. Pilots with less experience often constrained their searches outside of the cockpit to a small range of angles, whereas those more experienced widened their scanning angles to fill a much larger portion of the available Field-Of-View (FOV) within the cockpit. Other hypotheses about scanning patterns and pilot visual fixation are presented with empirical evidence throughout this report. The analysis of thousands of simulated encounters using the visual acquisition models for either a single pilot or a combination of two pilots scanning can impact the industry standards for Detect-and-Avoid (DAA).

For Uncrewed Aircraft Systems (UAS), DAA is the compliance approach for meeting the accepted SAA requirements for operating in the National Airspace System (NAS). As small UAS (sUAS) typically cannot be seen by manned aircraft pilots, a sUAS must meet or exceed the combined performance for a standard encounter between two different aircraft in the NAS. Using the updated models and scanning performance from 137 participating pilots, MSU researchers were able to determine the simulated see-and-be-seen performance of any two GA pilots coming within a close enough distance to be considered an encounter. The following report details the reasoning behind MSU researchers' suggestion that industry consensus standards, like the American Society and Testing and Materials (ASTM) International's DAA Performance Standard F3442/F3442M-23 (ASTM International, 2023), use required metrics like Risk Ratios that are at least as safe as the current interaction between two non-cooperative pilots in the NAS. Through extensive simulation, researchers have updated Risk Ratio tables for various parameters including beta value, intruder aircraft type, turn rate, and delay time and found that the Risk Ratio values presented in this report are in line with the currently accepted ASTM non-cooperative LoWC Risk Ratio of 0.5 and NMAC Risk Ratio of 0.3 for most of the beta ranges. Researchers caveat that as the NAS evolves, including the mass integration of sUAS and larger UAS in the future, probability of encountering an intruding aircraft will increase greatly, and the encounter simulations performed under this effort may need to be updated to accommodate this integration.

Lastly, researchers remark on the possibility of improvements to this line of research and to training of GA pilot scanning patterns given findings from the eye tracking dataset. As the technology and techniques utilized throughout the test campaign are affordable and repeatable, researchers make the case for continued analysis of pilot performance, specifically for terminal airspace, and any such airspace where critical flight may occur such as future vertiport airspace integration and advanced air traffic management concepts.



## 1 Introduction & Background

Unmanned Aircraft Systems (UAS) continue to be integrated into the National Airspace System (NAS) in increasing numbers and complexity of operations. These UAS will need to safely interact with the existing air traffic across the NAS, from commercial operations to general aviation cross country flights. In order to integrate as safely as possible, the UAS industry has turned to new and disruptive technologies that can enable a UAS to detect existing traffic and maneuver the UAS to avoid any possible escalation of a safety conflict with such traffic. Industry accomplishes this de-escalation through various technologies that enable a UAS to Detect-and-Avoid (DAA) an incoming intruding aircraft. Sensors either onboard the UAS or ground-based relay traffic information from those aircraft cooperatively broadcasting Automatic Dependent Surveillance-Broadcast (ADS-B) information or through sensing technologies that detect an aircraft flying non-cooperatively without broadcasted location and intent information. Industry has produced sensors based on acoustic science, computer vision, and traditional radar to detect these aircraft that are considered non-cooperative participants. As the capabilities of these sensors vary, and the industry seeks to push forward with integrating mass UAS operations into the NAS, regulators have funded various efforts to determine what an appropriate performance requirement or standard should be for DAA sensor performance and reliability. Traditionally, the Code of Federal Regulations (CFR), specifically 14 CFR Part 91.113 (General Operating & Flight Rules 14 C.F.R § 91, 2022) requires general aviation aircraft to "maintain well clear" of other aircraft while operating in the NAS. As an equivalent replacement of that requirement for UAS, industry consensus standards generated by the American Society of Testing and Materials (ASTM) International and Radio Technical Committee for Aeronautics suggested cylindrical volumes of "keep out" airspace that a UAS and its DAA system must comply with. However, no set of geometric values have been traditionally placed on the meaning of the phrase "well clear." This prompted a line of research questioning as to "how well do pilots actually maintain well clear in the current NAS?" To accomplish this, previous research determined models of subject pilots' ability to see another aircraft while flying in the NAS based on controlled flight test data. The ability of a pilot to visually acquire an intruder aircraft at distance coupled with assumptions on pilot maneuver helped build the narrative of the then current NAS's safety performance for general aviation. Although the research output convincing statistical reliability of the results, the range of possible intruders for a general aviation pilot was not thoroughly tested, and testing occurred many years ago, yet the NAS continues to change as aviation modernizes.

The following research report covers the effort done to both modernize the understanding of pilot visual acquisition performance and improve upon existing datasets through the integration of modern human factors technologies and the variance of test aircraft. Through the end of the A23 test program and this A65 effort, data was collected from 137 pilots at Delta State University's (DSU) Department of Commercial Aviation in multiple encounters between the pilot's fixed-wing aircraft and an intruder aircraft such as other fixed-wing aircraft, rotorcraft, and large UAS. Researchers produced pilot visual acquisition models based on the previous methodologies and present a new approach for estimating the scanning behaviors and performance of general aviation pilots in cruise flight. These models were then integrated with fast-time simulations to generate safety metrics for thousands of encounters between manned aircraft attempting to see and avoid one another. Outputs of the fast-time simulations are connected to industry standards safety requirements for small UAS (sUAS).

#### **Purpose**

The purpose of this research project is to expand on the results of the ASSURE A23: Validation of Low-Altitude Detect and Avoid Standards (Amerson, et al., 2023) project, thus increasing the statistical significance of the analysis performed to determine the ability of a GA pilot to See-and-Avoid other aircraft. The team addressed shortcomings of the previous research and attempted to fill the gaps in the research and continued to create a more robust dataset of flight-testing encounters between two crewed fixed-wing aircraft and encounters between a crewed fixed-wing aircraft and crewed rotorcraft as well as build a new



dataset to include encounters between a crewed fixed-wing aircraft and an UAS. The goal of these encounters was to capture human factors parameters that would allow the team to estimate the pilot's workload in the cockpit and estimate a pilot's ability to see other aircraft in Visual Flight Rules (VFR) flight conditions. These parameters also allowed the team to make updated estimates on the Risk Ratio values and make comparisons to prior research efforts to validate existing industry standards for UAS.

#### **Research Ouestions**

The research conducted for this project sought to answer the following questions:

- 1. What is the individual alerted and un-alerted pilot see-and-avoid risk ratio for a manned aircraft that encounters another manned aircraft?
- 2. What is the combined alerted and un-alerted see-and-be-seen risk ratio for two manned aircraft that are attempting to avoid one another?
- 3. How does pilot performance vary under different variable conditions? (i.e., environmental, aircraft/encounter related such as closure speed, and personal factors)
- 4. Are proposed DAA "well clear" distances by standards bodies appropriate?
- 5. What are adequately safe DAA risk ratio targets for a variety of drone size including sUAS (< 55 lbs.) and midsize UAS (55 1320 lbs.)?
- 6. What is the risk ratio trade space between surveillance capability and avoidance capability for achieving risk ratio targets for Ground Based and Airborne DAA systems?
- 7. Based on lessons learned through flight testing, what additional DAA safety performance metrics and performance targets are needed for advanced air mobility DAA operations?

#### 2 Experimental Planning

As previously mentioned, the goal of this research effort was to derive the minimum safety performance requirements of UAS so DAA systems could be used as an adequate alternative means of compliance. To do this, the team needed to create a series of flight tests to capture the human factors data necessary to determine the existing safety requirements of GA pilots in the NAS. The following sections describe the flight test planning, types of aircraft used, procedures followed, types of data that were collected, and the means for collecting the desired data.

#### Personnel

To keep everyone on task during flight operations, designated roles and duties were created. These roles were defined as follows:

- Test Director The Test Director was responsible for ensuring a flight test was completed in accordance with the flight test plan. They participated in the Flight Readiness Review meeting where the flight test plan, flight test cards, and hazard identification forms were discussed and finalized, ensured the test flight was conducted in a safe manner and in compliance with the flight test cards with accepted deviations, acted as backup to the Test Conductor, reviewed and approved flight test plans and flight test reports, had the responsibility of ensuring all members of the flight test team understood their roles and responsibilities and ensured that all members of the flight test team were properly trained in their assigned roles. The test director was the final authority on alterations to any test cards or the test plan.
- Test Conductor The Test Conductor was responsible for coordinating personnel, aircraft, and equipment to meet the objectives of Test Cards during a test flight. The Test Conductor took guidance from the Test Director. The Test Conductor was the lead for generating the flight test plans and flight test cards. The Test Conductor also chaired the Flight Readiness Review meeting where the flight test plan, flight test cards, and hazard identification forms were discussed and finalized. The Test Conductor also participated in flight execution briefings and oversaw the execution of the test flight.



- **Human Factors Researcher** The Human Factors Researcher was tasked with data recording, system operation, equipment emplacement, data analysis, and any other measurement duties onboard the aircraft. This role performed active data collection during the flights as well as provided all necessary post-flight documentation.
- Safety Pilot The Safety Pilot ensured that the flight was safe and that all applicable procedures were followed. The Safety Pilot was responsible for visually acquiring the other aircraft to ensure that safety thresholds were being met while in flight. This role was assisted by a traffic display allowing them to ensure that the ownship and intruding aircraft were at the correct altitudes and speeds. In the event of a possible unsafe encounter, the Safety Pilot had the authority to initiate an abort procedure. This role was typically occupied by a member of Delta State University's flight instructor team and sat in the right seat for the duration of each flight event.
- Subject Pilot The Subject Pilot was the participant being observed during each flight event. DSU's flight school students executed this role. New students were used for each flight event to ensure unbiased data was captured. The primary task of the Subject Pilot was to visually acquire the other aircraft that were in the air during the active flight test while safely operating the aircraft. Each Subject Pilot had varying degrees of experience and qualification. The Subject Pilot was considered the Pilot-In-Command (PIC) for manned encounters. Each Subject Pilot was not aware of the true nature of the test and were only informed of the actual test intent after signing the data use consent document following the test.
- UAS Pilot The UAS pilots were responsible for flying and maintaining the UAS before, during, and after the duration of the flight test. They flew prescribed flight paths and monitored the aircraft while they communicated with the Human Factors Researcher, Test Conductor, and Test Director. The UAS Pilot was also responsible for monitoring the traffic display and providing commands to the GCS operator.
- GCS Operator(s) The GCS Operators were responsible for sending flight commands to the aircraft once the UAS Pilot had set the flight mode to AUTO. They monitored the test cards and executed the appropriate commands by following the test cards. All the flight commands were executed using Mission Planner software.

#### **Equipment**

The following equipment list details each piece of hardware required for data collection during the flight test. The equipment listed was placed in the ownship aircraft prior to each flight.

• Tobii Pro Glasses 3 – These wearable eye tracking glasses were placed on the Subject Pilot to record the flight from a first-person view and provide pupil gaze tracking data throughout the duration of the flight. This data was used to analyze pilot scanning patterns and verify visual acquisition timestamps.





Figure 1. Tobii Pro Glasses 3, recording unit, and Glasses 3 application (Tobii, n.d.).

- Microsoft Surface Tablet This tablet was used to setup the Tobii Pro Glasses 3 and monitor their live video feed. A Microsoft Excel macro application was created and installed on these devices to record the visual acquisition timestamps. A button on the application was pressed by the Human Factors Researcher when the Subject Pilot verbally stated an acquisition of the test aircraft occurred. Both programs were open and monitored throughout the duration of the flight. A bookmark was created in the live video feed of the Tobii Glasses 3 Controller software directly after the visual acquisition's timestamp was recorded.
- Apple iPad The electronic flight bag app, ForeFlight Mobile, was installed on the iPad and used with a Sentry ADS-B Receiver for higher positional accuracy to record the Global Positioning System (GPS) track log of the crewed aircraft throughout the duration of the flight test.
- Sentry ADS-B Receiver This ADS-B receiver was used to provide accurate GPS track log data by pairing it via Wi-Fi to the iPad. The Sentry supports four GNSS systems (Wide Area Augmentation System GPS, Galileo, Global Navigation Satellite System, and BeiDu), and increased the accuracy of the GPS data. The device was mounted on the rear passenger window via suction cup mount in the ownship aircraft.
- Sony PX470 Digital Voice Recorder The digital voice recorder was used to record all communication that came through the Subject Pilot's headset. A split audio recording cable was plugged into the headphone audio port onboard the aircraft and then into the voice recorder's microphone port. The Subject Pilot's headset was plugged into the port audio cable and the other port onboard the aircraft, enabling the recording of all in flight audio whether from within the aircraft or via radio.





Figure 2. Sentry ADS-B receiver unit and Sony PX-470 audio recorder.

#### **Test Aircraft**

A variety of aircraft consisting of crewed fixed wing, rotorcraft, and a UAS were used throughout this flight-testing campaign. Additional performance metrics and descriptions can be found in Test Aircraft Characteristics. The ownship aircraft throughout this project was most often a Cessna 172P or Cessna 172R. The aircraft shown in the following images are representative of the multitude of different planes from DSU's fleet that were utilized. The Cessna 172Ps' panel used analog gauges while the 172Rs were Technically Advanced Aircraft (TAA) that utilized a "glass" cockpit.



Figure 3. DSU's Cessna 172P (Left) and Cessna 172R (Right) (FlightAware, n.d.).

There were ten flights accomplished with a Cirrus SR20 as the ownship aircraft as well, shown in Figure 4.





Figure 4. DSU's Cirrus SR20 (Duff, 2023).

The intruder aircraft varied depending on the testing format desired. The rotorcraft intruder aircraft was a Bell 206B provided by Provine Helicopters, shown in Figure 5.



Figure 5. Provine Helicopters' Bell 206B.

For encounters involving UAS, the intruder was a remotely piloted 60% scale model Piper Cub, referred to as the subscale Cub or MicroCub. The exact model used in testing is shown in Figure 6.





Figure 6. RFRL's Hempel 60% Clipped Wing Cub (MicroCub).

#### **Testing Location and Flight Paths**

All flight tests occurred in the Central Mississippi Delta region surrounding Cleveland, Mississippi where Delta State University's flight school is located. All flights began and ended at Cleveland Municipal Airport (KRNV), highlighted in the box in Figure 7, with an aerial view shown in Figure 8. Tests occurred in predominantly Class G airspace, although some routes occasionally entered Class E.



Figure 7. Sectional chart for KRNV (marked by red rectangle) and surrounding area.





Figure 8. Aerial view of KRNV.

#### Crewed Fixed Wing Overtake Geometry

Testing of the overtake encounter geometry consisted of a faster ownship aircraft at a higher altitude, typically 1500ft Above Ground Level (AGL), passing directly over a slower intruder aircraft, typically at 1000ft AGL. These aircraft were a Cirrus SR20 and Cessna 172, respectively. A simple triangle shaped path, shown in Figure 9, was flown by the intruder aircraft. Each leg is 13 nautical miles long, allowing enough distance for the overtake encounter to be completed.

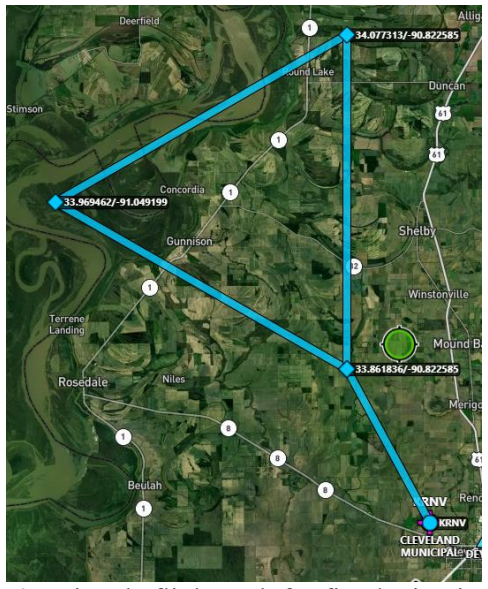


Figure 9. Triangle flight path for fixed wing intruder.

The ownship aircraft would follow the same path. However, large "teardrop" turns would occur at each corner to increase time of flight while losing sight of the intruder and allowing the slower aircraft to reach the next leg of the flight path. The intruders would typically cut the corners of the path to reach the next encounter path in a timely manner. The path was flown twice to generate a total of six encounters in each flight test.



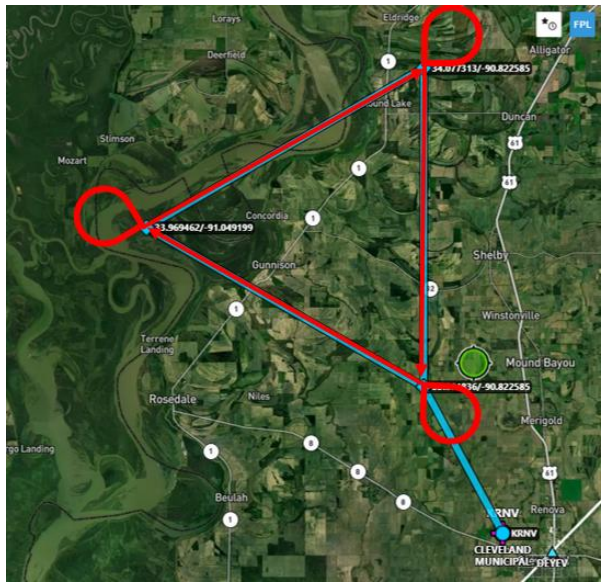


Figure 10. Triangle flight path for ownship aircraft.

#### Rotorcraft Crossing and Head On Geometry

For encounters with the rotorcraft, crossing and head on encounter geometries were executed in the same flight test by having an "hourglass" shaped flight path, shown in Figure 11. There were eight designated encounters throughout the flight which yielded four crossing encounters and four head on. Two circuits of the path were completed to generate the eight total encounters. This allowed for the four head on encounters to occur at the "top" and "bottom" of the hourglass shape (6.2 nautical miles long). The crossing encounters occurred directly in the center of the "X" (13.7 nautical miles long). The total flight time from wheels up to wheels down was roughly one hour and five minutes, depending on cruise speeds and wind conditions.

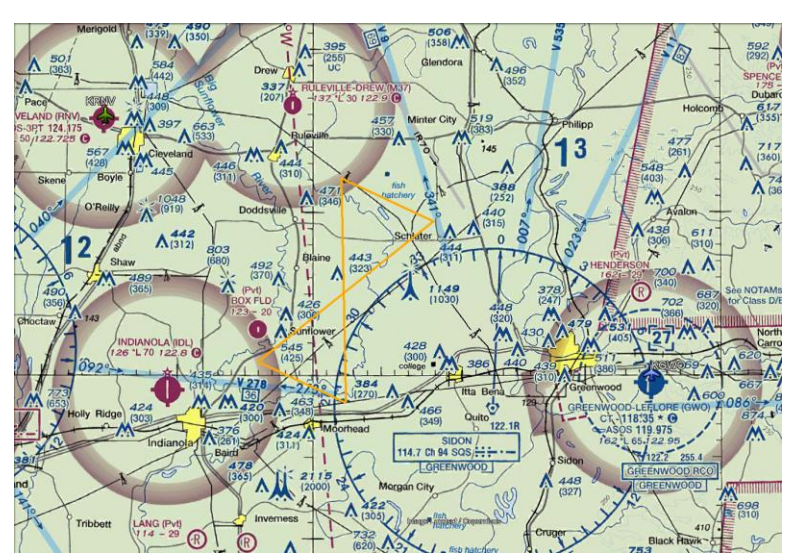


Figure 11. Hourglass flight path overlaid on sectional.

The fixed wing ownship and intruder rotorcraft flew the path in opposite directions to generate the designated encounters. The ownship aircraft was located at an altitude of 1600ft AGL and departed from KRNV. Its flight path direction can be found below.





Figure 12. Ownship hourglass flight path, in orange, and its direction, shown in blue.

The intruder rotorcraft departed from Greenwood-Leflore Airport (KGWO) and cruised at 1100ft AGL. The rotorcraft would proceed in the opposite direction of the ownship, as can be seen in Figure 13.



Figure 13. Intruder hourglass flight path, in orange, and its direction, shown in red.



#### Rotorcraft Overtake Geometry

The following paths were designed to generate overtake encounters between a fixed wing aircraft and a rotorcraft. The rotorcraft was located at a lower altitude of 1100ft AGL and was overtaken by the fixed wing ownship containing the Subject Pilot located at 1600ft AGL. Each of the overtakes was considered a single encounter. Figure 14 displays the two flight paths with numbered waypoints overlaid. There were four total encounters planned to occur before the conclusion of the one-hour flight. The green diamond shape is the ownship path and the red hexagon is the intruder path. The encounters occurred during the overlapping sections of the straight legs before the intruder broke off to the next portion of the path to setup for the next encounter.

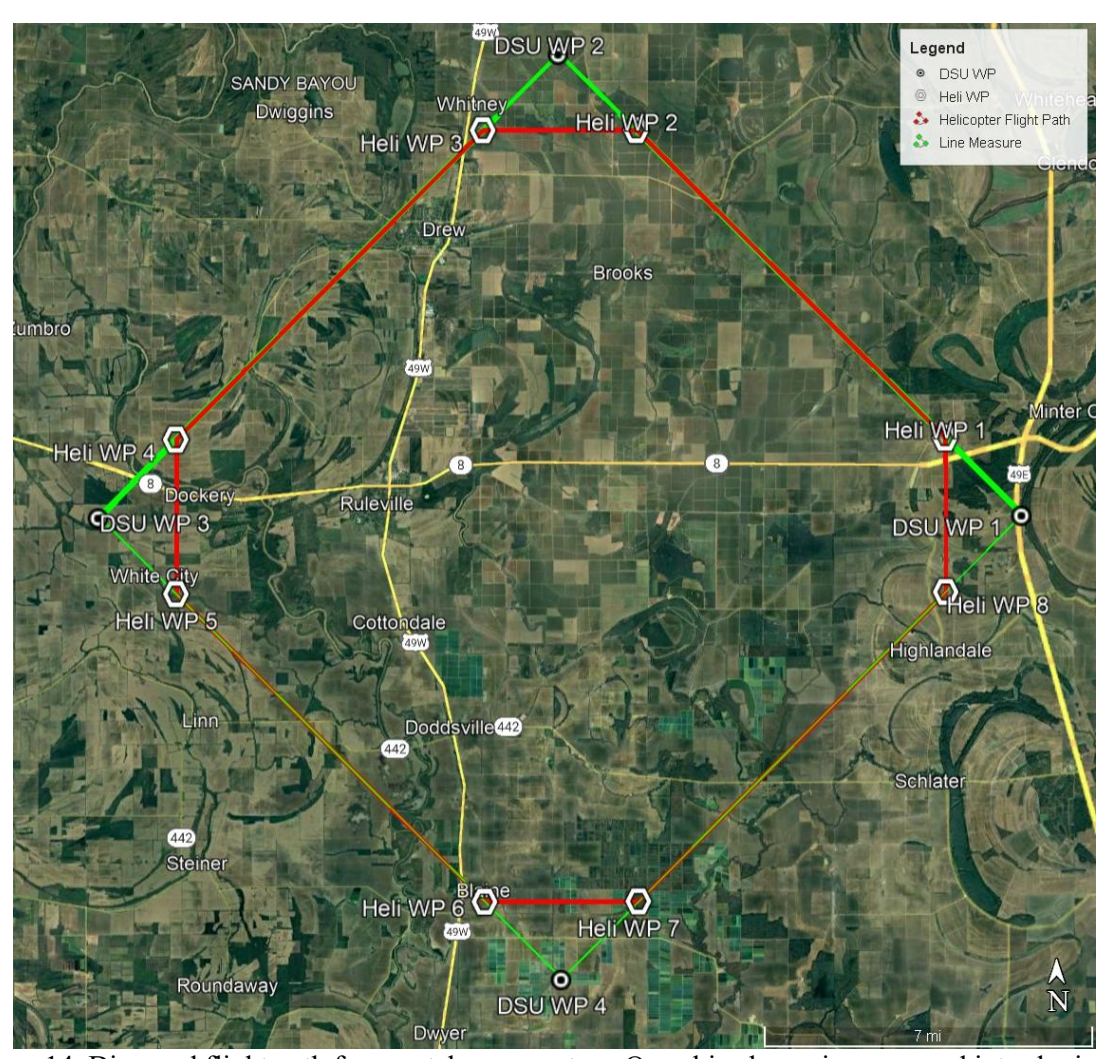


Figure 14. Diamond flight path for overtake encounters. Ownship shown in green and intruder in red.

The intruder rotorcraft maintained a speed of 50 to 80 knots during the encounters, dependent on the speed and location of the ownship aircraft. The ownship aircraft was expected to maintain at least 95 knots or above to ensure that it could overtake the intruder within the designated encounter distance of eight nautical miles. Both aircraft flew the path in a counterclockwise direction. The ownship aircraft's flight path is shown in the following images as a satellite view and the ForeFlight path, overlaid on a sectional chart, which was provided to the Subject Pilots. The Subject Pilots were instructed to perform a teardrop turn at each vertex, as can be seen in the right image. This was done to allow time for the intruder to set up on the



next leg of the flight path. This also increased the distance between the aircraft while allowing loss of visual acquisition upon the end of the overtake encounter.



Figure 15. Ownship's diamond shaped flight path for overtake encounters.

Figure 16 displays a satellite view of the intruder's flight path along with the ForeFlight path overlaid on a sectional chart that was provided to the rotorcraft pilot.



Figure 16. Intruder's diamond shaped flight path for overtake encounters.

#### UAS Overtake Geometry

Similar to the crewed fixed wing overtakes, the UAS overtakes required the ownship aircraft to fly 500ft above the UAS which acted as the intruder aircraft. The altitudes for these tests were typically set at 1000ft AGL for the ownship and 500ft AGL for the intruder. The ownship would follow a larger path that was intended to cross through two UAS test sites in which a UAS intruder would fly its own path to create the overtake encounters. The UAS test sites were limited to 1-mile radii due to radio range limitations. The crewed ownship path is shown below.



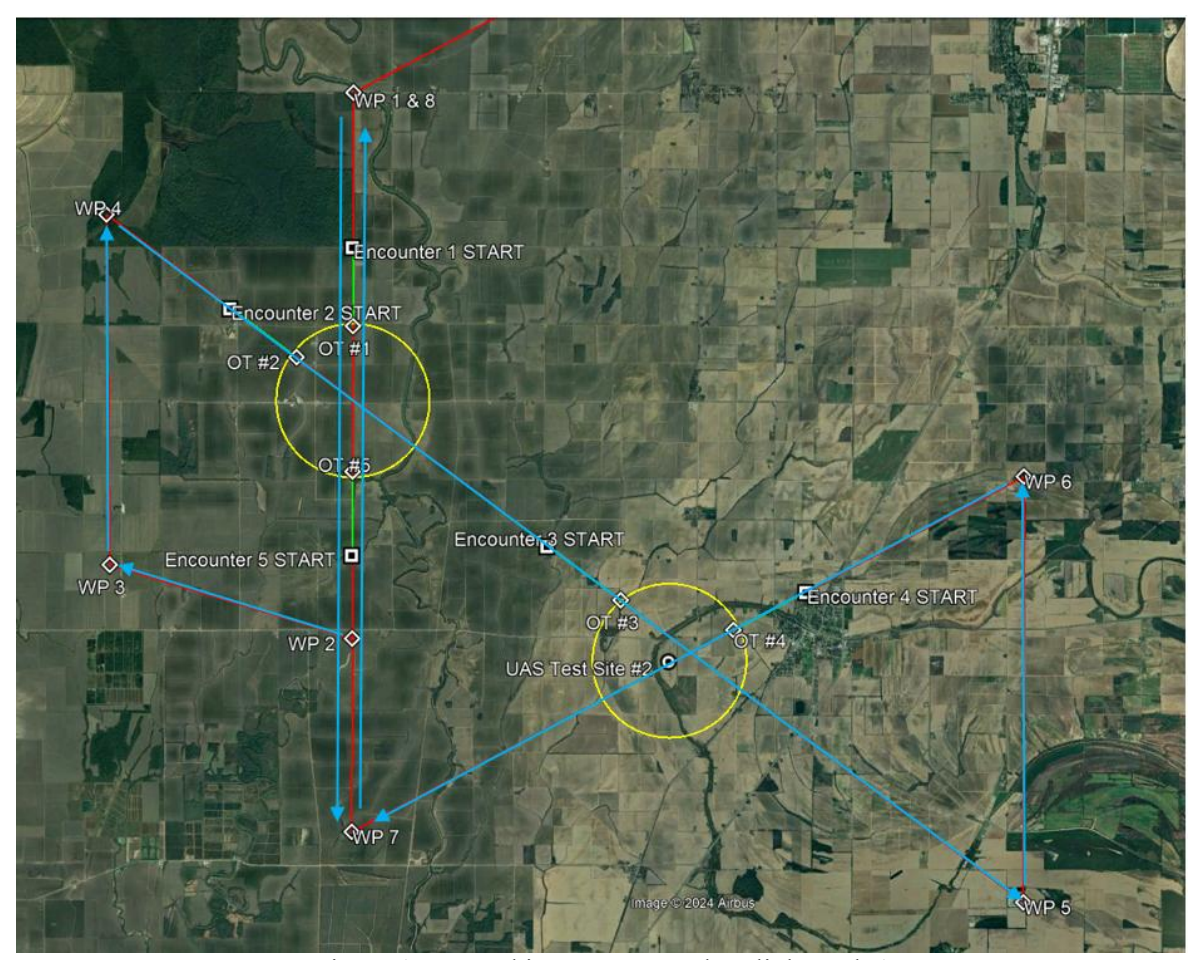


Figure 17. Ownship UAS-Overtake Flight Path 1

The ownship flew the blue path and was intended to create five overtake encounters. The first encounter would occur at the first test site in yellow on the left of the figure from North to South from WP1 to WP2. The second and third encounters would happen back-to-back starting at WP4 and ending at WP5 and would pass through both test sites. The fourth encounter would occur from WP6 to WP7 at UAS test site 2. The fifth and final encounter would occur from WP7 to WP8 from South to North at UAS test site 1. Each test site had its own path for the encounters and are both shown in Figure 18 and Figure 19. The flight paths for each of the UAS are shown in blue and labeled by encounter number.



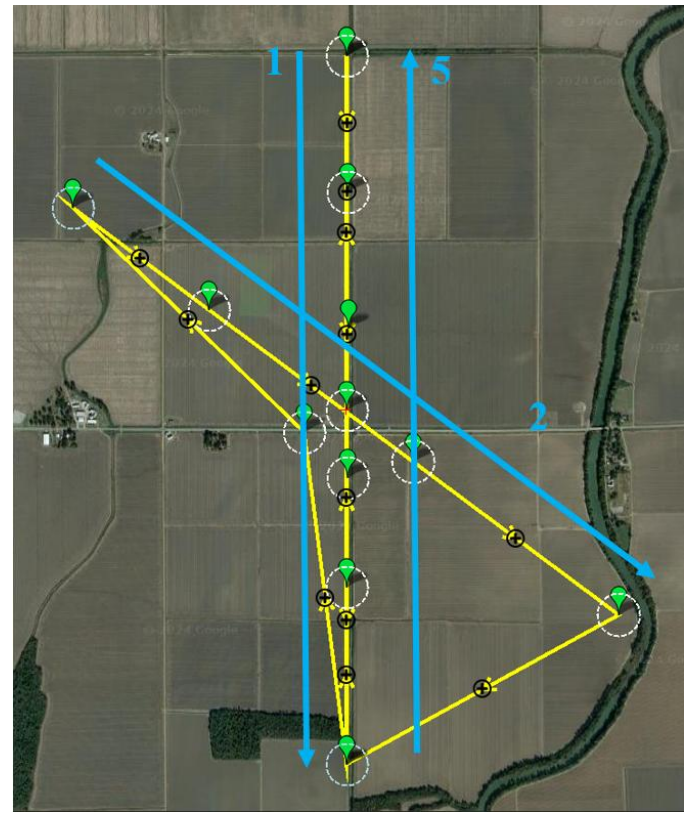


Figure 18. Site 1 UAS Intruder Flight Path 1



Figure 19. Site 2 UAS Intruder Flight Path 1



Due to issues with one of the UAS during the first round of flight-testing events, the second test site was removed from the following tests. The crewed flight path remained the same, but only generated three encounters per flight instead of five. Each flight would last approximately 45 minutes depending on winds.

Additionally, after reviewing the first few rounds of UAS overtakes, it was determined that the subject pilots had a better chance of visually acquiring the intruder during its loiter at the beginning of each leg of the encounters because the operational radius of the UAS was too short at 1 mi. To remedy this, the UAS intruder was outfitted with an upgraded radio receiver to allow the operational radius to be increased to 1.5mi giving an extra mile and more time for the overtake to occur. Ultimately this allowed the UAS to be sent on its path sooner so that the subject pilot had less of a chance to see the aircraft in its loiter at the beginning of each encounter leg. The new ownship flight path can be seen below. The new path allowed for the UAS to fly at 1000ft AGL and the ownship flew at 1500ft AGL keeping the 500ft vertical separation.

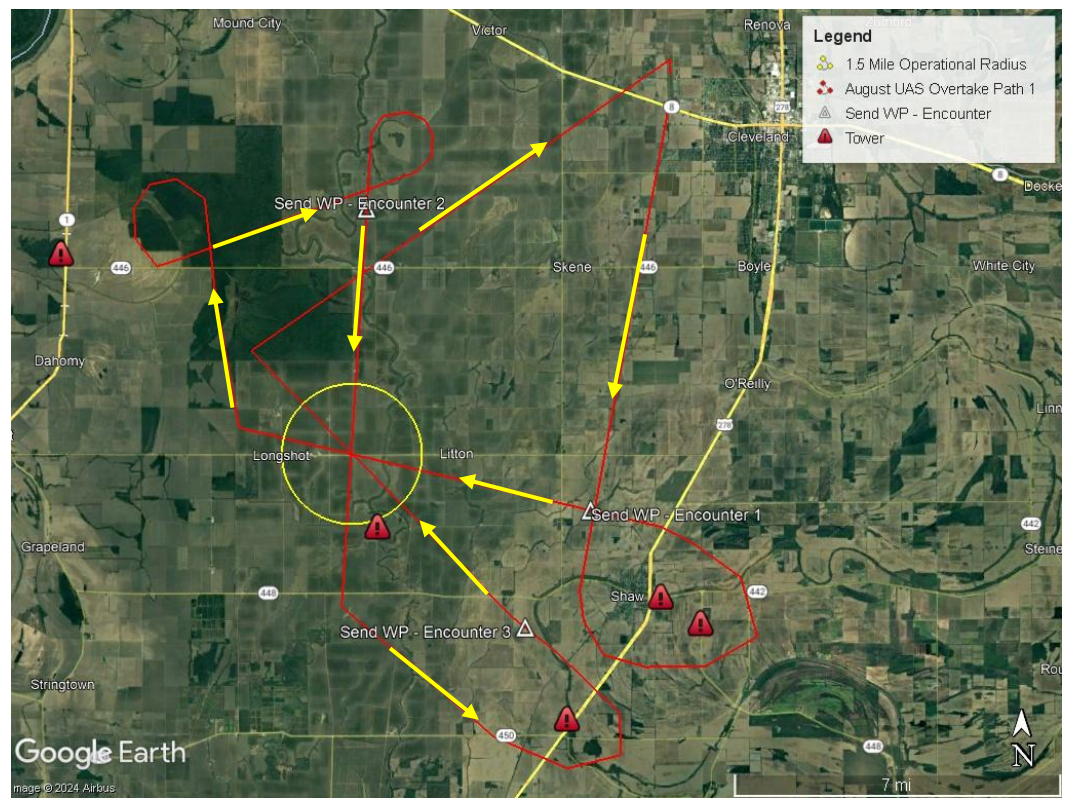


Figure 20. Ownship UAS-Overtake Flight Path 2

As shown in the figure above, the ownship flew along the red path until it reached the triangle waypoints called "send" points. Once the ownship reached a send point for a given encounter leg, the UAS GCS operator would send the UAS intruder out of its loiter and onto its encounter leg. The send it points were spaced from 2.5mi to 3.75mi away from the operational radius depending on timing needed for that run. The Mission Planner path for the UAS is shown below with overlays for each encounter leg. The path for the UAS would operate solely inside of the yellow operational radius at UAS Site 1 from Figure 20.



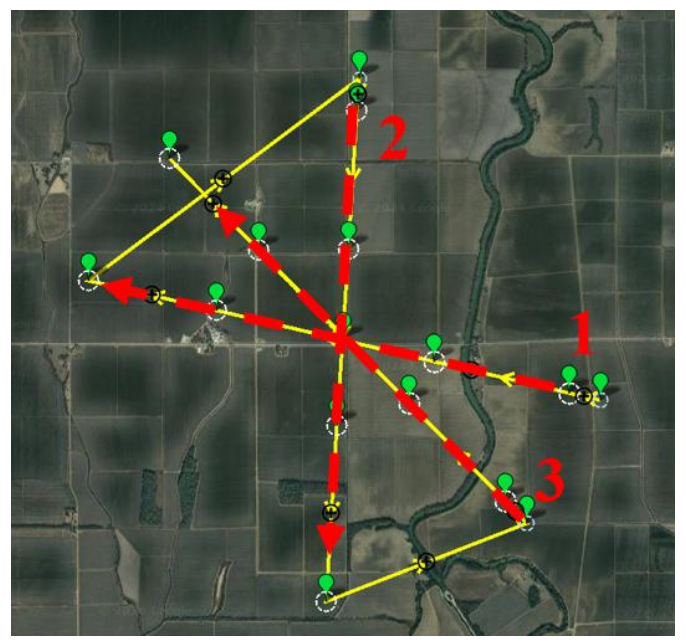


Figure 21. Site 1 UAS Intruder Flight Path 2

#### **Flight Test Procedure**

3

4

5

The test procedures discussed below were performed for every test window regardless of testing geometries or aircraft. Prior to arriving at the airport, the equipment would be fully charged, updated, and tested to confirm that all equipment was operational. Each test personnel role had its own procedure for a given phase of the testing. If a role was not listed for a phase, that role would act as support for the other personnel. Testing would typically last from Monday-Friday for a given week and would target up to five flights per day in two-hour windows for each flight. The flight windows are shown in Table 1.

 Flight Window
 Time

 1
 7:00 AM - 9:00 AM

 2
 9:00 AM - 11:00 AM

11:00 AM - 1:00 PM 1:00 PM - 3:00 PM

3:00 PM - 5:00 PM

Table 1. DSU's student pilot flight windows.

#### Preflight

Test Director, Test Conductor, and Human Factors Researcher: Power on iPad and Surface Tablet and perform a time synchronization before every flight window. Set up templates for the data capture software. Install all the necessary instrumentation into the test aircraft. Preflight brief to the Subject Pilot using the approved Institutional Review Board (IRB) brief in Subject Pilot Briefing Script. Brief the Safety Pilot on the path they will fly, what they should expect to encounter during the flight, and inform them to monitor air traffic and take over the aircraft if necessary. Inform the intruder on the path and timing to ensure that the encounters will happen when and where they were supposed to. The Human Factors Researcher boards test aircraft prior to engine startup.

Safety Pilot: Perform weight and balance to ensure that all crew onboard the aircraft met the limits of the aircraft as well as the policies and procedures set by DSU. Generally, the Safety Pilot also needed to request that the test aircraft to be filled to half tanks instead of full tanks to meet the weight and balance limits.



Subject Pilot: Preflight the test aircraft as normally would be done for any DSU training flight.

*UAS Pilot and GCS Operators:* For flights that required the UAS, the UAS Pilot and GCS Operators would perform all standard preflight procedures for the UAS and perform a warmup flight to ensure that the aircraft is operating nominally.

#### Inflight

Human Factors Researcher: Provide status updates of the aircraft and the testing to the Test Conductor/Test Director such as the time to takeoff and environmental factors that they encountered to be documented. Capture the visual acquisitions from the Subject Pilot and log them in the Human Factors Application as well as set a bookmark in the Tobii video recording to be reviewed later.

Test Director and Test Conductor: Keep communication with the intruder aircraft crew, two intruder Safety Pilots or the UAS Pilot and GCS Operators depending on the test requirements, relaying any critical information back and forth. Documented weather during each flight event and set up all postflight surveys to keep the test event running smoothly and limit the downtime between flights.

Safety Pilot: Monitor the flight path and instruct the Subject Pilot to apply corrections to the course heading, altitude, or speed as necessary to keep the flight safe and maintain the timing needed to generate an appropriate encounter. If a two-person crew of Safety Pilots was needed to act as the intruder aircraft for a test, monitor the path and fly the intruder aircraft to maintain the timing necessary to generate an encounter with the ownship.

Subject Pilot: Fly the given path as instructed while wearing the Tobii eye tracking glasses and having headset audio recorded through the audio recorder. Verbally call out any air traffic seen during the flight.

*UAS Pilot and GCS Operators*: The UAS Pilot should take off the UAS and fly to a specified altitude and switch the aircraft into autopilot. From there, the GCS Operator takes over and send the aircraft to specified waypoints to generate encounters while listening to radio traffic and coordinate with the Test Director/Test Conductor to ensure everything is running smoothly.

#### **Postflight**

Human Factors Researcher: Save all data from the flight and prepare the next template for the following flight. Swap batteries in equipment as necessary. Conduct the Postflight Survey with the Subject Pilot. The Postflight Survey can be found in Demographics and Situational Awareness Survey / Semi-Structured Interview. After the survey, have the Subject Pilot read and sign an informed consent document.

Test Director and Test Conductor: File all documentation from the Human Factors Researcher and organize the next test window by ensuring that everyone is in place and there were no issues from the previous flight or no negative developments in weather that would impact the next test window.

Safety Pilot: Inform the Test Director or Test Conductor of any issues or comments regarding the previous flight. If there was a two-person crew acting as the intruder aircraft, prepare the aircraft for the next window of flight testing as necessary.

Subject Pilot: Conduct DSU standard postflight procedures and then meet with the Human Factors Researcher in a private area to participate in the postflight interviews and documentation.

*UAS Pilot and GCS Operators*: Perform a post flight inspection, charge the avionics batteries, refuel the UAS, and wait for the call from the Test Director or Test Conductor to begin operations for the next flight window.



#### **Data Management**

There was a plethora of data captured during each flight window. Most of the data was captured and stored on its local recording format during the flight to keep all of the data separate and organized. The typical types of data and their corresponding storage devices are shown in Table 2.

Table 2. Data and metrics recorded during flight testing.

Data Type	Storage Device
Ownship Track Log	ForeFlight Application on iPad
Subject Pilot Audio	Voice Recording Unit
Eye Tracking Data	Tobii Recording Unit
Human Factors Log	Surface Tablet
Intruder Track Log (Non-UAS)	ForeFlight Application on iPad
Intruder Track Log (UAS)	Pixhawk Autopilot
Post Flight Survey	Paper Copy
Informed Consent Document	Paper Copy

After each flight, all associated data was compiled and uploaded to an encrypted Solid-State Drive (SSD) hard drive to keep the human factors data secure and organized. The SSD always remained in the possession of the Test Director in a secured location when not in use. The data remaining on the original recording devices would be erased and the recording devices would be set up for the next flight window. This ensured that all data was in a secure place and that the storage on the recording devices would not fill up during a test. The paper copies of the post flight survey and informed consent document were filed into a binder and then scanned and uploaded to the SSD with the other data. All Personally Identifiable Information was stored according to the IRB documents and made inaccessible to anyone that was not listed as a performer for the research.

#### **Safety Considerations**

Before conducting any of the flight testing for this project, MSU went through the full flight test development process. This involved participating in a flight test plan and card(s) development meeting, creating both the test cards and test plan, and reviewing the plan and cards for accuracy with all parties involved in the testing through a flight test plan review. After that, the team would meet with the Aviation Safety Officer (ASO) to identify any risks associated with the tests and create a hazard document. If necessary, the hazard document was reviewed in a safety review board consisting of the research team and the ASO. Finally, the entire flight testing team participated in a flight readiness review to ensure that all questions were addressed, and all parties had all required knowledge and resources to safely execute the flight test.

While not a direct hazard, the ownship was typically required to fly at the minimum allowed altitude limit of 1000ft AGL during the testing. This was atypical for standard DSU training flights. This kept a 500ft vertical offset between the test aircraft. The Safety Pilots were instructed to intervene if either aircraft waivered in altitude by 150ft. Since the flight testing took place in the NAS, the Safety Pilot would monitor the airspace during the flight to keep separation from non-test aircraft and apply avoidance maneuvers as necessary to maintain safe offsets. For each flight test, specified Hazard Identification Forms were created to capture all notable hazards of the testing along with mitigations for each hazard. The Collision Hazard Identification Form for the risk of aircraft collision is shown below, additional risk identification forms are shown in Additional Hazard Identification Forms.





#### Raspet Flight Research Laboratory

114 Airport Road Starkville, MS 39759

P. 662.325.3274 F. 662.325.3864 www.raspet.msstate.edu

## Hazard Identification Form

Hazard Cause Test aircraft in close proximity to each other

Hazard Effect Collision

Basic Risk Probability 2 Severity 5

Probability Mitigations: Aircraft must maintain a 500 ft vertical separation at all times. Safety pilots are aware of the encounter locations and will monitor the location of other aircraft with ForeFlight. Safety pilots can assume control of the aircraft in unsafe situations.

Severity Mitigations:

Mitigated Risk Probability 1 Severity 5

Emergency Procedure: In the event separation is lost, the aircraft will follow the standard right of way rules to avoid the collision. Pilots will also inform the other aircraft of the change in altitude to maintain a safe flight test.

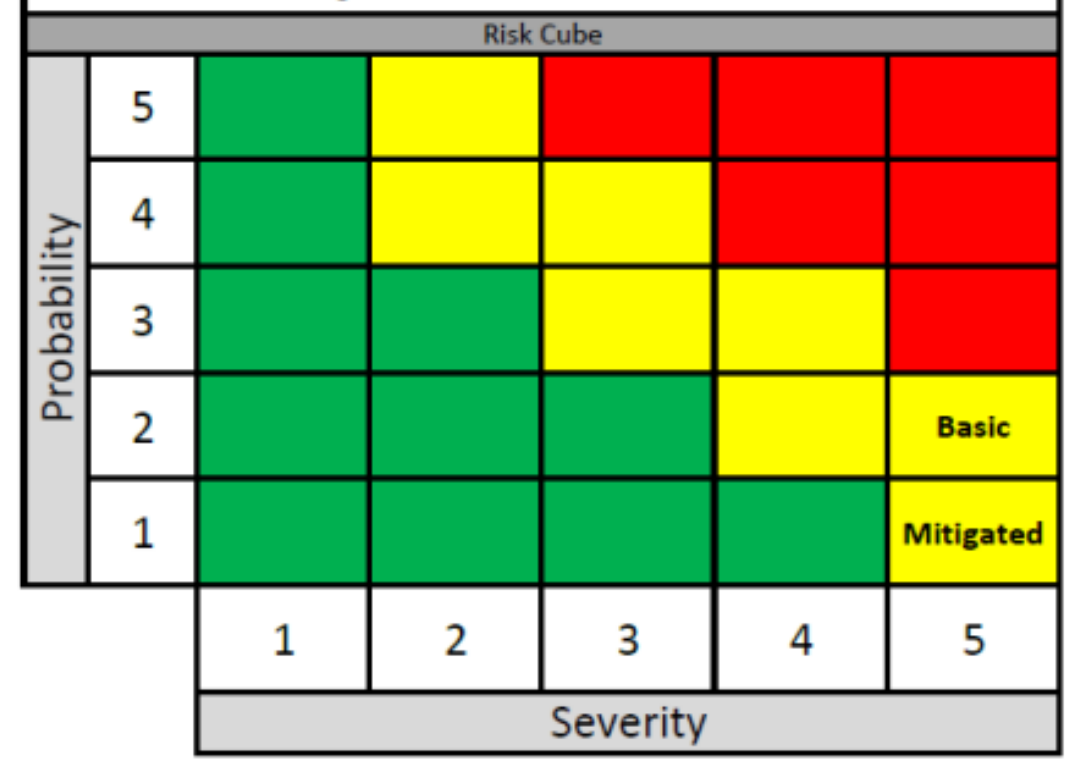


Figure 22. Hazard identification form for a collision hazard.



## 3 Flight Test Results

#### **Participant Demographics**

Subject Pilot experience levels varied from pilots with less than a total year of flight experience up to six years, with the average age of the Subject Pilots being around 21 years old. Ages ranged from 18 to 35. This is due to the research team's utilization of the DSU flight school which consists mainly of student pilots. The Subject Pilots predominantly flew single engine aircraft such as Cessna 152 and Cessna 172 models as these are the most numerous at the flight school, although 26 of the pilots also possessed a multi engine rating.

Table 3. Demographics overview of test participants.

Parameter	Unit	Minimum	Maximum	Average	Mode	Median
Age	Years	18	35	21.7	20	21
Pilot experience	Years	0.5	6	2.6	2	2
Single-engine, non-complex experience	Hours	65	750	182.9	180	180
Multi-engine experience	Hours	0	120	14.9	0	0
Complex experience	Hours	0	120	15.4	0	0
Cross-country flight time in last 6 months	Hours	0	50	11.8	0	10.35

Of the 78 Subject Pilots tested, 74.4% held an instrument rating. 42% of the Subject Pilots were rated commercially and only 12.8% were certified flight instructors.

Table 4. Ratings overview of test participants.

Rating	Percentage of Subject Pilots holding rating
Commercial	42.3%
Instrument	74.4%
Certified Flight Instructor	12.8%

The years of experience for each Subject Pilot were recorded as shown in Figure 23. Many of the Subject Pilots were relatively new to flying, exhibited by the two most numerous ranges being between 1 and 2 years.



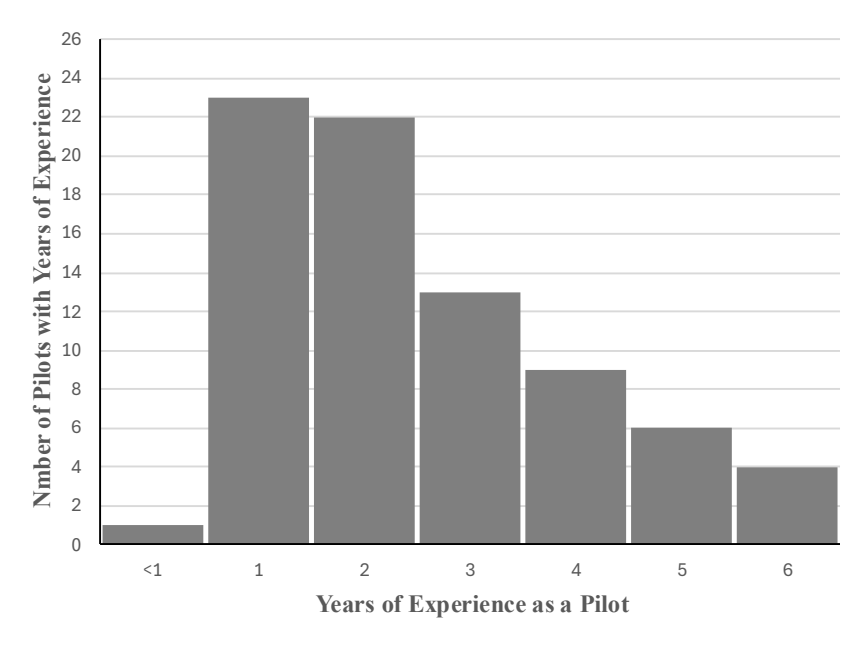


Figure 23. Years of experience as a pilot for each Subject pilot tested.

Most of the Subject Pilots were rather comfortable with the aircraft they were asked to fly, although 17 of them stated they were either "Not at all" or "Slightly" familiar with the aircraft, as shown in Figure 24.

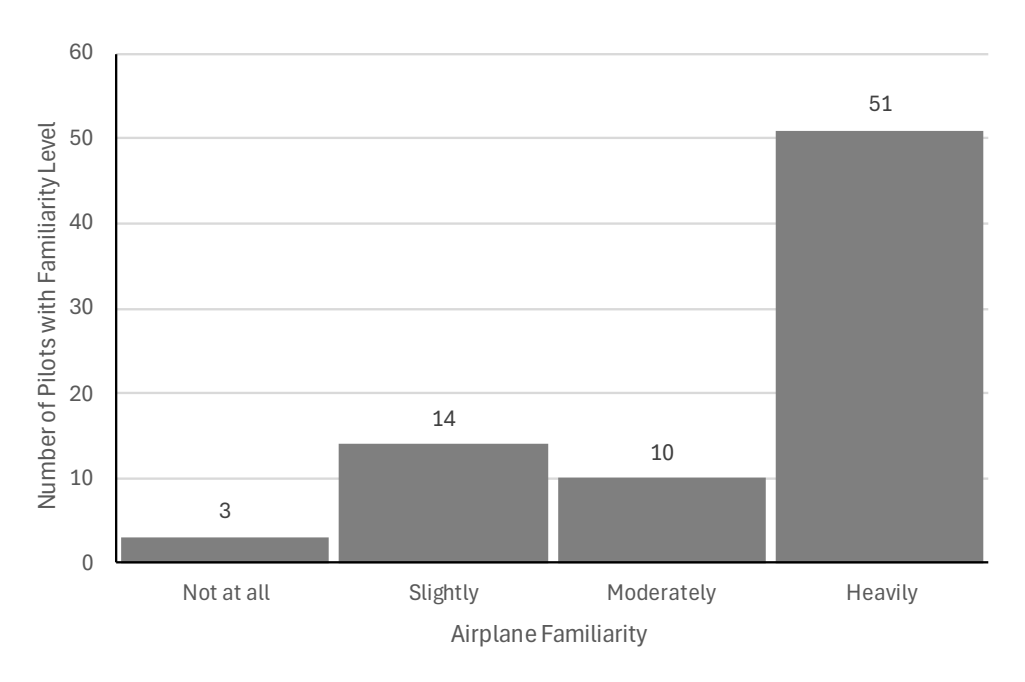


Figure 24. Subject Pilot's familiarity with aircraft flown.

Ten of these pilots flew the Cirrus SR20 during the fixed wing overtake encounters and were new to the aircraft, as many had just recently started receiving training in or recently been approved to fly the aircraft. The remaining six flew a Cessna 172R (TAA) and had more time in a Cessna 172P with analog instruments, or vice versa, and stated that they were "slightly" familiar with the aircraft due to its similarity but slight



differences in cockpit layout and performance compared to the aircraft they had spent the most time in during the six months prior to their participation in the research.

41 pilots stated they paid more attention than usual to traffic throughout the flight. This is most likely attributed to them being aware of their evaluation by the Human Factors Researcher and the presence of the eye tracking glasses. Another reasonable hypothesis is the pilots were aware the research was for the FAA and may have attempted to abnormally pay more attention to different cockpit duties. A similar number, however, stated that they paid around the same amount of attention to traffic as they would in any other flight. In either case a visual acquisition was no more likely in pilots that stated they paid more attention to traffic than to pilots that paid the same amount of attention to traffic. More information on pilot scanning can be found in Section 4, Visual Acquisition Performance, where the data from the Tobii Glasses has been analyzed.

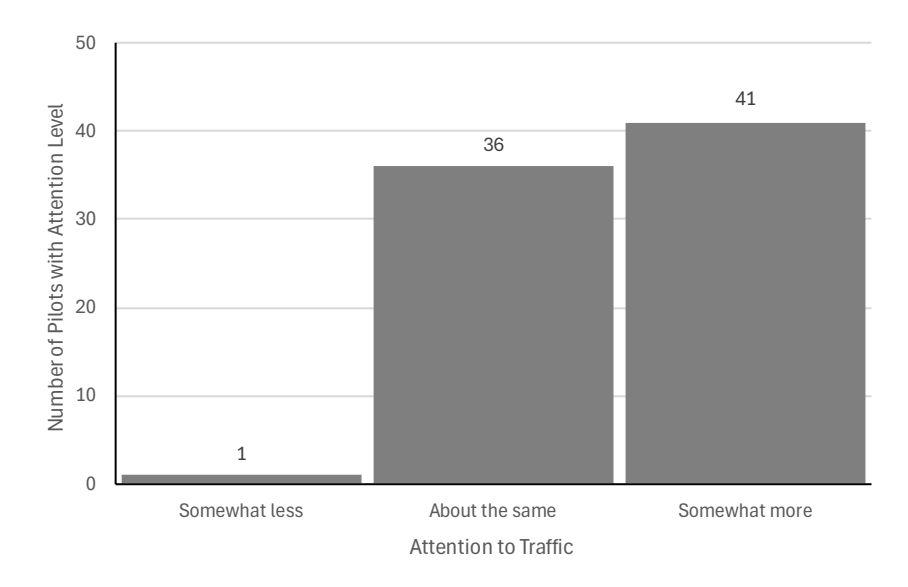


Figure 25. Subject Pilot's attention paid to scanning for traffic.

#### **Survey and Interview Analysis**

As the final portion of the questionnaire, the Human Factors Researcher would ask the following questions about the flight and the aircraft the Subject Pilot visually acquired. Their answers were recorded and transcribed onto the surveys by the Human Factors Researcher.

For each positive visual acquisition, answer the following questions:

- What were the characteristics of the aircraft that made it easy or difficult to spot?
- What were the environmental conditions that made it easy or difficult to spot?
- Was there anything else that made detection easy or difficult to spot?

Table 5 and Table 6 show the factors that Subject Pilots stated as having made visual acquisition of the intruder aircraft easier. The tables have been divided by intruder type due to the difference in characteristics between the aircraft. Many of the Subject Pilots stated similar factors, however, there were slight differences in the flight tests leading to a few specific factors mentioned for the different intruders.

Table 5. Factors that made acquisition easier for fixed wing intruder.

Tueste 2: I deteste didt made dequisition east	ter for finted wing mutater:
Made Visual Acquisition Easier (Fi	xed Wing Intruder)
Intruder Aircraft Charac	cteristics



- Looking down on high wing aircraft provided more visual surface area.
- Aircraft moving against static background made it stand out more.
- White paint at low altitude contrasted against ground when flying above intruder.
- Low wing ownship: Easier to look up at higher altitude traffic without FOV being blocked.

#### **Environmental Conditions**

- Sun reflected off of intruder causing glint that was noticeable.
- Clear weather with low winds was easy to fly in and allowed for more attention to be paid to scanning for traffic.
- Lower altitude ownship: Looking up on cloudy day, the intruder aircraft would contrast against the clouds in the background.
- During the summer, much of the background was green providing high contrast for the white intruder aircraft.

#### Other

• Windshield being cleaned made it much clearer and easier to see out.

#### Table 6. Factors that made acquisition easier for rotorcraft intruder.

## **Made Visual Acquisition Easier (Rotorcraft Intruder)**

#### Intruder Aircraft Characteristics

- Red color of aircraft stood out to Subject Pilots.
- The motion of the rotors was noticeable to Subject Pilot's and assisted some of them in initially spotting the rotorcraft.
- Relative motion of the aircraft was spotted in peripheral vision of the Subject Pilot.
- During head on encounters, the rotorcraft was easier to spot over the nose when further away.

#### **Environmental Conditions**

- The sun reflected off of the rotor blades or the windows of the rotorcraft and caused Subject Pilot to spot the intruder.
- Clear days with calm winds allowed Subject Pilot to spend more time scanning outside.
- Rural area with little to no air traffic made spotting intruder easier because it would stand out more due.

#### Other

- Side profile of the helicopter provided a larger visual area making it easier for the Subject Pilot to visually acquire it.
- Encountering the rotorcraft multiple times caused Subject Pilot to increase their awareness and try to predict its location throughout the flight test.

#### Table 7. Factors that made acquisition easier for UAS intruder

#### **Made Visual Acquisition Easier (UAS Intruder)**

#### Intruder Aircraft Characteristics

- White aircraft stood out against brown fields below it.
- Flashing lights on intruder aircraft spotted, especially on early morning flights when sun was lower
- Intruder aircraft spotted during turn from further distance due to the wing's larger visual surface area.
- Likewise, high wing intruder provided higher visual surface area when spotted from above.
- Red/Maroon accent stripes on wing broke up the intruder's silhouette.

#### **Environmental Conditions**

• Clear days with calm winds allowed Subject Pilots to spend more time scanning for intruder.



- Brown fields and flat landscape below intruder improved contrast, making the intruder stand out.
- Sun bouncing off of wrapped paint job on wings causing glint.
- On slightly cloudy days, the sun was not shining in Subject Pilot's eyes making it easier to scan for traffic.

#### Other

- Normal VFR flight with low activity and workload.
- Easier to look down in a high wing aircraft and spot traffic below you due to wings not blocking FOV.

The following tables detail the factors that Subject Pilots stated as having made their visual acquisition of the intruder aircraft more difficult. Like the above tables, they have been broken down by intruder type.

Table 8. Factors that made acquisition harder for fixed wing intruder.

## Made Visual Acquisition Harder (Fixed Wing Intruder) Intruder Aircraft Characteristics

• There was lower visual area during head on encounters.

#### **Environmental Conditions**

- Sun shining in the Subject Pilot's eyes during afternoon/evening flights.
- Sun glare off of ponds, flooded areas, and windshield.
- Hazy sky obscuring intruder aircraft, especially at further distances.

#### Other

- Looking for a higher altitude intruder while in a high wing aircraft due to blocked FOV.
- Looking for a lower altitude intruder while in a low wing aircraft due to blocked FOV.
- Traffic on roads in the distance (close to horizon) being mistaken for potential air traffic.

Table 9. Factors that made acquisition harder for rotorcraft intruder.

## Made Visual Acquisition Harder (Rotorcraft Intruder)

## **Intruder Aircraft Characteristics**

• Intruder moving out of the Subject Pilot's FOV during head on encounters.

#### **Environmental Conditions**

- Sun shining in the Subject Pilot's eyes during afternoon/evening flights.
- Sun glare off of ponds, flooded areas, and windshield.
- Hazy sky obscuring intruder aircraft, especially at further distances.
- Wind causing turbulence and made it harder to follow path and stay at altitude; this took the attention of the Subject Pilot away from traffic scanning.

#### Other

- Blind spots created by nose of ownship and wing struts.
- Higher amount of radio traffic to focus on during flight.
- Flying at a lower altitude than Subject Pilot is accustomed to.
- Lack of traffic awareness data.
- Instructor pilot usually assists in traffic scanning to the right and Subject Pilot may not have scanned in this direction as often as others.
- FOV blockages due to the Safety Pilot in the right seat.
- Subject Pilot does not usually wear sunglasses while flying.



Table 10. Factors that made acquisition harder for UAS intruder

### Made Visual Acquisition Harder (UAS Intruder)

### Intruder Aircraft Characteristics

- Small aircraft
- Lack of maneuvering and relative motion
- Looked like a car or pond

### **Environmental Conditions**

- Hazy weather conditions, especially towards horizon
- Wind causing turbulence and made it harder to follow path and stay at altitude; this took the attention of the Subject Pilot away from traffic scanning
- Sun shining in eyes

### Other

- Due to lower altitude, Subject Pilot was more concerned about potential tower hazards than usual
- Glasses reduced Subject Pilot's FOV
- Tall Subject Pilot had to duck to fully see out of the windshield
- Subject Pilot's first time flying with third person in plane caused them to spend time adjusting to weight and balance difference
- Following the flight path on the screen while also scanning for traffic
- Subject Pilot recently finished their IFR training and was not accustomed to flying under VFR
- Have not flown in left seat recently

Many of the factors mentioned by pilots that made the visual acquisition easier or more difficult align with previous research accomplished in the A23 – Validation of Low Altitude Detect and Avoid Standards (Amerson, et al., 2023) effort. The main factors that many pilots mentioned as making it easier to see most often related to aircraft color and its contrast with the background or a higher visual surface area when they would spot the aircraft from above. Many pilots mentioned weather as a factor in making it harder to spot the intruder aircraft, most often stating the sun would be in their eyes. This was especially prominent on flights that took place in the evening when the sun was lower on the horizon. Haziness on otherwise clear days also proved challenging for many as the intruder aircraft would be "hidden" at greater distances, although weather conditions were within normal VFR boundaries.

### **Flight Testing Environment**

Limits for clouds were in place according to the Class G airspace weather requirements present in 14 CFR § 91.155 (General Operating & Flight Rules 14 C.F.R § 91, 2022). Weather data was collected from the Meteorological Aerodrome Report for Greenville Mid-Delta Airport, located 23 miles southwest of KRNV, prior to every flight.

Subject Pilots were asked to self-assess their attention paid to weather throughout the test flight when compared to other "normal" VFR flights. Out of the 78 Subject Pilots, 55 paid the same attention to the weather as they would in a normal flight, illustrated in Figure 26. 10 Subject Pilots stated they gave more attention to the weather throughout the flight than usual. Most of these pilots flew in conditions with a low cloud ceiling or higher sustained and gusting winds. They have been denoted with an asterisk in Table 11.



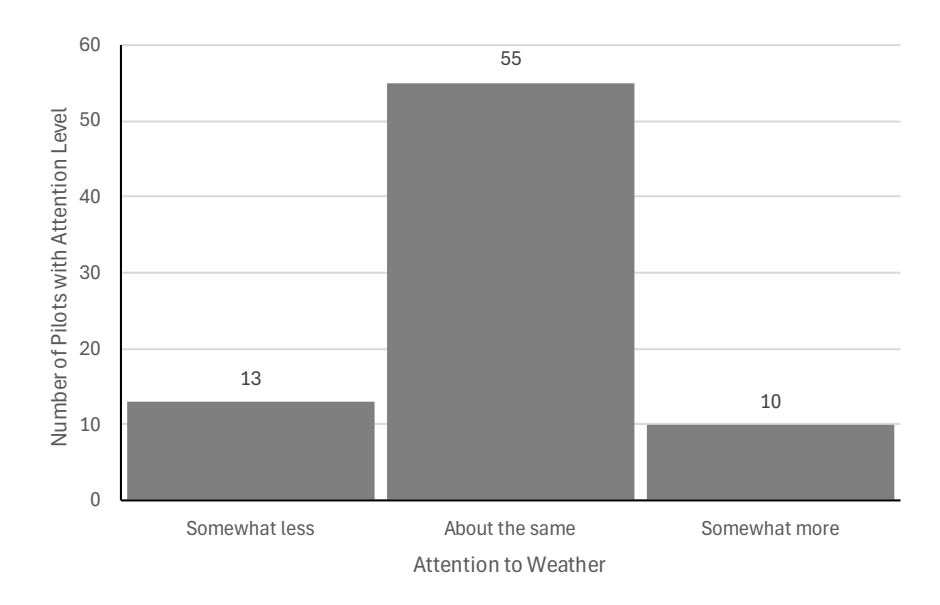


Figure 26. Subject Pilot's attention paid to weather conditions during flight.



Table 11. Weather conditions during testing.

Participant #	Date	Temp (°F)	Visibility (mi)	Wind Speed (mph)	Wind Direction	Clouds
1	7/11/2023	90	10	3	SSW	SCT031 OVC043
2	7/11/2023	90	10	3	SSW	SCT031 OVC043
3	7/12/2023	85	10	14	S	FEW015 FEW021
4*	7/12/2023	85	10	14	S	FEW015 FEW021
5	7/12/2023	87	10	12	SW	CLR
6	7/12/2023	87	10	12	SW	CLR
7	8/21/2023	97	10	5	ESE	CLR
8	8/22/2023	91	10	4	NNW	CLR
9	8/22/2023	95	19	2	NNW	CLR
10	8/22/2023	97	10	5	S	CLR
11	8/23/2023	87	16	4	ENE	CLR
12	8/23/2023	93	10	4	SWS	FEW040
13	8/23/2023	93	10	4	SWS	CLR
14	8/24/2023	88	10	1	ESE	CLR
15	8/24/2023	95	19	2	E	CLR
16	8/24/2023	99	17	3	E	CLR
17	8/25/2023	93	18	4	SW	CLR
18	11/28/2023	46	22	8	N	CLR
19	11/28/2023	52	25	6	NNE	CLR
20	11/28/2023	53	25	4	NNW	CLR
21	11/29/2023	30	20	5	S	CLR
22	11/29/2023	45	20	5	S	CLR
23	11/29/2023	62	25	11	SW	CLR
24	11/29/2023	60	28	9	SSW	CLR
25	11/30/2023	59	25	9	SW	FEW100
26	1/10/2024	31	19	7	SSW	CLR
27	1/10/2024	33	19	8	SSW	CLR
28	1/10/2024	47	19	12	SSW	CLR
29*	1/10/2024	51	22	13	SSW	CLR
30*	1/11/2024	34	14	7	SSE	FEW028 BKN036
31	1/11/2024	44	10	9	S	FEW026 FEW035
32	1/11/2024	56	16	9	SSE	FEW031
33	1/11/2024	63	18	11	SSE	SCT060
34	3/19/2024	54	21	10	SW	CLR
35	3/19/2024	56	22	10	SW	CLR
36	3/19/2024	59	25	10	WSW	CLR
37	3/20/2024	49	17	6	SW	CLR
38*	3/20/2024	59	21	8	SW	CLR





39	3/20/2024	68	25	9	SW	CLR	
40	3/21/2024	45	13	3	ESE	CLR	
41	3/21/2024	54	16	4	SSE	CLR	
42	3/21/2024	64	16	3	Е	CLR	
43	3/21/2024	71	25	7	ESE	SCT070	
44*	4/15/2024	65	13	13	SSW	BKN023	
45	4/15/2024	74	14	11	SSW	FEW027 OVC036	
46	4/15/2024	79	15	12	S	BKN039	
47	4/15/2024	81	18	13	S	FEW041	
48*	4/17/2024	79	15	9	SSW	FEW013 BKN022 OVC028	
49	4/17/2024	80	17	9	SSW	FEW017	
50	4/17/2024	81	17	9	SSW	FEW049	
51*	4/18/2024	76	14	12	S	FEW018 SCT029 OVC036	
52	4/22/2024	43	13	3	NE	CLR	
53	4/22/2024	60	22	4	Е	CLR	
54	4/22/2024	61	23	4	Е	CLR	
55	4/22/2024	64	25	2	SE	CLR	
56	4/22/2024	66	25	2	S	CLR	
57	4/23/2024	49	12	7	S	CLR	
58	4/23/2024	61	16	10	S	CLR	
59	4/24/2024	63	14	6	WSW	CLR	
60	4/24/2024	67	15	7	WNW	SCT060	
61	5/6/2024	81	15	10	SSW	FEW027 FEW033	
62	5/6/2024	85	16	12	S	FEW038	
63	5/6/2024	86	16	12	SSW	SCT042 SCT055	
64*	5/9/2024	80	6	6	S	CLR	
65*	5/9/2024	80	6	6	S	BKN017	
66	5/9/2024	83	5	5	WNW	BKN023 BKN030 OVC047	
67	5/9/2024	87	18	7	WNW	FEW033	
68	5/9/2024	90	20	7	NNW	CLR	
69	5/10/2024	67	17	11	N	CLR	
70	8/12/2024	72	14	5	ENE	CLR	
71	8/14/2024	88	18	4	ESE	SCT085 BKN150	
72*	8/14/2024	94	19	5	NE	FEW 130	
73	8/15/2024	89	17	5	S	SCT 070	
74	8/15/2024	89	17	5	S	SCT 055	
75	8/15/2024	95	18	3	S	CLR	
76	8/15/2024	97	19	3	SE	CLR	
77	8/16/2024	78	13	5	SSW	BKN 080	
78	8/16/2024	84	15	7	SW	CLR	
						·	



### 4 Visual Acquisition Performance

### **Tobii Eye Tracking Data Structure**

Using the Tobii Pro Glasses 3, the team collected pilots' eye tracking data, which encompasses various metrics such as 2D and 3D Gaze Points, Gaze Direction, Pupil Position, Pupil Diameter, and Fixation Points. The team identified essential variables for subsequent analysis.

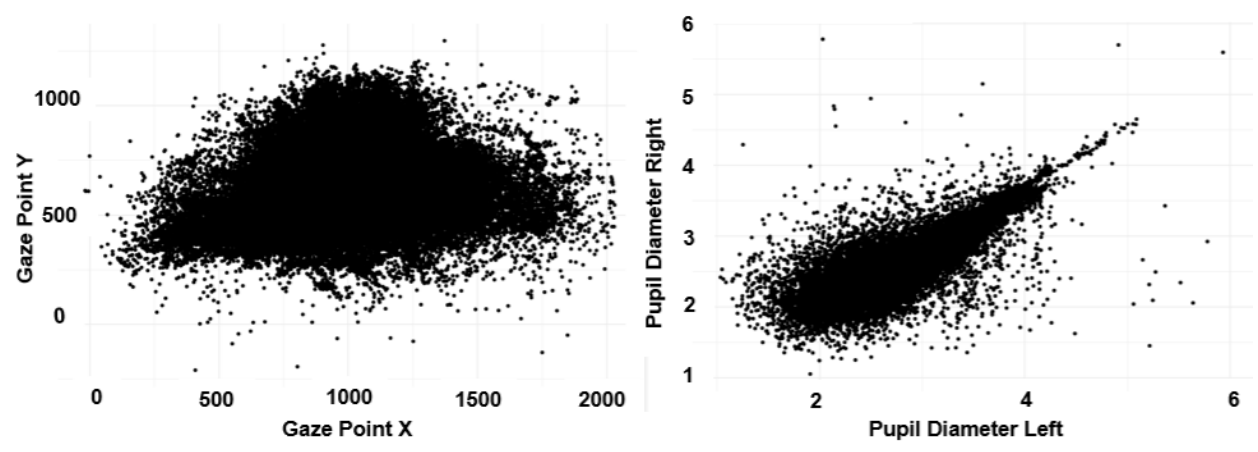


Figure 27. Subject Pilot's gaze point on left and pupil diameter on right.

The analysis is substantiated by two key visualizations. The first scatter plot does not indicate any significant correlation between the x (gaze point x in 2D) and y (gaze point y in 2D). This dispersion suggests that both dimensions provide distinct and valuable insights into the gaze behavior, implying that the exclusion of either variable could result in a loss of critical information. Therefore, it is recommended that both dimensions be retained for a comprehensive analysis of gaze patterns. In contrast, the second plot exhibits a correlation between the diameters of the left and right pupils. This correlation suggests redundancy since pupil dilation is generally symmetrical and influenced by similar physiological or environmental factors. It suggests the pupil diameter with a single variable (either left or right), thereby streamlining the dataset without compromising the analytical value.



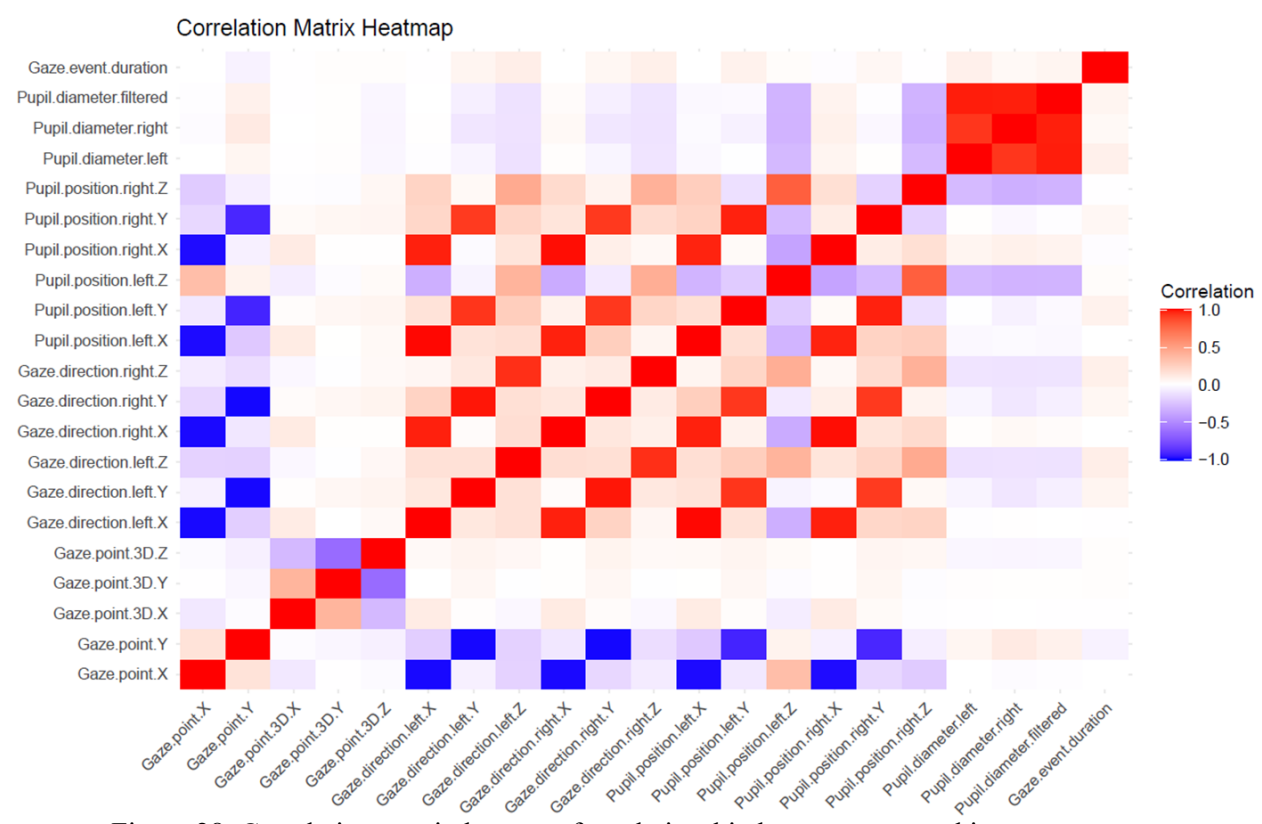


Figure 28. Correlation matrix heatmap for relationship between eye tracking parameters.

The correlation matrix heatmap provides a comprehensive view of the relationships between various eyetracking parameters measured by Tobii Eyeglasses. Each cell in the heatmap represents the correlation coefficient between two variables, with the scale ranging from -1 (perfect negative correlation) to +1 (perfect positive correlation). Colors closer to red indicate a higher positive correlation, and colors closer to blue indicate a higher negative correlation.

From the heatmap, one can observe high positive correlations among similar types of data points, particularly within the gaze direction and pupil position variables. For example, the X, Y, and Z coordinates within the gaze direction and pupil position categories show significant mutual correlations, suggesting that these measurements tend to vary together in a predictable manner. This correlation is expected as movements in one axis often accompany shifts in others when the eye changes direction or position. Conversely, the relatively lower correlations between Gaze Point 2D coordinates and 3D Gaze Directions suggest these variables provide unique details. This distinction is crucial for analyses where detailed spatial orientation and eye movement patterns are necessary, such as in studies aimed at understanding how people interact with complex visual interfaces.

Additionally, the variables with low or no correlation, such as the duration of gaze events compared to physical measures like pupil diameter, highlight various aspects of eye behavior, indicating the importance of retaining these distinct data types for comprehensive behavioral analysis. Table 12shows the actual



correlation values between the variables. The detailed analysis of those variables will be demonstrated in Section 0.

Gaze.point.X Gaze.point.Y Gaze.point.3D.X Gaze.point.3D.Y Gaze.point.3D.Z Pupil.diameter.left Pupil.diameter.right Pupil.diameter.filtered Gaze.event.duration 0.15 -0.1 -0.02 -0.01 Gaze.point.Y 0.15 -0.02 -0.04 -0.06 0.05 0.11 0.07 -0.05 Gaze.point.3D.X -0.1 -0.02 1 0.39 -0.3 0 0 0 Gaze.point.3D.Y -0.04 0.39 1 -0.64 0.01 0.01 0.01 0.01 Gaze.point.3D.Z -0.02 -0.06 -0.3 -0.64 1 -0.04 -0.04 -0.04 0.01 Gaze.direction.left.X -0.99 -0.21 0.1 0 0.03 -0.01 0.01 0 0 Gaze.direction.left.Y -0.06 -0.99 0.01 0.04 0.06 -0.04-0.11 -0.07 0.05 Gaze.direction.left.Z -0.19 -0.03 0.04 -0.13 -0.12 -0.12 0.09 -0.2 0 Gaze.direction.right.X 0.02 -0.99 -0.1 0.11 0.01 0.01 0.01 0.03 Gaze.direction.right.Y -0.99 0.04 -0.17 0.02 0.04 0.06 -0.04 -0.1 -0.07 Gaze.direction.right.Z -0.14 -0.03 0.03 -0.11 -0.12 -0.12 0.08 Pupil.position.left.X -0.98 0.1 0.03 -0.03 -0.02 -0.03 Pupil.position.left.Y -0.1 -0.93 0.01 0.04 -0.01 -0.06 0.07 Pupil.position.left.Z 0.06 -0.08 -0.02 0.03 0.02 0.34 -0.3 -0.32 Pupil.position.right.X -0.98 -0.06 0.1 0.05 0.07 0.06 -0.01 Pupil.position.right.Y -0.17 -0.92 0.03 0.04 0.05 0.01 -0.03 -0.01 0.04 Pupil.position.right.Z -0.22 -0.07 -0.01 -0.01 0.04 -0.29 -0.34 -0.33 Pupil.diameter.left 0 0.05 0 0.01 -0.04 1 0.92 0.97 0.08 Pupil.diameter.right -0.02 0.11 0 0.01 -0.04 0.92 0.97 0.03 Pupil.diameter.filtered -0.01 0.07 0 0.01 -0.04 0.97 0.97 0.05 Gaze.event.duration -0.05 0.01 0.01 0.08 0.03 0.05

Table 12. Correlation between eye tracking variables.

### **Sequence Analysis**

I-F-S-Y-K-N-I-M

# Research hypothesis 1: The eye scanning patterns of pilots differ significantly between various mission stages of a flight.

This hypothesis is grounded in the observation that the complexity and frequency of gaze shifts vary between the more demanding take-off phase and the relatively routine cruise phase. During take-off, pilots are required to monitor multiple instruments and controls rapidly to ensure a safe ascent, whereas during cruise, the focus tends to be more on maintaining course and altitude, resulting in more repetitive and less varied gaze patterns.

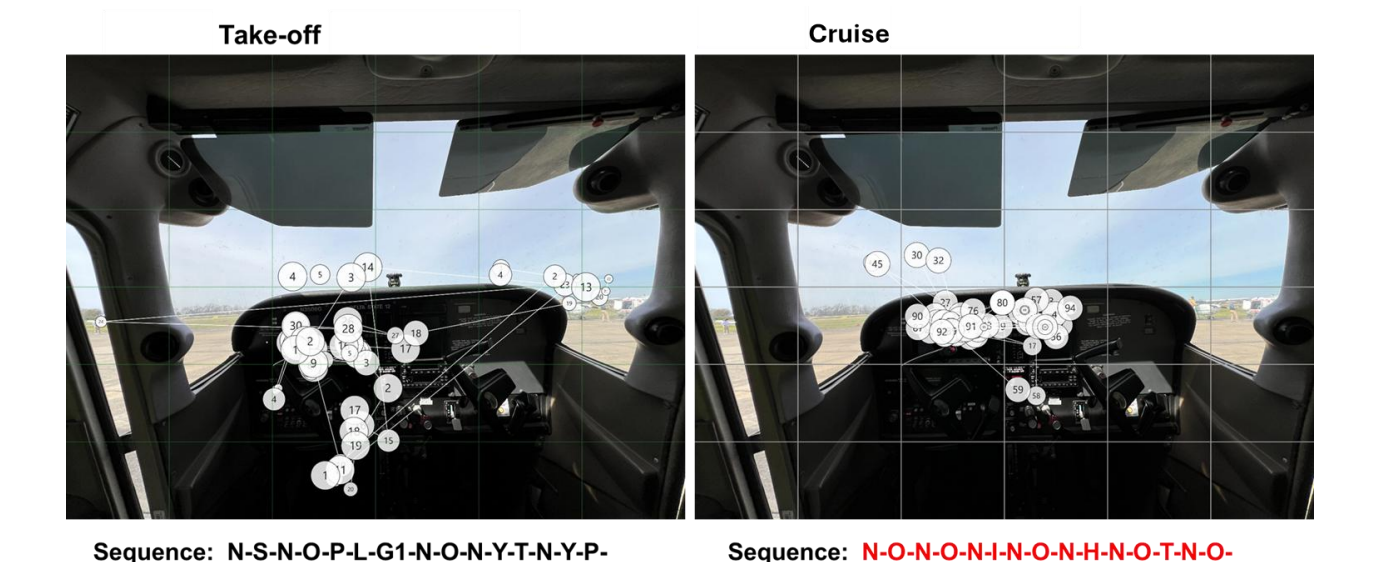


Figure 29. Eye movement sequence of a pilot during two phases of flight.



Figure 29 illustrates the eye movement sequences of a pilot during two distinct phases of flight: take-off and cruise. These sequences are captured using eye-tracking technology fitted within the cockpit, allowing for a precise recording of where and how frequently the pilot's gaze shifts to different instruments and controls. Each numbered marker represents a specific Area Of Interest (AOI) within the cockpit that the pilot looks at, and the sequence of numbers below each image represents the order in which the pilot's gaze moved between these points.

During take-off, the sequence is more complex and varied: N-S-N-O-P-L-G1-N-O-N-Y-T-N-Y-P-I-F-S-Y-K-N-I-M. This sequence indicates frequent shifts between numerous controls and instruments, reflecting the high demands placed on the pilot during this critical phase of flight. The pilot must monitor a wide range of indicators and systems to ensure a safe ascent. The gaze points include essential flight instruments and navigation systems, which are crucial for adjusting the aircraft's speed, altitude, and trajectory during the initial climb.

# Research hypothesis 2: The eye scanning patterns of pilots, as indicated by average relative frequency of gaze points, do not show significant differences across different aircraft types.

This hypothesis demonstrates that despite variations in cockpit design and layout across different aircraft types, the fundamental eye-scanning patterns of pilots remain consistent. The heatmaps display prominent areas of gaze concentration which appear quite similar in terms of the locations on the instrument panels that attract the most attention. This suggests a level of uniformity in the critical zones that pilots monitor, regardless of aircraft type. If these focal areas correspond to similar instruments in both aircraft (e.g., primary flight displays, and engine monitors), it supports the hypothesis that pilots maintain a consistent scanning pattern, adapting to where essential information is displayed.



Figure 30. Scan pattern in C172 on left and Cirrus SR20 on right.

Research Hypothesis 3: Pilots exhibit significant differences in eye scanning patterns during head-on versus overtaking encounters in flight.



In the "Head-on" scenario, the distribution of AOI shows a concentration of gaze points around central and upper portions of the instrument panel, as well as some focus on the forward view and peripheral areas. This pattern indicates that the pilot is actively maintaining situational awareness of the airspace directly ahead. The scattered distribution across a wide array of instruments suggests a high level of alertness and comprehensive monitoring.

For the "Overtake" scenario, the gaze points are more focused towards specific areas of the instrument panel, particularly around navigation and communication instruments. This suggests that while the pilot is overtaking another aircraft, the focus is on maintaining precise control over the aircraft's trajectory. The concentration of gaze points in fewer areas could indicate a more targeted approach to monitoring, reflecting the different priorities in this type of encounter compared to a head-on situation.

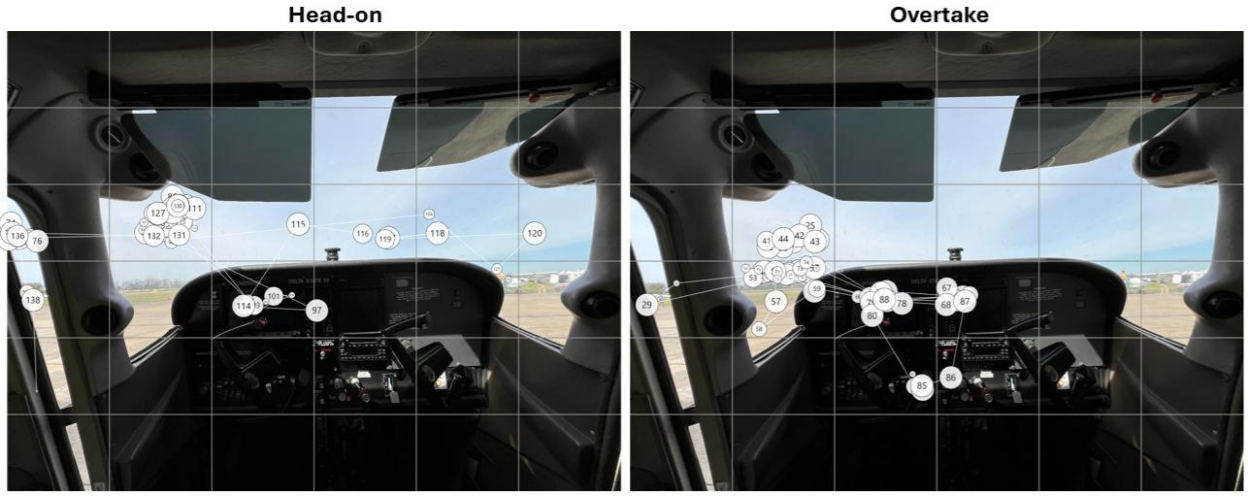


Figure 31. Scan pattern in a head-on encounter on left and overtake encounter on right.

## Research Hypothesis 4: Experienced pilots exhibit more diverse and comprehensive eye scanning patterns compared to novice pilots during standard flight operations.

This could be indicative of a higher level of situational awareness and an ability to integrate information from multiple sources more effectively. In Figure 32, the experienced pilot's gaze points are spread across a broader array of instruments and controls, reflecting a refined capability to monitor and respond to multiple aspects of the flight environment simultaneously. This expansive scanning behavior might allow experienced pilots to maintain better control and readiness, adapting quickly to any situational changes by having a holistic view of the cockpit and external conditions. On the other hand, the novice pilot seems to focus on fewer points, which might suggest a more concentrated but possibly limited scope of attention. This could be due to the novice's need to concentrate more on essential controls and instruments as they



are still mastering the basics of flight management. Their scanning pattern might be less diverse as they have not yet developed the confidence or skill to simultaneously monitor multiple information sources.

# Novice Single Engine Hours (150) Single Engine Hours (750) Single Engine Hours (750)

Figure 32. Scan pattern based on approximate engine hours with 150hrs on left and 750hrs on right.

# Research Hypothesis 4A: Pilots' engine hours significantly impact eye-scanning patterns, causing the scanning behavior to broaden as engine hours increase.

Figure 33 illustrates the eye-scanning patterns of inexperienced pilots, each with engine hours under 120. As depicted, the scanning pattern for these pilots remains relatively narrow and focused. Pilot with 60-70 hours, exhibits a concentrated scanning pattern around the central instruments. Similarly, a pilot with 80-90 hours, shows a narrow scanning pattern with slight expansion, but still primarily focused on a small area. Another pilot with 90-100 hours, demonstrates minor broadening of the pattern, yet it remains centered on key areas. Finally, a pilot with 100-110 hours, has a somewhat broader scanning pattern, though it is still relatively constrained compared to that of more experienced pilots. These observations support the team's hypothesis that less experienced pilots (with fewer engine hours) tend to have narrower and more focused eye-scanning patterns. As pilots gain more experience, their scanning patterns become wider, covering more of the cockpit displays and surroundings.



# 90-100 hours 90-110 hours 100-110 hours

Figure 33. Experience impacts on scan pattern for pilots with less than 120 single engine hours.

Figure 34 illustrates the eye-scanning patterns of more experienced pilots, each with varying hours on single and multiple engines. The broader scanning patterns are observed, indicated by the number of engine hours, which significantly influence eye-scanning behavior. For instance, pilots with higher single and multiple engine hours demonstrate eye-scanning patterns that cover a larger portion of the cockpit. This broad scanning pattern indicates a heightened level of situational awareness and an ability to monitor multiple cockpit instruments simultaneously. Indeed, experienced pilots tend to develop a more comprehensive and proactive scanning strategy. This allows them to effectively integrate information from various sources within the cockpit, enhancing their overall flight management and decision-making capabilities. Overall, these observations align with the team's hypothesis that increased engine hours, encompassing both single and multiple engine experiences, contribute to wider and more distributed eye-scanning patterns.



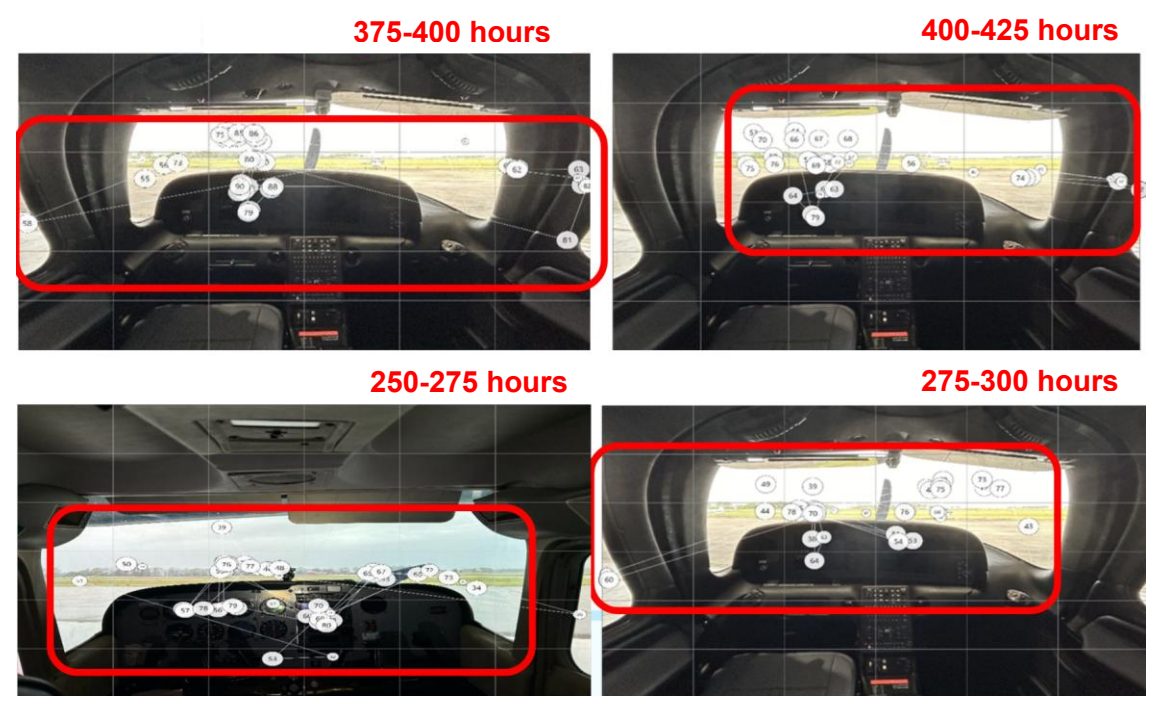


Figure 34. Experience impacts on scan pattern for pilots with more than 120 single engine hours.

Research Hypothesis 5: Increased pilot engine hours lead to wider scanning behavior, regardless of the type of intruders (both in UAS and rotorcraft overtakes) and the missions (both overtakes and head-on/crossing).

Figure 34 and Figure 35 provide evidence supporting the hypothesis that pilots with more engine hours exhibit broader and more expansive scanning behaviors. This trend is observed consistently across different types of intruder scenarios, such as rotorcraft and UAS overtakes. For example, a pilot, who has accumulated 250-275 engine hours, demonstrates a scanning pattern that covers a vast area of both the cockpit and the external environment. Moreover, regardless of the missions (both in overtakes and head-on), this extensive scanning pattern by experienced pilots suggests a high level of situational awareness, where the pilot is actively monitoring multiple instruments and external cues to effectively manage the overtake, head-on, and crossing encounter.

Similarly, in the case of UAS overtakes, experienced pilots exhibit wider scanning patterns as their engine hours increase. As shown in Figure 36, pilots with higher engine hours display scanning behaviors that encompass significant portions of the cockpit and external surroundings. In contrast, pilots with fewer engine hours show narrower and more focused scanning patterns, primarily directed at specific instruments and the windshield.

These observations indicate that experienced pilots, regardless of the type of intruders encountered, engage in more extensive scanning patterns. This behavior likely reflects their enhanced ability to maintain situational awareness and manage multiple information sources simultaneously. Overall, the analysis demonstrates a clear correlation between pilot experience, as measured by engine hours, and the breadth of scanning behavior. This insight has important implications for understanding how pilot training and experience influence situational awareness and scanning strategies during flight encounters with different types of intruders.



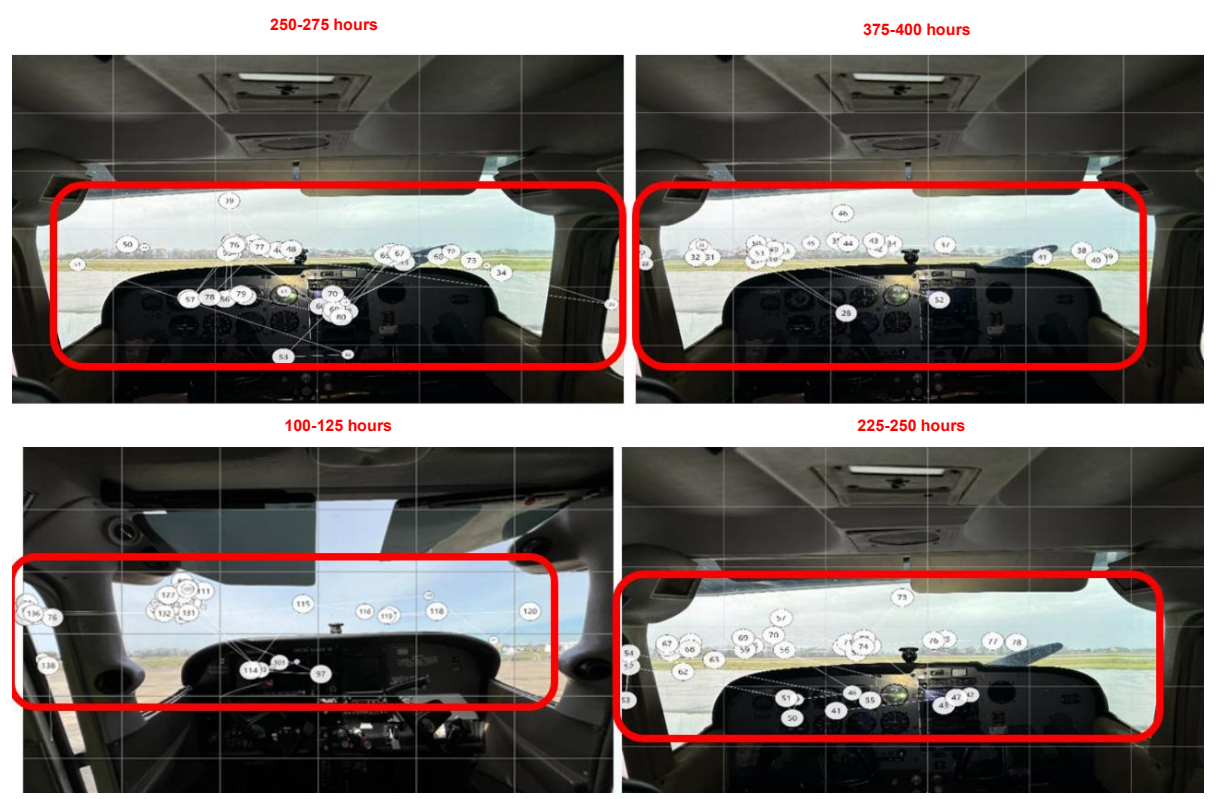


Figure 35. Typical Subject Pilot scan patterns in rotorcraft encounters.

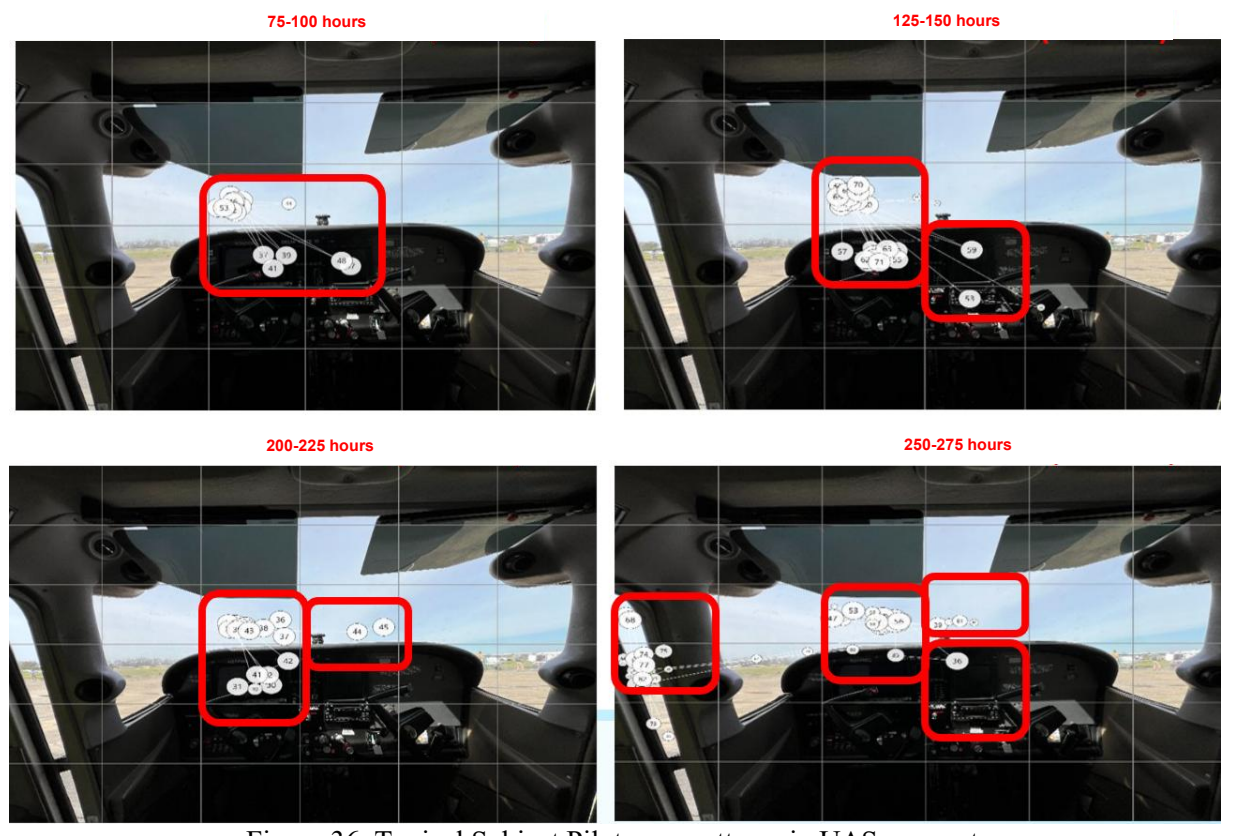


Figure 36. Typical Subject Pilot scan patterns in UAS encounters.



### Scanning Behaviors and Cognition Awareness based on Flight/Pilot Configuration

Figure 37 illustrates the relationship between engine hours and eye-scanning patterns in pilots. The two key metrics analyzed are the average duration of eye fixations and the total duration of eye fixations, both measured in milliseconds, across different ranges of engine hours. The left graph shows the average duration of eye fixations for pilots grouped by their engine hours: less than 150, between 150 and 300, between 300 and 450, and more than 450 hours. From the graph, it is evident that pilots with fewer engine hours (<150) tend to have higher variability in their average fixation duration, with some fixations reaching up to 7000 milliseconds. As pilots gain more experience, their average fixation duration decreases and becomes more consistent. For instance, pilots with engine hours between 150 and 300 show a tighter cluster of fixation durations around 1000 milliseconds, indicating more stable and focused scanning patterns. This trend continues for pilots with 300 to 450 hours and those with over 450 hours, where the average fixation durations are shorter and less variable.

The right graph illustrates the total duration of eye fixations for pilots within the same engine hour groups. Here, a similar trend is observed. Pilots with fewer than 150 engine hours have a wider range of total fixation durations, with some pilots reaching up to 60,000 milliseconds. As pilots accumulate more hours, the total fixation duration decreases and stabilizes. For example, pilots with 150 to 300 engine hours show a clustering of around 40,000 milliseconds, and this clustering becomes even more pronounced in the 300 to 450 and > 450-hour groups, indicating more efficient and targeted scanning behavior. From these observations, researchers can conclude that pilot experience, as measured by engine hours, has a significant impact on eye-scanning patterns. Less experienced pilots tend to have longer and more variable fixation durations, reflecting a less efficient scanning strategy. As pilots gain more experience, their scanning patterns become more focused and consistent, with shorter average fixation durations and more stable total fixation times. This suggests that experienced pilots are better at quickly and effectively processing the information in their cockpit environment, leading to improved situational awareness and flight performance.

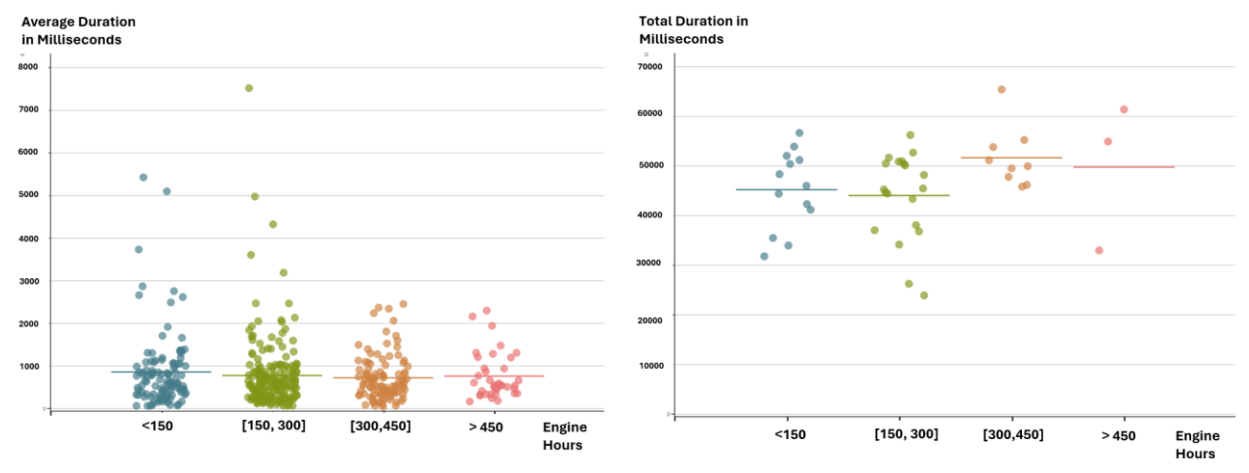


Figure 37. Relationship between engine hours and eye fixation.

The graphs in Figure 38 illustrate the relationship between years of experience and two key eye metrics: average pupil diameters in millimeters and the number of saccades. The graphs categorize pilots into three groups based on their years of experience: less than 2 years, between 2 and 4 years, and more than 4 years. The left graph shows the average pupil diameters for pilots across the different experience groups. Pilots with less than 2 years of experience exhibit a relatively wide range of pupil diameters, with an average of less than 2.5 millimeters. The variability in this group suggests that their scanning patterns are highly individual-specific. Compared to the more experienced groups, their pupil diameters are smaller. Indicating that they might not be collecting data as efficiently. Pilots with 2 to 4 years of experience have a slightly



more consistent pupil diameter, indicating a more uniform physiological response. This consistency might reflect a more stable emotional state as pilots gain more experience and confidence in their flying abilities. Pilots with more than 4 years of experience show average pupil diameters around 2.5 to 3 millimeters. This suggests that experienced pilots have a stable physiological response during flights, indicating better situational awareness.

The right graph depicts the number of saccades for pilots within the same experience groups. Saccades are rapid eye movements between fixation points, and their frequency can indicate cognitive workload and attention distribution. Pilots with less than 2 years of experience show a moderate number of saccades, averaging around 80. In the 2 to 4 years' experience group, the number of saccades is slightly higher, averaging around 85. This group shows the second group is better at distributing their attention across the cockpit. Pilots with more than 4 years of experience exhibit the highest number of saccades, averaging around 90, with some pilots reaching up to 140 saccades. This higher frequency of saccades suggests that experienced pilots are highly active in scanning their environment, maintaining high situational awareness. From these observations, one can clearly conclude that pilot experience significantly impacts both physiological and cognitive responses during flights. The key findings are that less experienced pilots exhibit smaller values in pupil diameter and a smaller number of saccades, indicating less efficient attention distribution. As pilots gain more experience, their physiological responses stabilize, and their eye movement patterns become more efficient.

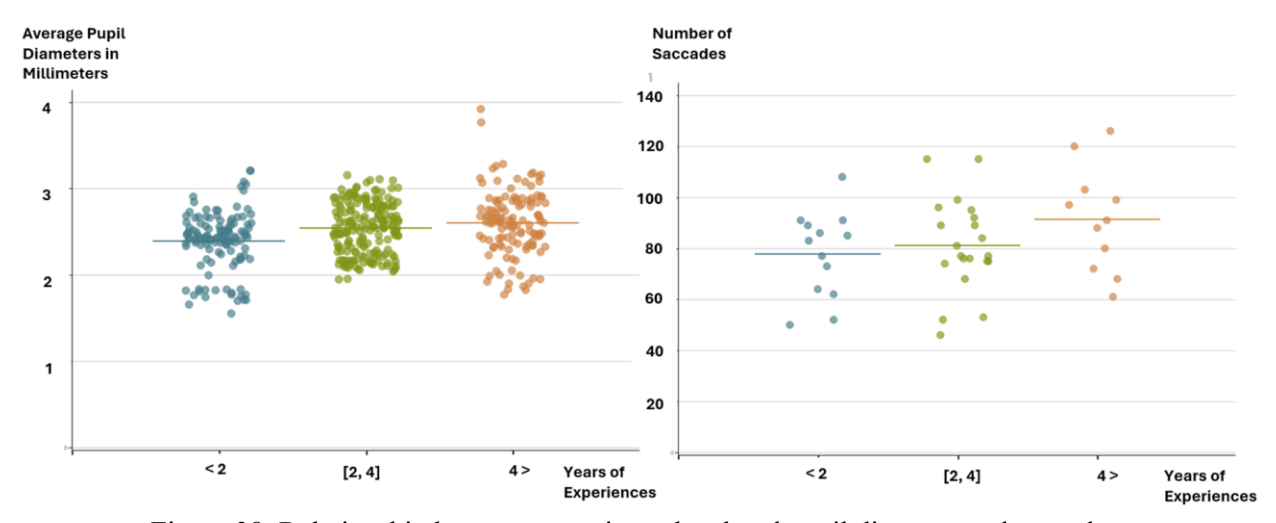


Figure 38. Relationship between experience level and pupil diameter and saccades.

Figure 39 illustrates the relationship between reliance on visual landmarks and two key eye metrics: average pupil diameters in millimeters and the time to first fixation in milliseconds. The pilots are grouped into three categories based on their reliance on visual landmarks: not at all, slightly, and moderately to heavily. The left graph shows the average pupil diameters for pilots across these various levels of reliance. Pilots who do not rely on visual landmarks at all exhibit a relatively narrow range of pupil diameters, averaging around 2 millimeters. This consistency suggests that these pilots have a stable physiological response, indicating lower cognitive load during flight. In contrast, pilots who rely slightly on visual landmarks show a wider range of pupil diameters, averaging around 2.5 millimeters. The increased average pupil size and variability suggests a higher cognitive load, as these pilots use visual landmarks to aid in their navigation and situational awareness. Pilots who rely moderately to heavily on visual landmarks exhibit the largest average pupil diameters, around 3 millimeters, with significant variability. This indicates that these pilots experience the highest cognitive load and stress levels, relying heavily on visual landmarks for navigation.



The substantial increase in pupil diameter suggests a heightened state of effort as they process a greater amount of visual information to maintain situational awareness.

The right graph illustrates the time to first fixation for pilots within the same reliance categories. Pilots who do not rely on visual landmarks at all have the shortest time to first fixation. This quick response time indicates efficiency in identifying and focusing on relevant visual information, likely due to their familiarity and confidence in their environment. Pilots who rely slightly on visual landmarks have a longer time to first fixation. The increased time suggests that these pilots take longer to identify and focus on relevant information, possibly due to the additional cognitive processing required to incorporate visual landmarks into their navigation. Pilots who rely moderately or heavily on visual landmarks show the longest time to first fixation. The extended time indicates that these pilots take the most time to process and focus on relevant information, reflecting the higher cognitive load and mental effort associated with their heavy reliance on visual landmarks.

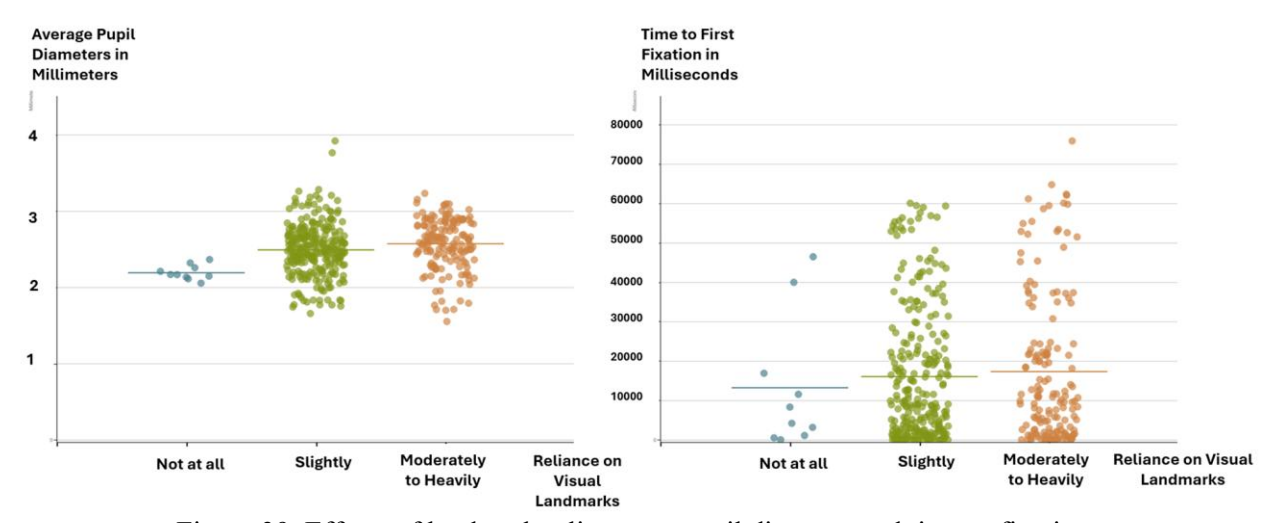


Figure 39. Effects of landmark reliance on pupil diameter and time to fixation.

The provided graphs in Figure 40 illustrate the relationship between wearing sunglasses and two key eye metrics: the number of saccades and the time to first fixation, both measured in milliseconds. The left graph shows the number of saccades for pilots wearing sunglasses versus those not. Saccades are rapid eye movements between fixation points, and their frequency can indicate cognitive workload and attention distribution. For pilots wearing sunglasses, the number of saccades averages around 80, with some pilots reaching up to 140 saccades. There is considerable variability, indicating a range of cognitive workloads and attention distribution strategies among these pilots. In contrast, pilots not wearing sunglasses show a slightly lower average number of saccades, also around 80, but with fewer outliers reaching above 100. This group exhibits a tighter clustering of saccades, suggesting more consistent eye movement patterns.

The right graph depicts the time to first fixation for pilots with and without sunglasses. Time to first fixation measures how quickly pilots can fixate on a target after a stimulus. Pilots wearing sunglasses show a wide range of fixation times with a higher average time. This indicates potentially due to visual interference or discomfort caused by sunglasses; it takes longer time to get fixated. On the other hand, pilots who do not wear sunglasses demonstrate slightly quicker and more consistent fixation times, with lower time. Pilots who do not wear sunglasses exhibit more consistent saccade patterns, indicating a potentially more stable cognitive workload and attention distribution. This consistency might be due to the absence of visual interference from sunglasses, allowing for clearer and more focused vision. Conversely, pilots wearing



sunglasses have a broader and higher range of reaction times, suggesting that sunglasses may cause some visual interference or discomfort, leading to delayed fixation times for some pilots.

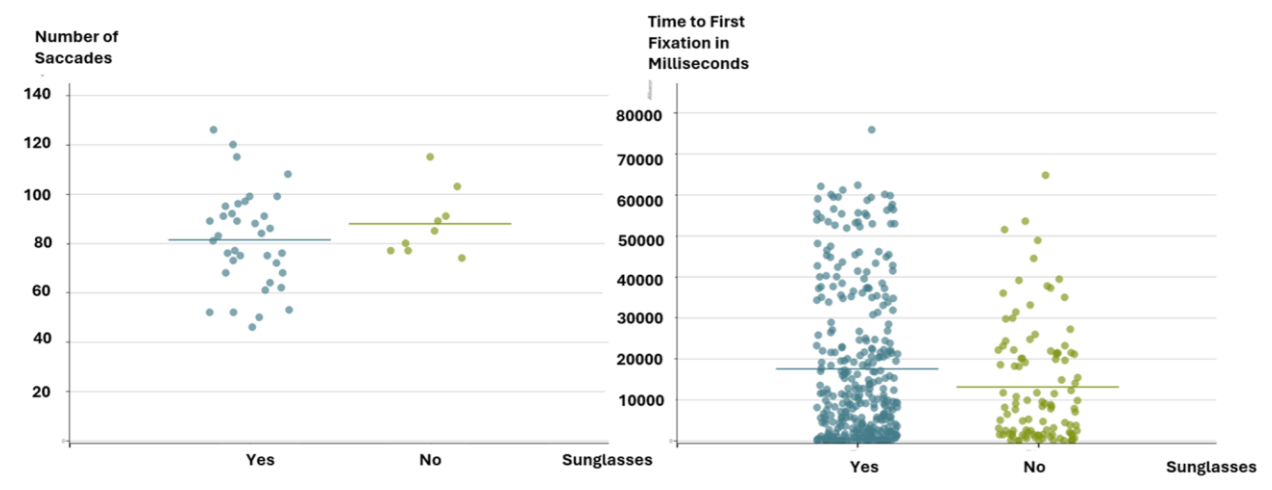


Figure 40. Effects of sunglasses on saccades and time to fixation.

### **Encounter Set**

As mentioned, a variety of encounter geometries were performed against different intruder aircraft. An overview of the encounters can be seen in Table 13. Detailed tables containing information about each individual encounter are in

A65 Encounter Data. Overall, 189 encounters were conducted with crewed aircraft in this research effort, 60 against a crewed fixed wing intruder, 79 against a rotorcraft intruder, and 50 against a UAS intruder.

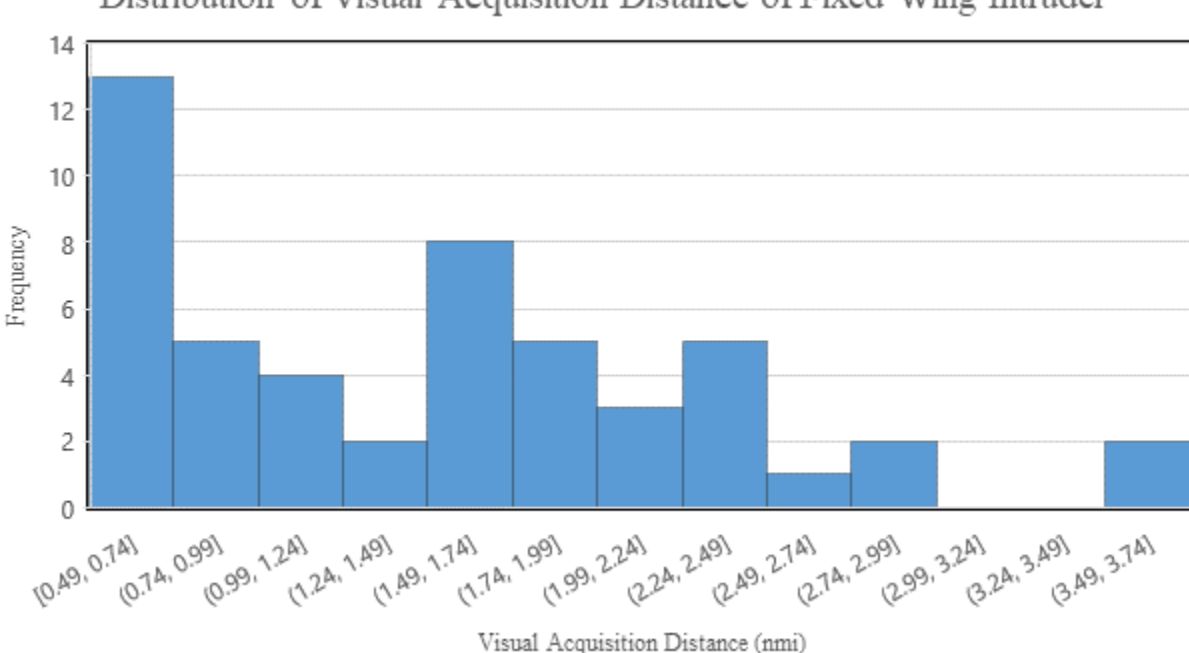
the 13. Types and number of encounters generated in hight test						
Intundou Tymo	Encounter	# of Encounters Generated				
Intruder Type	Type					
Crewed Fixed Wing	Overtake	60				
Rotorcraft	Head On	24				
Rotorcraft	Overtake	33				
Rotorcraft	Left Crossing	11				
Rotorcraft	Right Crossing	11				
UAS	Overtake	50				

Table 13. Types and number of encounters generated in flight testing.

### Fixed Wing Encounters

Encounters against a fixed wing intruder were overtake scenarios where the ownship aircraft would pass directly over the top of the intruder aircraft. There was one test where this was swapped due to the Subject Pilot being a repeat test participant. Out of the 60 encounters, 55 resulted in the Subject Pilot visually acquiring the intruder aircraft. The distribution of these visual acquisitions is shown in Figure 41. None of the visual acquisitions occurred within the currently accepted Well-Clear Volume (WCV) of 0.33 nmi (2000ft) or Near Mid Air Collision distance (NMAC) of 0.082 nmi (500 ft). The average detection distance was 1.35 nmi (8,203 ft).





### Distribution of Visual Acquisition Distance of Fixed Wing Intruder

Figure 41. Detection distances of the fixed wing intruder during overtake encounters.

The probability of detection at each visual detection range is shown in Figure 42. At distances below 1.5 nmi (9,114 ft), Subject Pilots were more likely to spot the aircraft during the overtake encounters. When the intruding fixed wing aircraft is at distances of 2.5 nmi (15,190 ft) and beyond the probability of detection is greatly diminished to 10% and below.

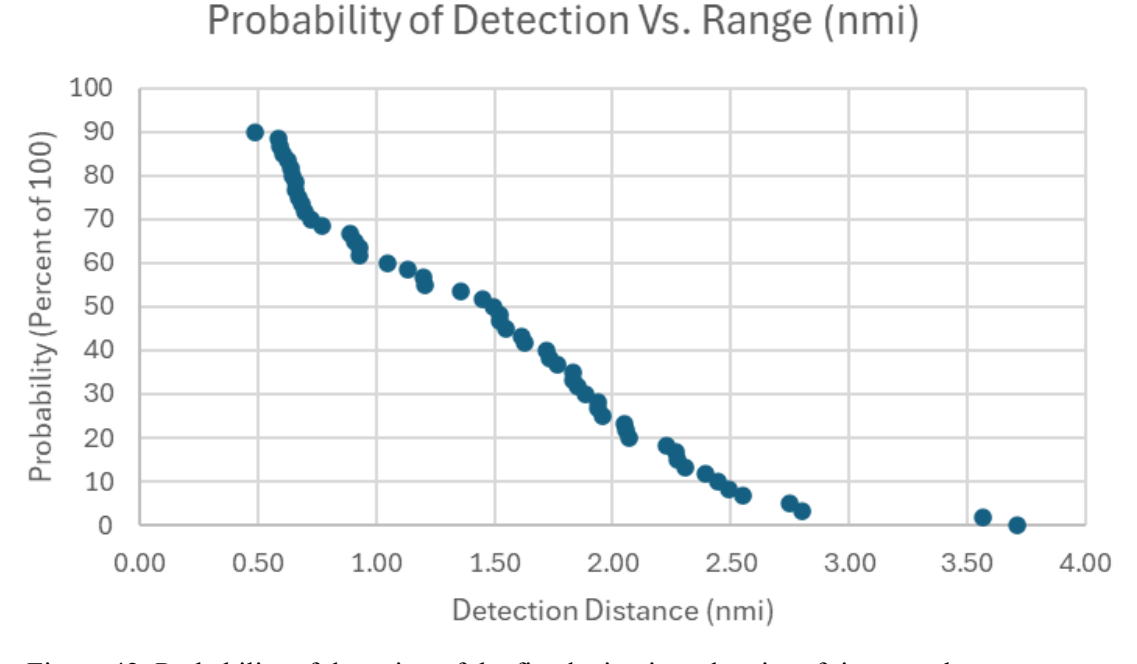


Figure 42. Probability of detection of the fixed wing intruder aircraft in overtake geometry.



Due to the nature of the test, a horizontal Closest Point of Approach (CPA) of zero was desired for a "perfect" encounter. The CPA for fixed wing encounters, shown below, was within 1 nmi (6076 ft) for all encounters with a maximum of 0.83 nmi (5043 ft) and a minimum of 0.01 nmi (61 ft). In the 60 overtake encounters conducted, 47 of them occurred within the WCV and 24 would be considered NMACs. It is important to note that the tests were not designed to perfectly complete an overtake as the slower intruder aircraft needed time to setup for the next leg of the flight path before the ownship arrived. In many instances, the intruder aircraft broke off of the flight path after the ownship reasonably could no longer see the intruder without making exaggerated or unnatural body movements or physical displacement within the aircraft. For these reasons, the CPA values tend to be larger than if the test had been designed to minimize the tested CPA. Researchers determined that once the intruder was below the dashboard of the ownship's cockpit, that this approach would still yield, and did yield, good test data.

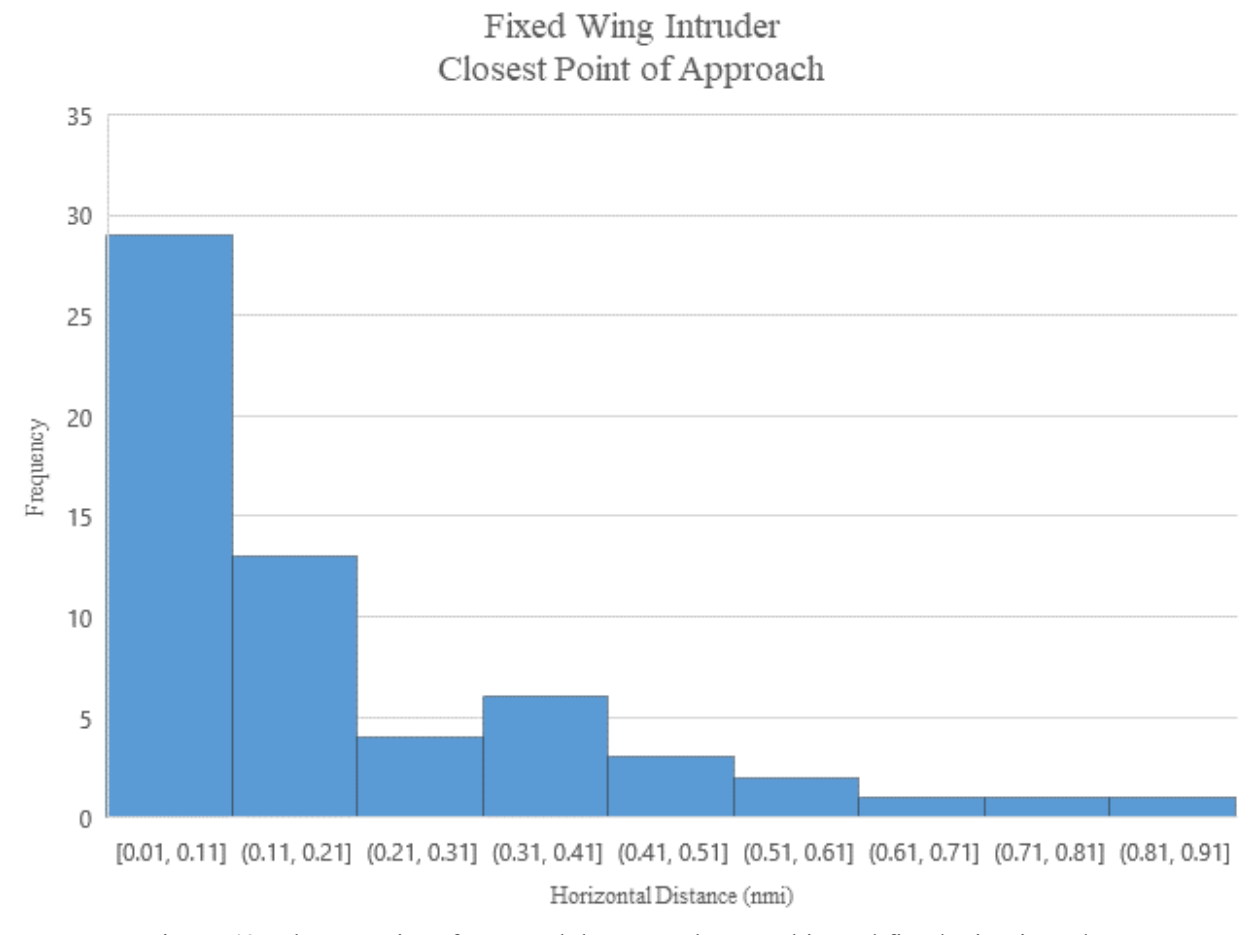


Figure 43. Closest point of approach between the ownship and fixed wing intruder.



Figure 44 shows that of the five missed detections in the overtake encounters, four of them had CPAs within the WCV and three were within the accepted horizontal NMAC volume.

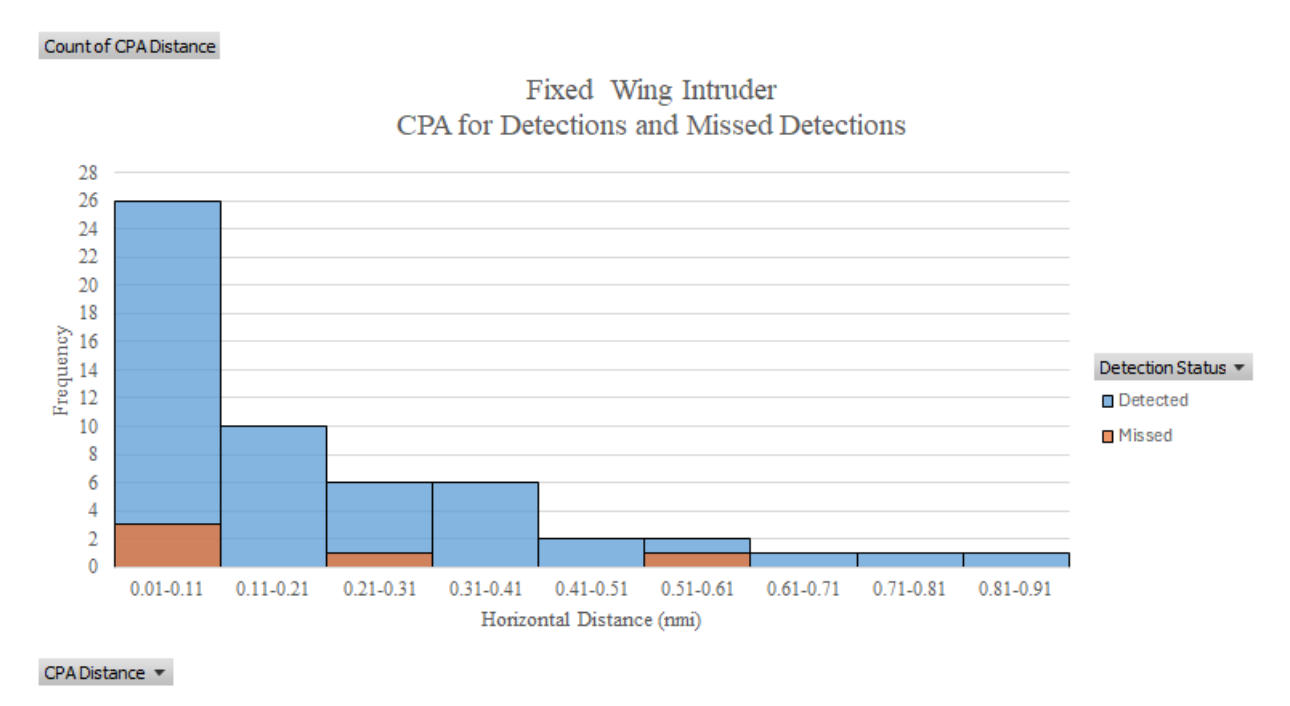


Figure 44. Closest point of approach between the ownship and fixed wing intruder separated by detection status.

The closing speed between the two aircraft, shown in Figure 45, was determined at the time of detection, if there was one, and at the time of CPA for those with no detection. The ownship aircraft was typically moving 35 to 60 knots faster than the slower ownship, a speed difference that was necessary to achieve the desired overtake encounter in an appropriate amount of time.



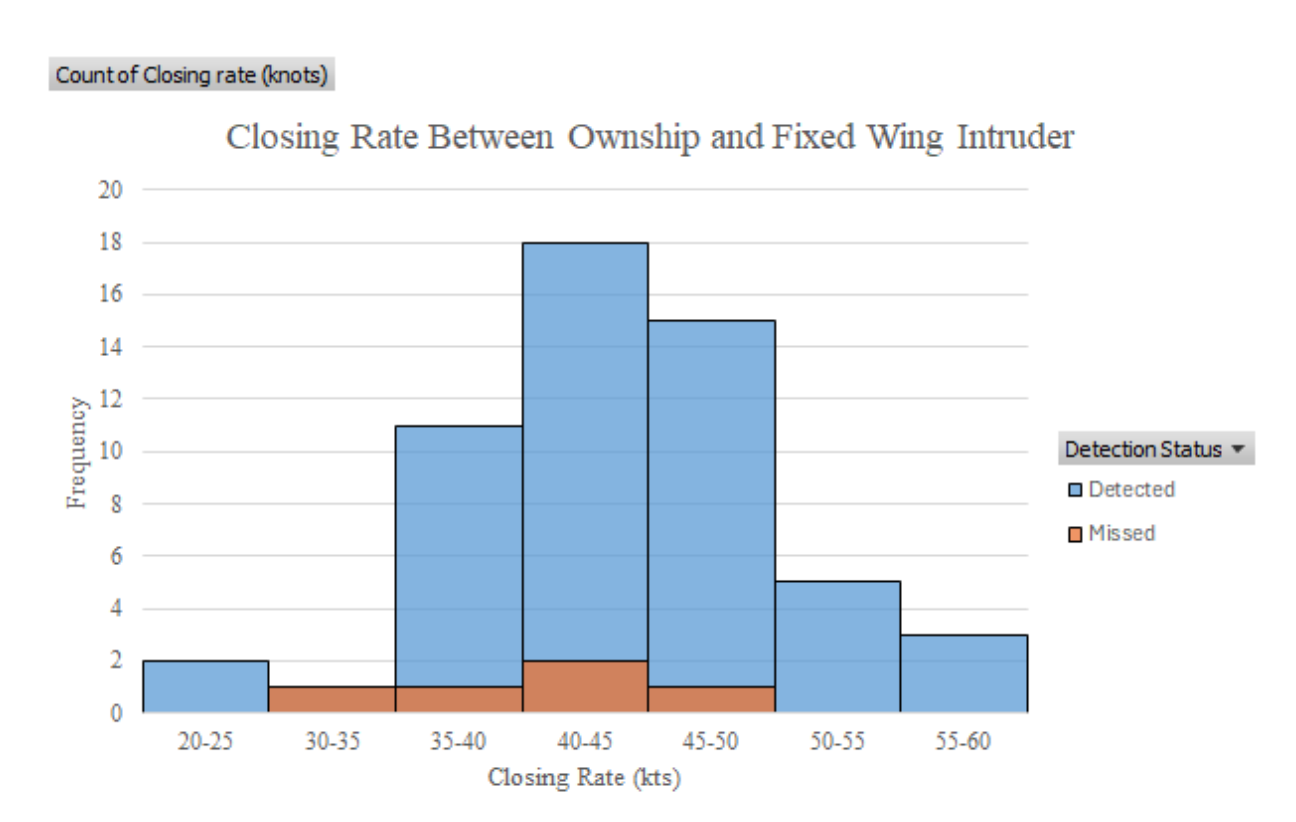


Figure 45. Closing rate between ownship and fixed wing intruder.

### Rotorcraft Encounters

Closing rate (knots) ▼

Encounters between a fixed wing ownship and rotorcraft intruder consisted of head-on, crossing, and overtake geometries. The rotorcraft was always at a lower altitude during all tests. There were 79 total encounters across the three geometries, as shown in Table 14. Out of these encounters, only 33 resulted in a positive visual acquisition of the rotorcraft by the Subject Pilot. These encounters are broken down further in the following table and Figure 46.

Table 14. Summary of encounters with rotorcraft intruder.

Encounter Geometry	Detections	Missed Detections	Total Encounters	Avg Detection Distance (nmi)	Min Detection Distance (nmi)	Max Detection Distance (nmi)
Overtake	15	18	33	0.77	0.17	1.74
Head On	6	18	24	0.45	0.12	0.89
Left Crossing	8	3	11	0.73	0.16	1.49
Right Crossing	4	7	11	1.02	0.91	1.21



# Visual Acquisition Distance of Rotorcraft Intruder All Encounter Geometries

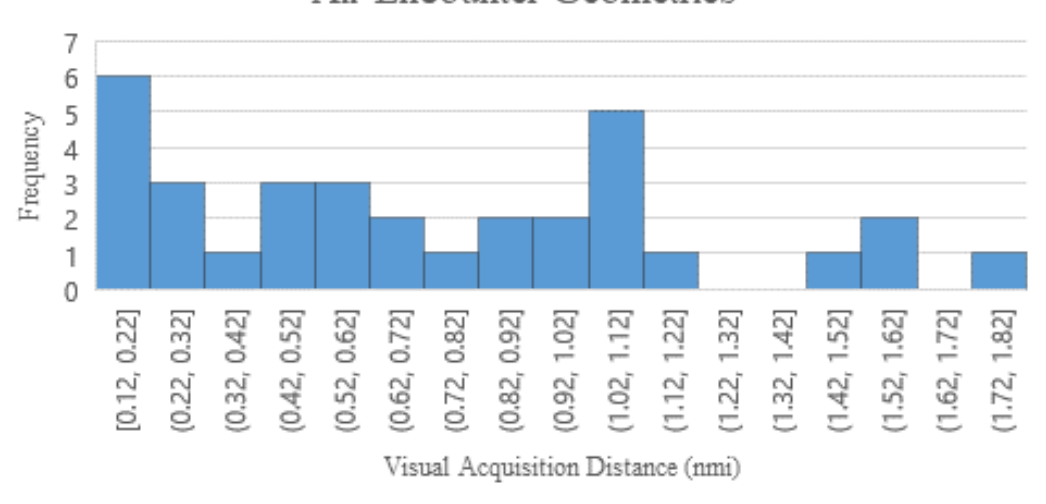


Figure 46. Detection distances of the rotorcraft intruder in all encounter geometries.

Out of the 33 positive visual acquisitions, nine occurred within the WCV, however, none were within the NMAC volume. Five were in overtake encounters and the remaining four being an even split of head-on and left crossing geometries. The following figures contain the visual acquisition distances for each encounter geometry type.

### Visual Acquisition Distance of Rotorcraft Intruder Head-On Encounter Geometry 4 3.5 3 2.5 Frequency 2 1.5 1 0.5 0 [0.12, 0.38] (0.38, 0.63] (0.63, 0.89]Visual Acquisition Distance (nmi)

Figure 47. Detection distances of the rotorcraft intruder in head-on encounter geometries.



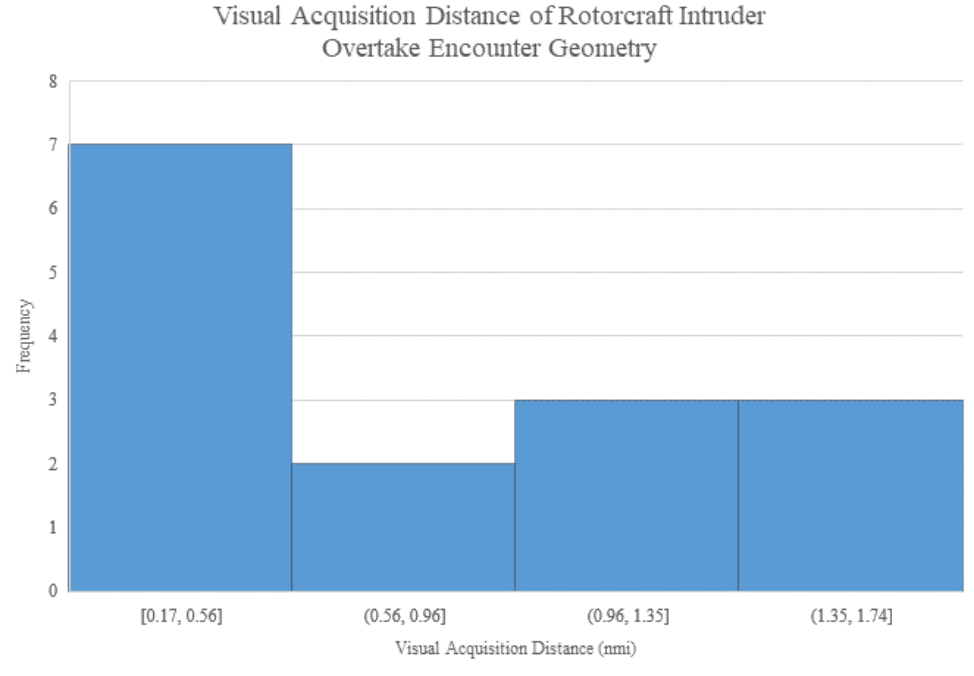


Figure 48. Detection distances of the rotorcraft intruder in overtake encounter geometries.

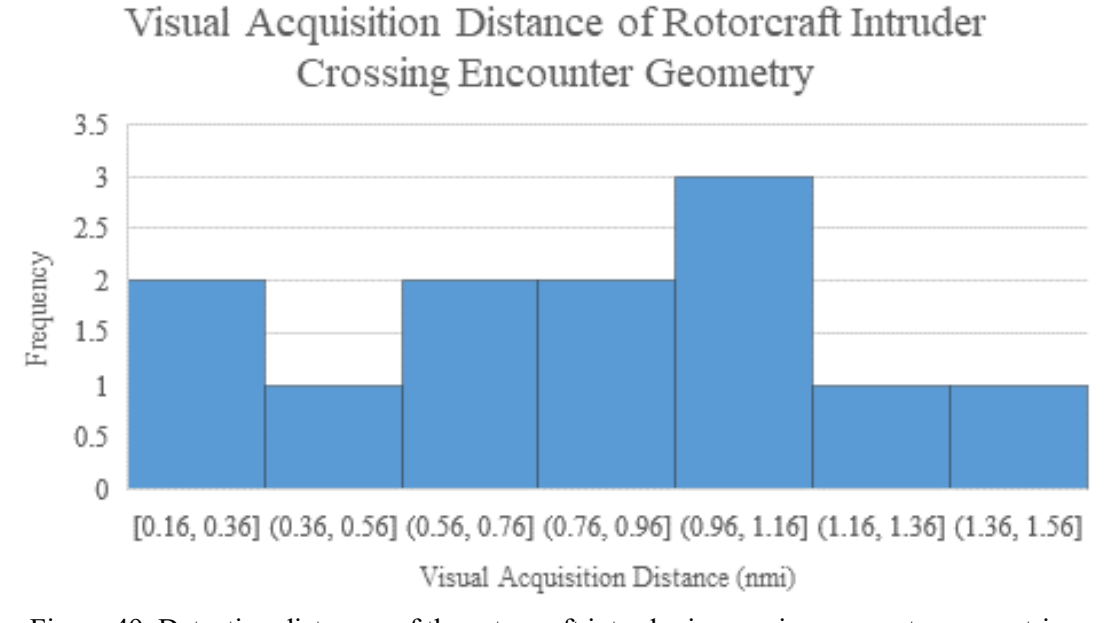


Figure 49. Detection distances of the rotorcraft intruder in crossing encounter geometries.

The probability of detection for the rotorcraft intruder is given in Figure 50, where it can be seen that the probability of detection and detection distances themselves are much lower when compared to the fixed wing encounters.



### Probability of Detection Vs. Range (nmi)

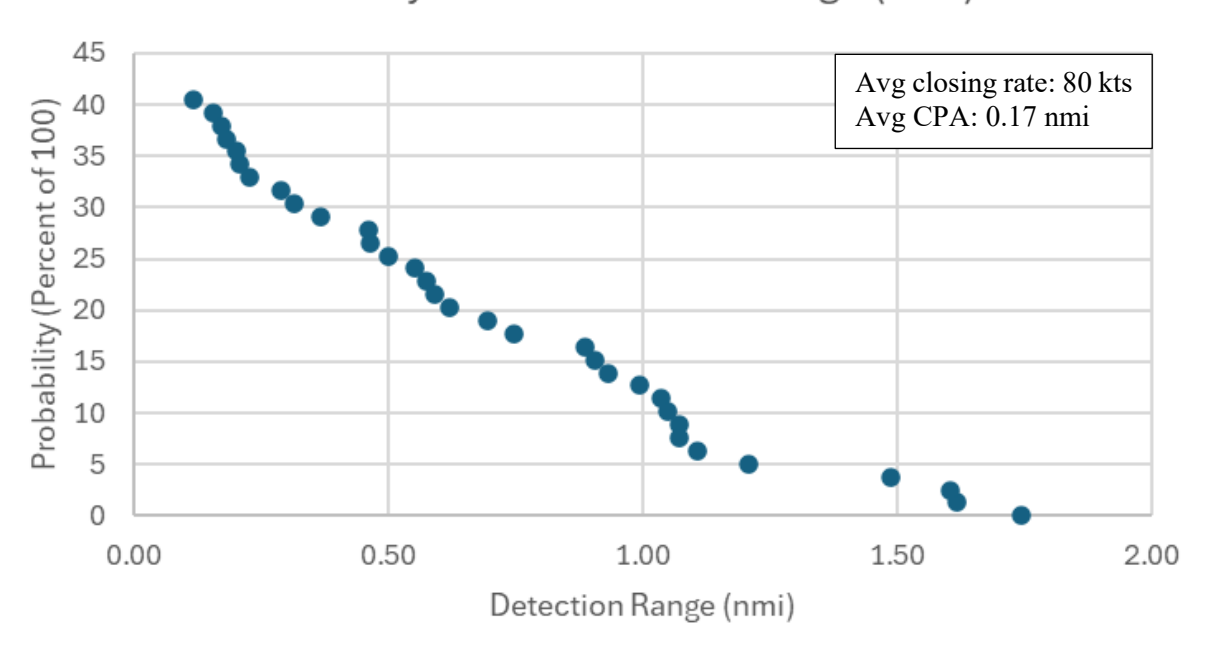


Figure 50. Probability of detection of the rotorcraft intruder aircraft all encounter geometries.

In Figure 51, the rotorcraft overtake geometry resulted in a slightly larger probability of detection than the larger rotorcraft dataset with a 45.5% probability of detection under 0.2 nmi. This is reasonable due to the significantly lower closing rates of overtakes when compared to the other geometries.

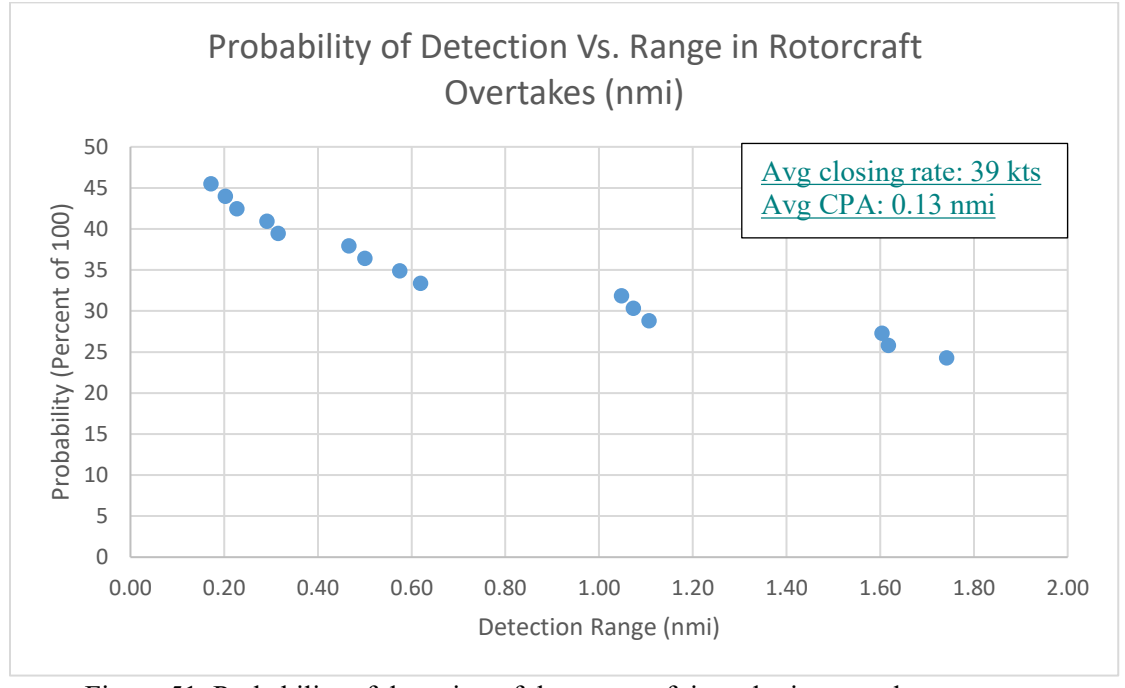


Figure 51. Probability of detection of the rotorcraft intruder in overtake geometry.



The head-on geometry posed a greater challenge for subject pilots to acquire the rotorcraft with a probability of detection around 25%. Additionally, the head on encounters have a smaller dataset than the overtake geometry, but a general trend of probability of detection versus range can be seen in the figure below.

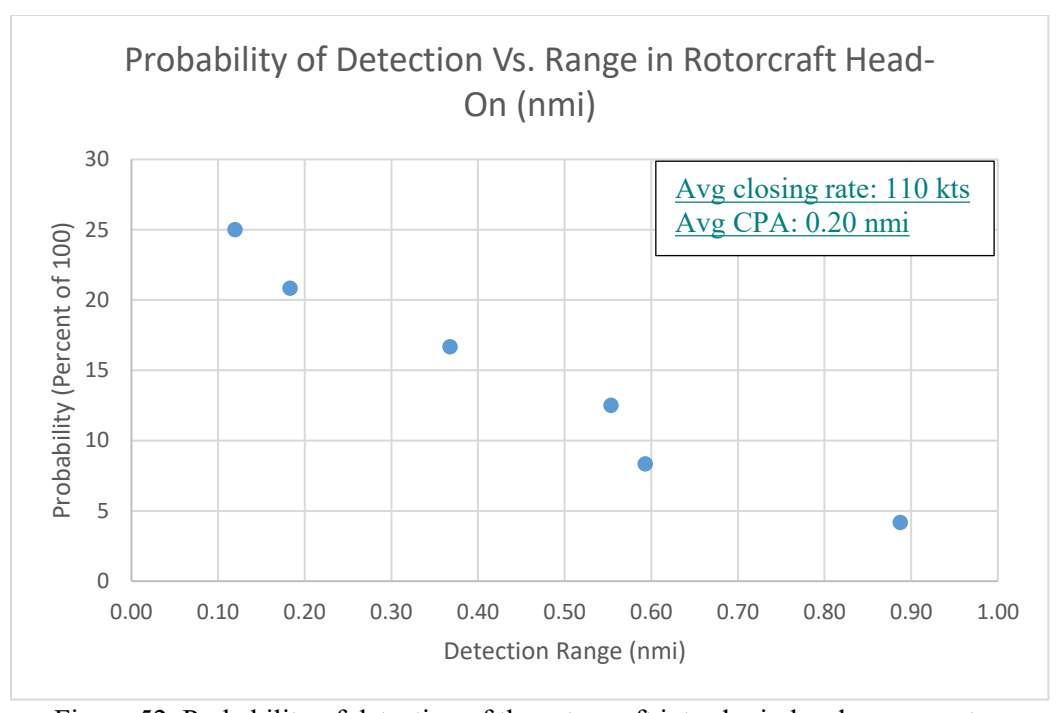


Figure 52. Probability of detection of the rotorcraft intruder in head on geometry.

The crossing encounters provided the largest probability of detection out of the rotorcraft encounter geometries tested despite have a large closing rate of 107 kts. In general, the rotorcraft was spotted further than 0.8 nmi. The side profile of the rotorcraft provided an easier target to spot, and a few pilots attributed their ability to see the rotorcraft to the sun flickering off the rotors as is traversed. As shown in Table 14, pilots were more likely to acquire the rotorcraft if it was crossing from left to right as opposed to right to left. This is most likely due to the subject pilot sitting in the left seat if the aircraft and having more visibility on the left side of the aircraft, if the subject pilot scans to the right side of the aircraft the nose and instrument panel block most of the pilot's vision. The eye tracking data from the previous section also agrees with this conclusion.



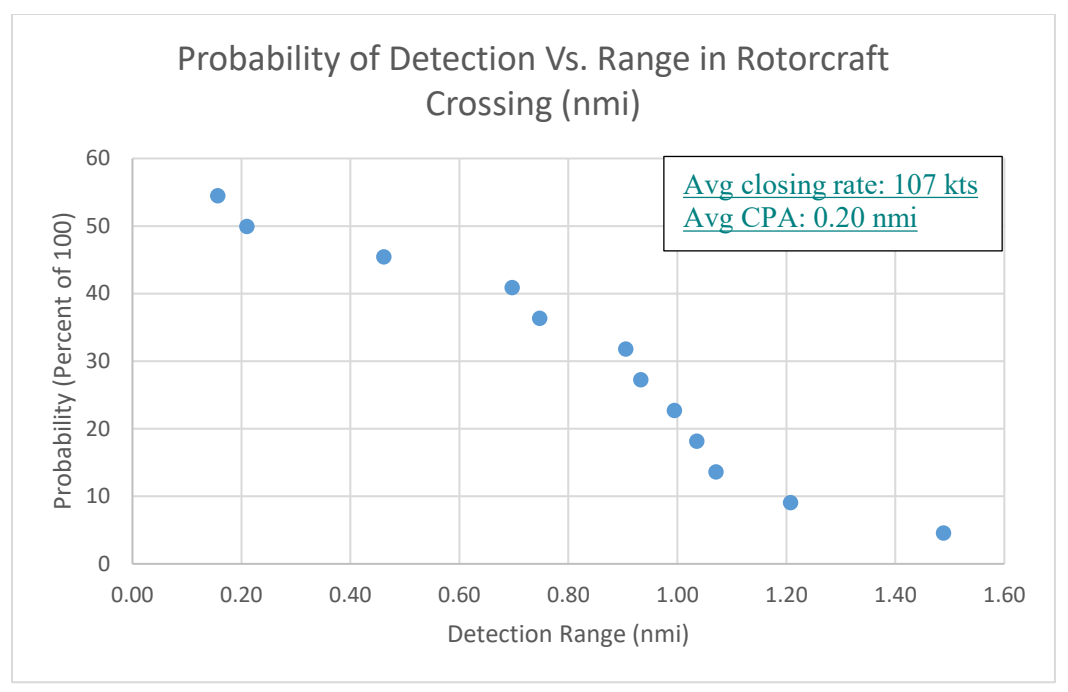


Figure 53. Probability of detection of the rotorcraft intruder in crossing geometry.

The CPA distances for all rotorcraft encounters are given in Figure 54. The lowest CPA was zero, a result of an overtake encounter where the ownship passed directly overhead with no lateral separation, and the largest 0.94 nmi (5712 ft). Nearly half of the encounters had a CPA that would be considered an NMAC and 69 resulted in WCV violations.

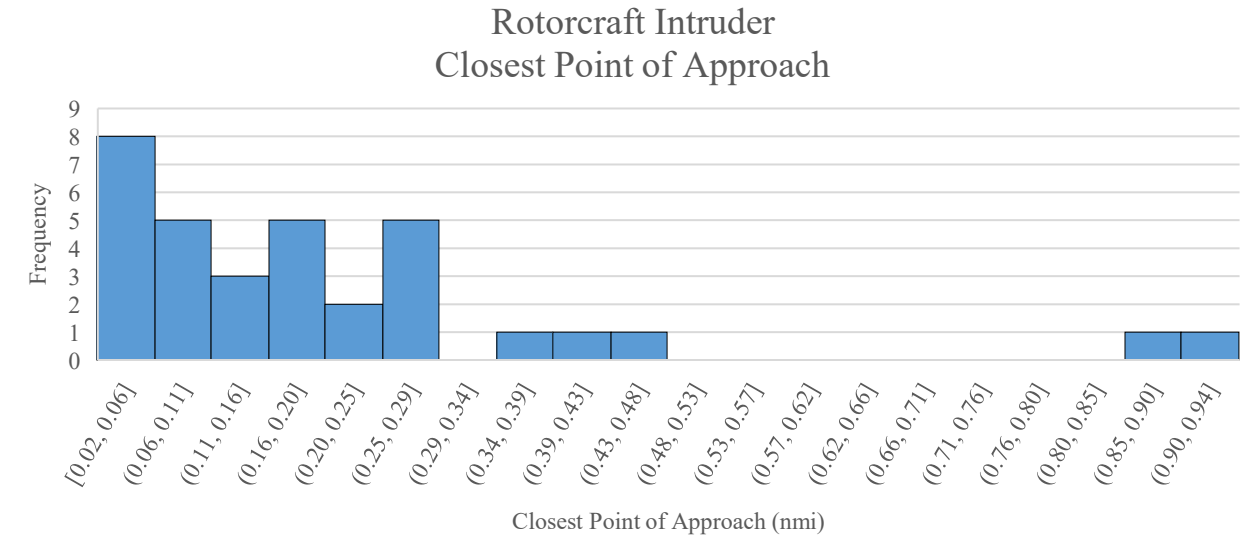


Figure 54. Closest point of approach between the ownship and rotorcraft intruder.

Figure 55 displays the CPA for encounters with detections and those without detections. Out of the 46 missed detections, 41 of them occurred in encounters with a loss of well clear and 28 in an NMAC.



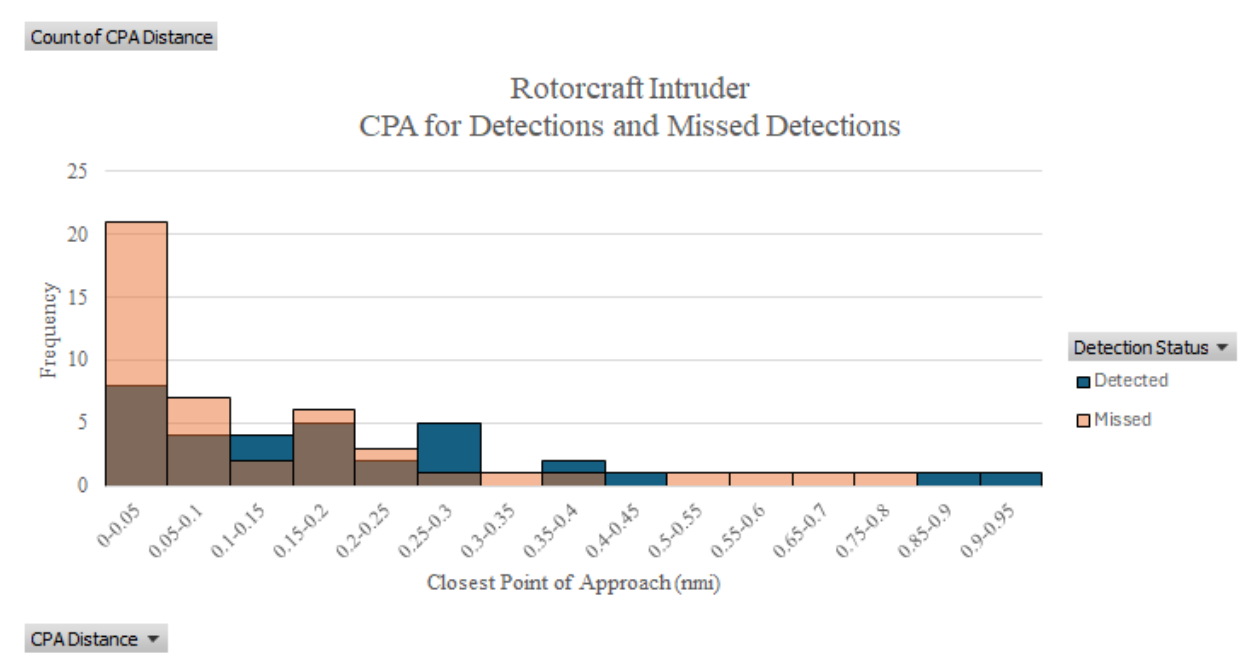


Figure 55. Closest point of approach between the ownship and rotorcraft intruder separated by detection status.

There was a wide range of closing rates exhibited across the three encounter geometries with three distinct speed ranges being present. In Figure 56, the first bin consists entirely of overtake encounters, all having closing rates below 50 knots. The crossing encounters all had closing rates of between 50 knots and 100 knots and all head-on encounters. The final speed range between 100 knots and the highest closing rate of 168 knots were all head-on encounters.

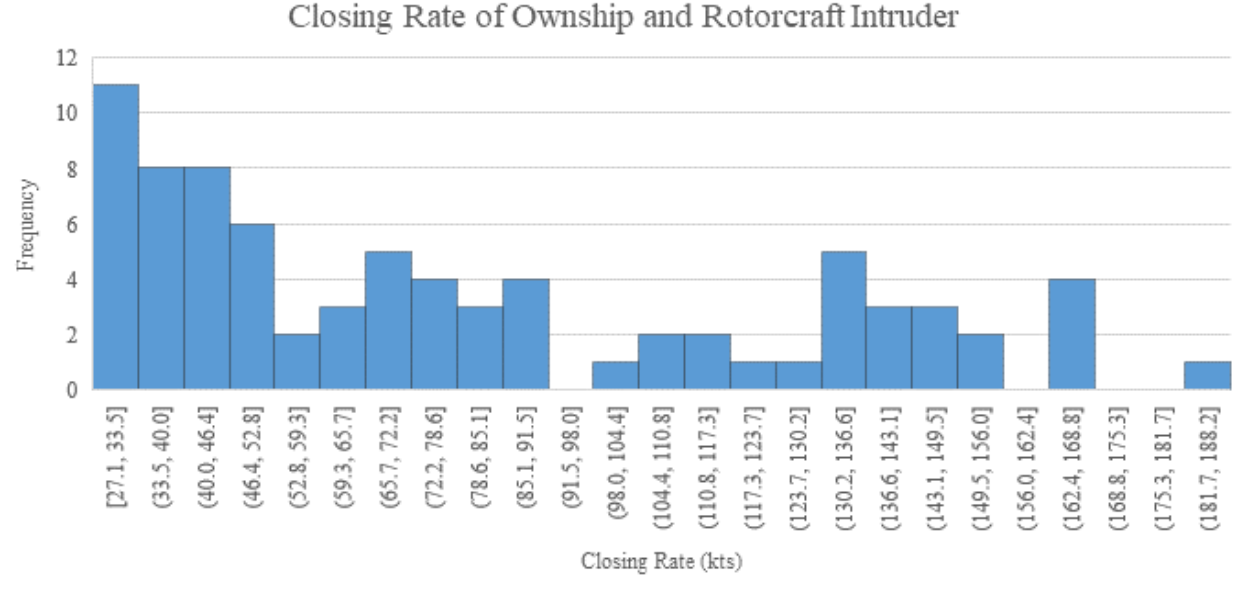


Figure 56. Closing rate between ownship and rotorcraft intruder.

The closing rate between the ownship and rotorcraft intruder sorted by detections and missed detections is shown below.





Figure 57. Closing rate between ownship and rotorcraft intruder sorted by detection status.

### **UAS** Encounters

Through the flight testing campaign of A65, the researchers captured 50 UAS encounters across 44 pilots. Unfortunately, due to various technical issues with the testing aircraft as well as timing for the encounters, many of the encounters resulted in the intruder aircraft being spotted in the loiter before the start of an overtake leg. The glare from the wings of intruder in the loiter caused the pilots to notice the intruder much further away than in the case of an ideal overtake scenario. Cases where the pilot saw the intruder UAS in a loiter were removed from the following analyses.

The overtakes between the ownship and UAS intrude occurred with the ownship flying at an altitude of 1000 ft AGL or 1500 ft AGL and the UAS flying at 500 ft AGL or 1000 ft AGL depending on the overtake flight path that was performed. Both paths were designed to generate three encounters per flight window. Out of the 50 encounters gathered during the testing, 22 resulted in the subject pilot visually acquiring the UAS intruder during the overtake meaning that only 44% of the encounters resulted in a positive visual acquisition. This is comparable to the overall A65 dataset which suggests that overall, pilots were only able to spot intruder aircraft 43% of the time. Figure 58 shows the probability of detection vs range between the ownship and the UAS intruder. The average detection distance for the UAS overtakes was approximately 2073 ft (0.34 nmi). All the visual acquisitions occurred before the NMAC volume was breached.



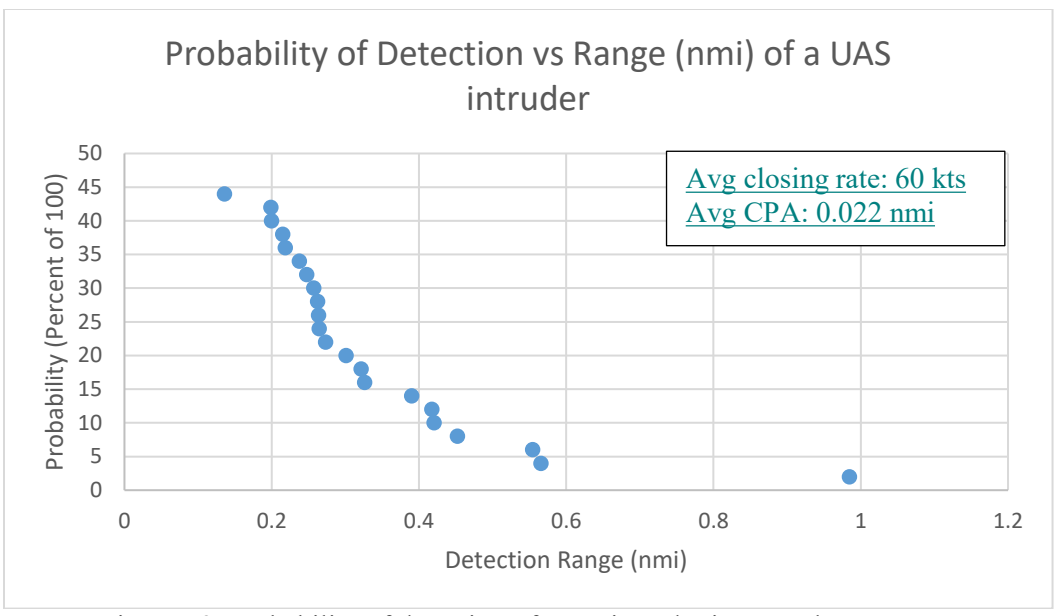


Figure 58. Probability of detection of UAS intruder in overtake geometry

Additionally, Figure 59 compares the UAS overtakes to the previously mentioned fixed wing overtakes. As shown, the smaller visual area of the UAS as well as faster closing rate greatly impacted the distance at which the subject pilot was able to see the aircraft. The UAS intruder moves much slower than a manned aircraft which means that an overtake occurs much faster than encounters where a manned aircraft overtakes another manned aircraft. UAS overtakes give the pilot less time to see the intruder before it goes out of the pilot's FOV.

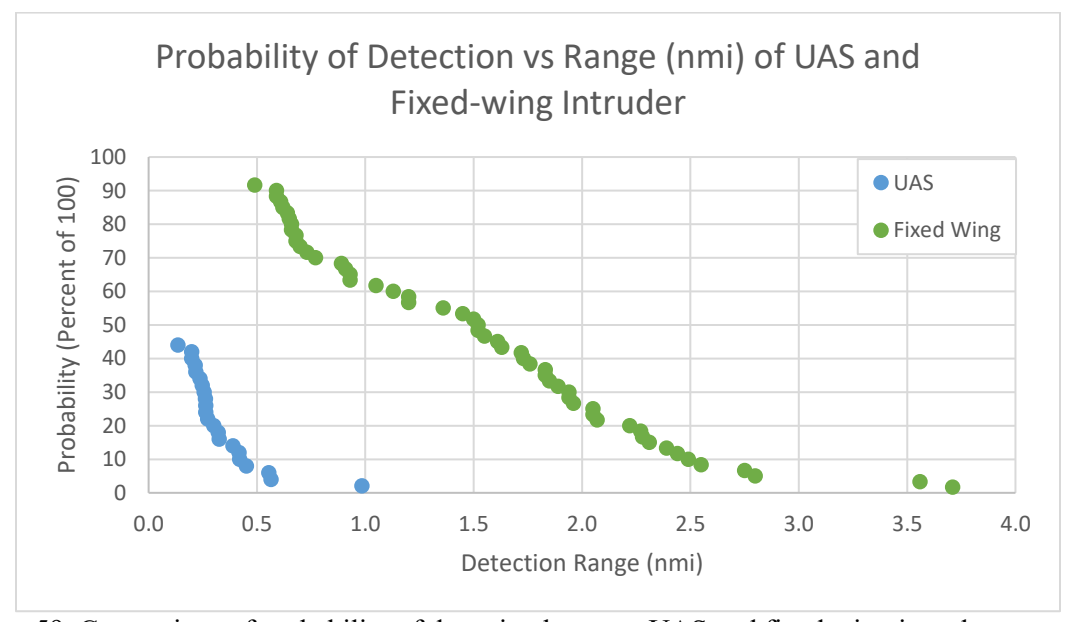


Figure 59. Comparison of probability of detection between UAS and fixed wing intruder encounters

The distribution of visual acquisition distances shown in Figure 60 shows that the majority of the visual acquisitions occurred within the WCV, but before breaching the NMAC volume. When compared to the fixed wing encounters, the visual acquisition occurred at much closer distances, this can be attributed to the scale of the UAS with a wingspan of 18 ft compared to the fixed wing intruder's 36 ft wingspan. Another



factor to consider is the closing rates between the fix wing encounters and the UAS encounters. The UAS had an average closing rate of 60 kts while the fixed wing encounters had an average closing rate of 43 kts. This means that the subject in the UAS overtake testing approached the UAS at a higher rate than in the fixed wing encounters, so there was less time to acquire the UAS before the overtake occurred.

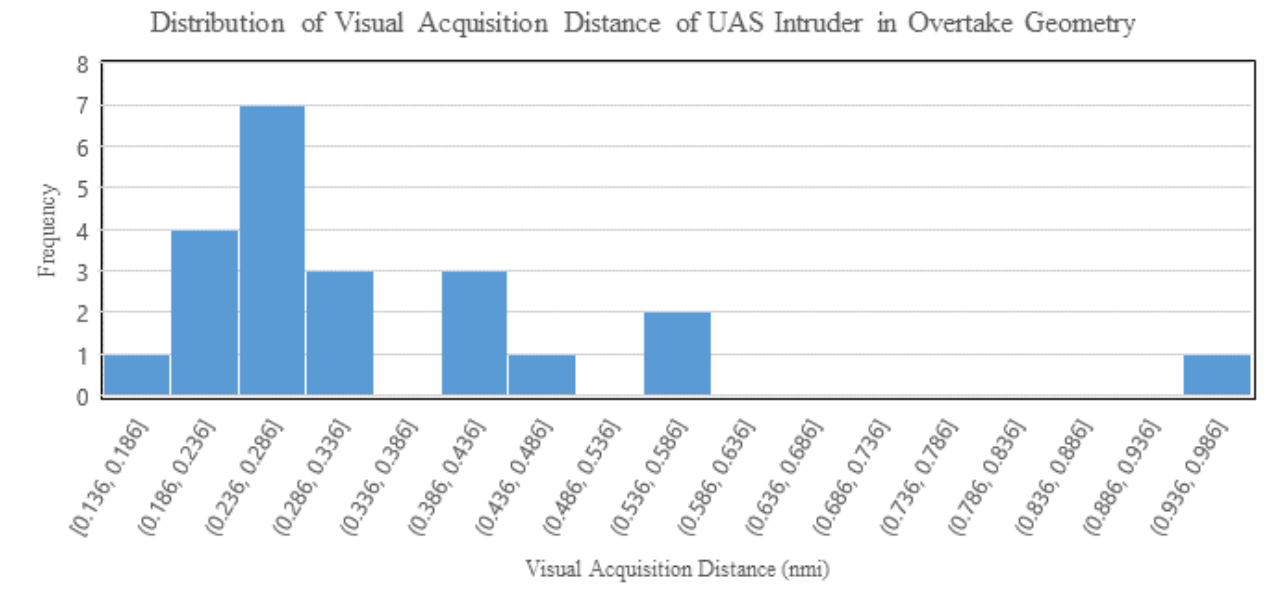


Figure 60. Detection distances of the UAS intruder during overtake encounters.

Figure 61 and Figure 62 show the breakdown of closest point of approach during the UAS overtake encounters. The first figure represents the CPA for all of the UAS encounters with the second figure providing a breakdown of CPA with respect to status of detection. The majority of the encounters resulted in CPA values less than 200 ft of horizontal separation. This is much better than the CPAs found in the fixed wing encounter set where the majority of the CPAs fell between 61 ft and 670 ft. This difference is mostly due to the fact that the UAS is following a course with GPS data feeding directly into the autopilot keeping the aircraft on its flight path while the fixed wing aircraft has to be manually flown by a human following a path given on the instrument panel or given audible headings to follow resulting in slight deviations from the true course.



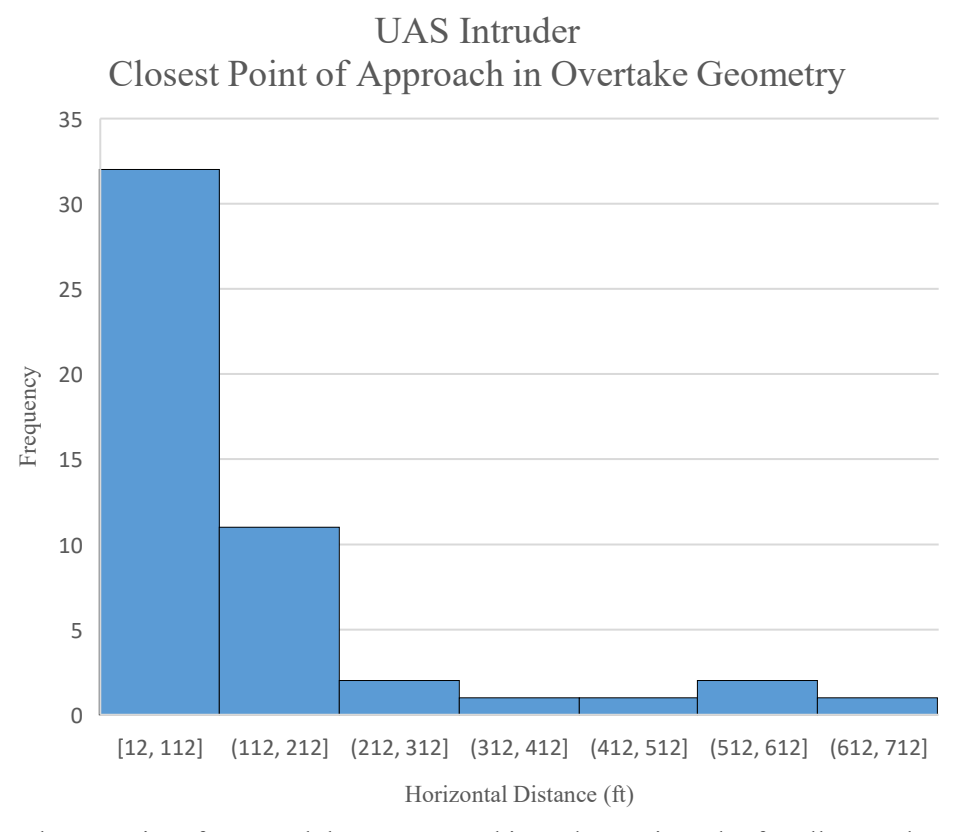


Figure 61. Closest point of approach between ownship and UAS intruder for all overtake encounters

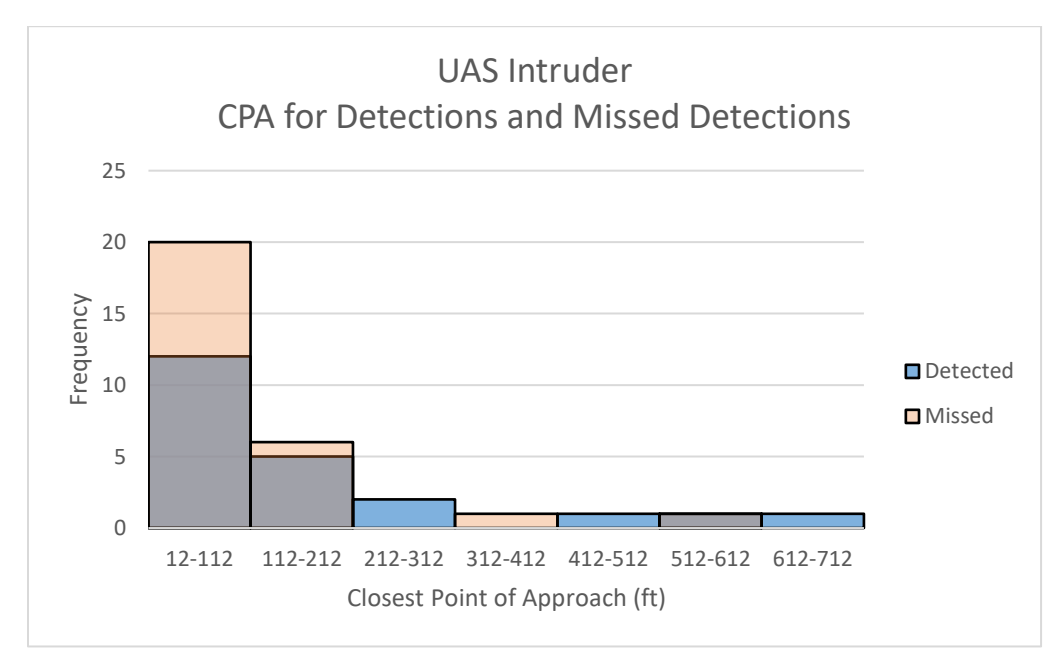


Figure 62. Closest point of approach between the ownship and UAS intruder separated by detection status.

The closing rate for the UAS encounters was generally between 44 kts and 64 kts. This is due to the limitations of test aircraft. The subject pilots were told to fly at 100 kts ground speed for the UAS tests



while the UAS is limited to a top cruise speed of 50 kts so the on average the closing rate should be 50 kts. Disregarding the two large closing rates, the average is 54 kts. The two large closure rates are due to the closing rate being calculated at the CPA, for those two encounters the CPA occurred at the end of the encounter leg when the UAS was turning back to set up the next encounter.

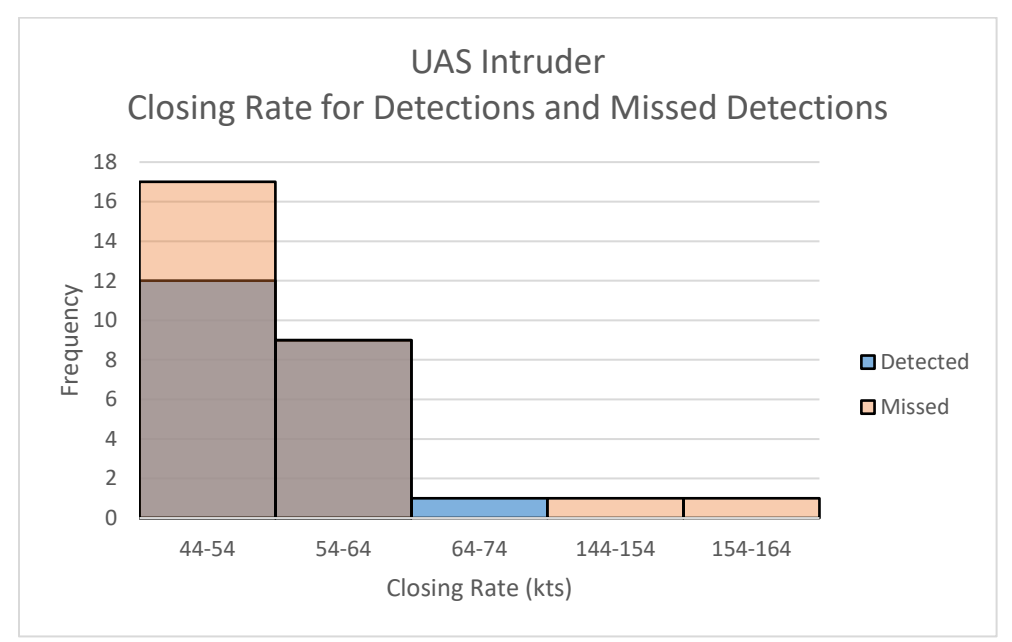


Figure 63. Closing rate between ownship and UAS intruder sorted by detection status.

### 5 Modeling and Simulation

Three encounter sets were measured for the A65 project. The value of the pilot attentiveness factor,  $\beta$ , was determined independently for all measurements, as well as by combining all the measurements with the measurements from the A23 project. The team's method for deriving  $\beta$  from the encounter tests followed the original method of (Andrews, 1991). The "instantaneous" probability of visual acquisition of a target is given by:

$$P = e^{-\lambda} \tag{1}$$

Where  $\lambda$  is the visual acquisition rate, which can be modeled as

$$\lambda = \frac{\beta A}{r^2} e^{-\frac{2.996r}{R}} \tag{2}$$

In this equation, r [nmi] is the range between the ownship and intruder,  $\beta$  [nmi2/sr] is the pilot attentiveness factor, A is the visual cross section of the intruder [nmi2], and R [nmi] is the visibility. The cross section versus angle was taken from existing models for the intruder vehicles used in this work (Cessna 172, Bell 206, and Microcub), and the value for r could be estimated from the flight data that was logged in one second intervals. All tests were conducted at high visibility; R=10 was assumed for this fitting process. Because these factors are known and controlled across all encounter sets, one can either combine datasets or fit the encounter sets individually.

To determine  $\beta$  from the flight tests, previous work (Andrews, 1991) has suggested integrating the time varying parts of Equation 2 into a single value, the "opportunity integral", Q:



$$Q = \int_0^t \frac{A}{r^2} e^{-\frac{2.996r}{R}} dt \tag{3}$$

The integration begins when the intruder enters the Field-Of-View (FOV) of the ownship and ends when the intruder either leaves the FOV or is detected by the ownship pilot. The value of Q is evaluated by integrating over the duration of the encounter. Therefore, this approach results in one datapoint each encounter, with each point having a Q value and a Boolean value indicating whether there was a detection or not. Since the integration starts and ends when the intruder enters the ownship FOV, the exact definition of the FOV will influence the results of the final analysis. In the A23 project, researchers considered several FOV definitions from previous works, as shown in Figure 64. Researchers also established a model that used weighted FOV with preference given to directions closer to the forward direction of the cockpit. The team found that this approach yielded similar results to the FOV defined in (Underhill & al., 2023). Therefore, the FOV defined in (Underhill & al., 2023) is used in this work, which places the horizontal angle from  $[-120^{\circ}, 80^{\circ}]$  and the vertical angle from  $[-15^{\circ}, 15^{\circ}]$ . Following (Andrews 1991), the FOV is restricted to ranges greater than 0.3 nautical miles.

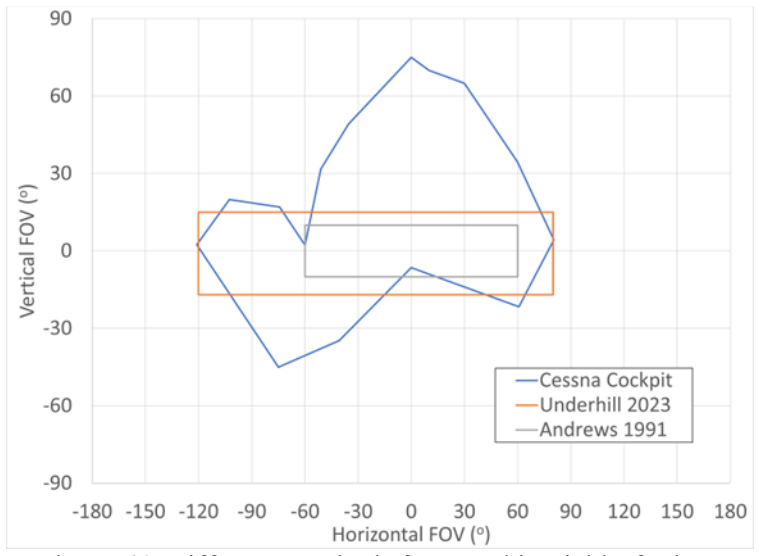


Figure 64. Different standards for ownship Field-of-View.

To estimate a probability of detection versus Q, all the data points are binned into a histogram with bins in Q and the probability being the number of points with a detection in a particular bin divided by the total number of points in that bin. With this process complete, it is only necessary to fit the equation.

$$P(d) = e^{-\beta Q} P(d) = e^{-\beta Q} \tag{4}$$

The value of  $\beta$  is the free parameter in the fit; Q is derived directly from the flight logs and aircraft geometries.

Since each encounter set had a different number of total encounters, the number of bins was different for each fit of Equation 4. The following table summarizes the fitting results for each dataset. The results from the A23 project are included for reference. The value for  $\beta$  is listed with one  $\sigma$  confidence intervals in parentheses. The research team used the field of view proposed by (Underhill 2023) and the range limits (r>0.3 Nm) proposed by (Andrews 1991).



Table 15. Beta values for each encounter set.

<b>Encounter Set</b>	Num. Enc.	Num. Det.	β	Num Bins	$\mathbb{R}^2$
A23 Crossings	298	118	4081 (1536)	10	0.759
A65 Overtakes	60	48	1831(1048)	8	0.691
A65 Rotorcraft	73	20	2592 (318)	10	0.938
A65 Microub	50	11	3410 (1700)	8	0.7051
Crosses +Rotor + Overtakes	431	186	2859(486)	15	0.8948

The data in the table above are plotted with one  $\sigma$  confidence intervals in Figure 65. From this figure it is clear that, within the measured confidence intervals, all encounter sets coincide with a value of  $\beta$ =2545-2879, indicated by the gray bar in Figure 65. Additionally, a simple average of the values in the Table 15 above, with error bars included, gives an average measured value of  $\beta$ =2859±486, indicated by the green bar in Figure 65. Therefore, the researchers recommend a value of  $\beta$ =2859±486 for encounter simulations. We note that although there are significant differences between the  $\beta$  values for the different encounter datasets, we cannot say for certain if these differences are due to encounter geometry. This is primarily because the visual acquisition model (Equation 2) does not provide a way to account for other factors like visual contrast that may have influenced the results. Additionally, and perhaps most importantly, there was a completely different set of test pilots from A23 and A65. Therefore, we cannot rule out that any differences in  $\beta$  may be due to differences in the pilots' scan strategies. Combining this with the fact that the uncertainties in the  $\beta$  measurements suggest that all the flight tests agree with  $\beta$ =2859, within uncertainty, the most defensible position is to adopt this as the value derived from our measurements. Future work may be able to distinguish between overtakes and crossing geometries by designing experiments that eliminate other sources of uncertainty such as uniform pilot selection processes and identical intruder aircraft.

The  $\beta$  value for the Microcub is somewhat higher than the average from the other tests. However, 11 of 22 "detection" events were excluded from the analysis because the detection window defined in previous work (Andrews 1991) states that datapoints with range less than 0.3 nautical miles should be excluded. This is because the exponential form of the visual acquisition equation (Eq 4) may not be valid at these close ranges. In these flight tests, 11 of the 22 total detections of the Microcub occurred within this range. Therefore, this may suggest that for the smaller Microcub and other drone-sized aircraft, the limits on the visual acquisition equations may need to be adjusted in future analysis.



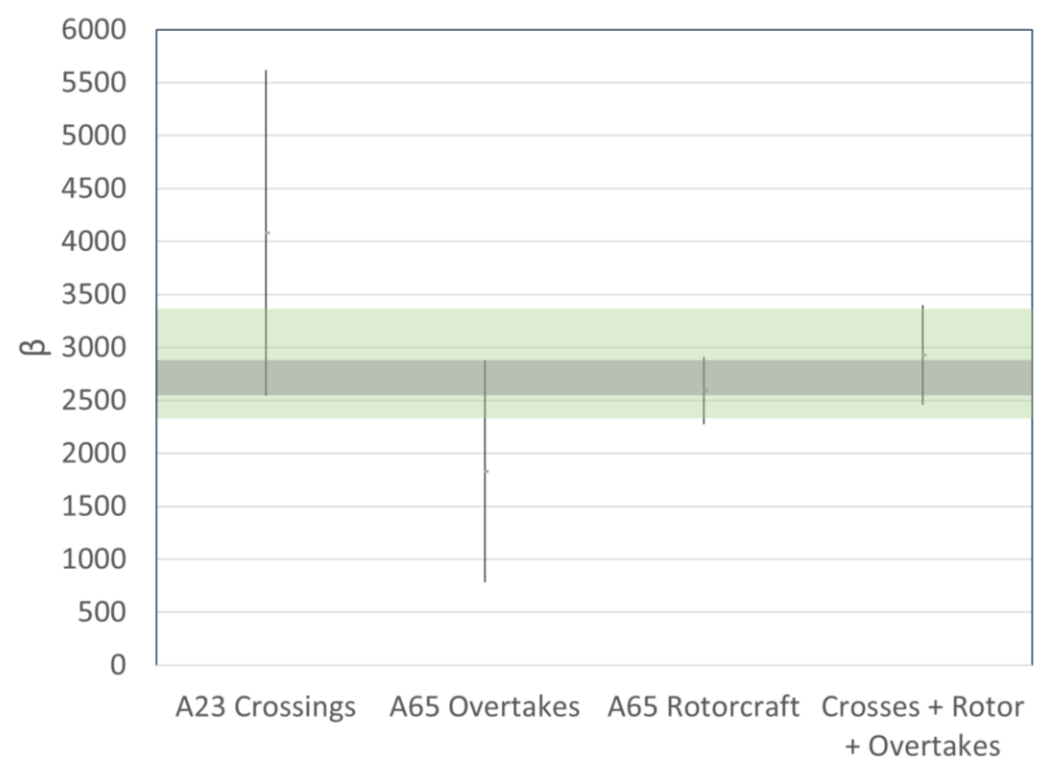


Figure 65. Comparison of results for different encounter datasets.

Figure 65-68 show the results of the fitting procedure used to estimate  $\beta$  from the encounter flight tests. Figure 65 shows the fixed-wing encounters only, while Figure 66 shows the rotorcraft and fixed wing sets. Finally, Figure 67 shows all datasets combined, including the A23 dataset. Figure 68 shows the results of fitting the Microcub experiments. The researchers recommend using the larger combined dataset (excluding the Microcub) to estimate  $\beta$  due to the improved counting statistics of the larger set. The Microcub is excluded because the researchers believe the range fitting constraints for the larger aircraft may not be comparable for the Microcub, as discussed above. Note that the quality of the fits in Figures 65 and 68 are limited by the overall size of the encounter dataset. Nevertheless, the  $R^2$  values of the fits are reasonable, as listed. The encounter data were fit to the exponential in Equation 4; therefore, there is limited flexibility to adjust the form of the fitting equation to better match the measured data.



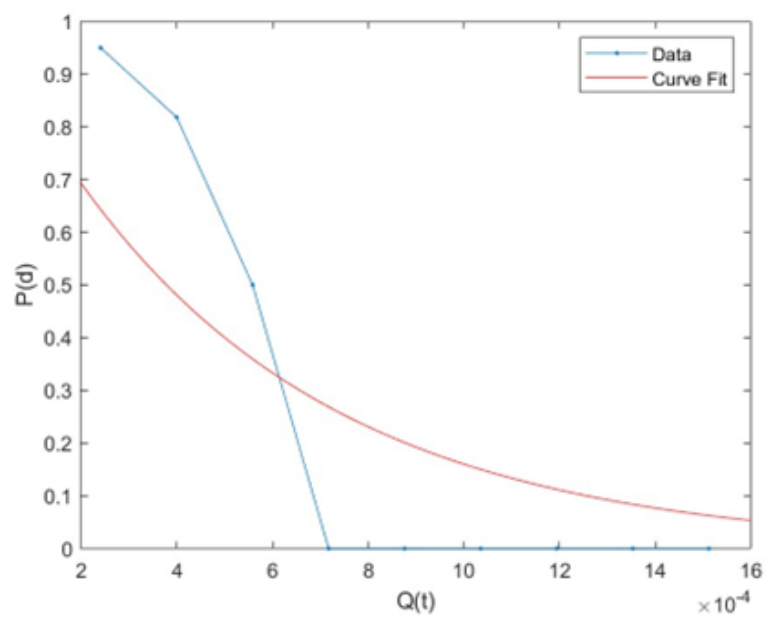


Figure 66. Fitting result for fixed wing overtake encounters.

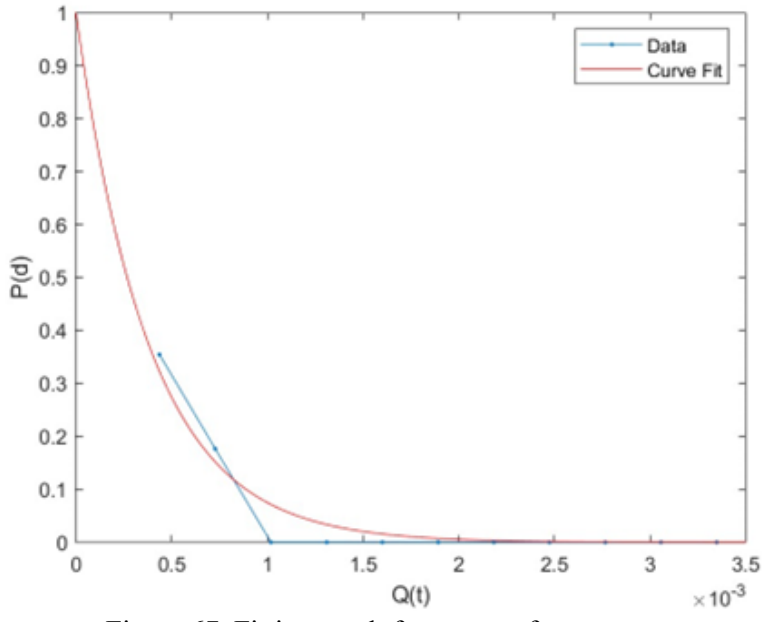


Figure 67. Fitting result for rotorcraft encounters.



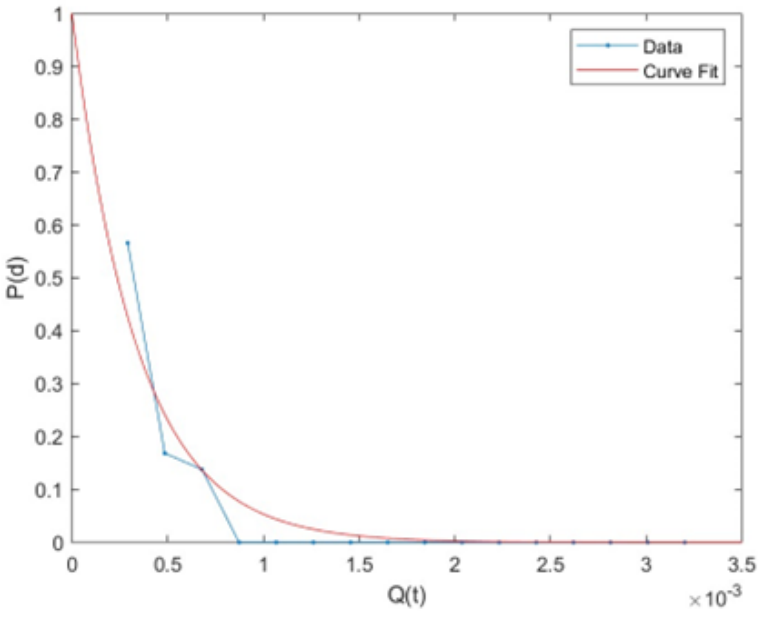


Figure 68. Fitting of combined dataset with A23 results included.

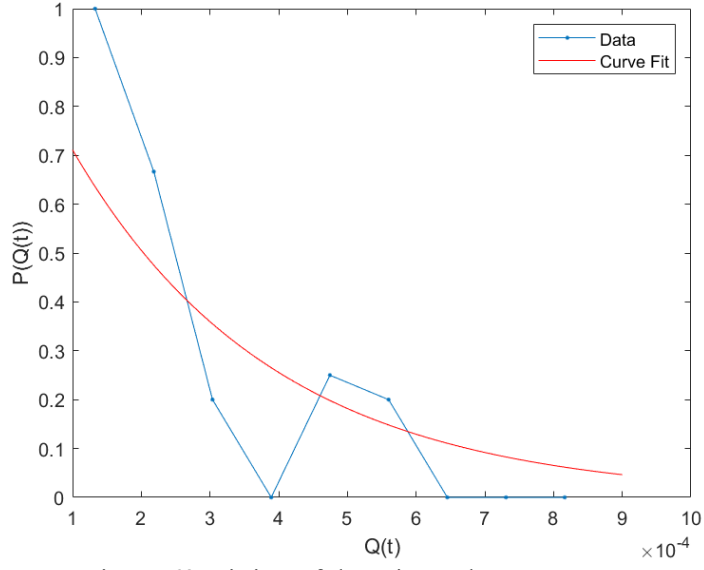


Figure 68. Fitting of the microcub encounter set.

#### **Encounter Simulations**

Encounter simulations were run for the rotorcraft vehicle using a fast-time simulator implemented in C++. The fast-time simulator uses a point mass flight kinematics model (Weitz, 2015) to simulate the motion of the ownship and intruder. Encounters geometries are created using an encounter set created by the Massachusetts Institute of Technology - Lincoln Laboratory Airspace Encounter Model (Korchenderfer, Espindle, Kuchar, & Griffith, 2008). The visual acquisition model was the same as the one described in the previous section, with the intruder cross section being the intruder represented by a Bell 206 rotorcraft calculated for each the Bell 206 and Cessna 172 using measured data in one-degree increments. The Microcub is 60% the size of the Cessna with a similar shape, so its cross section was calculated as 0.36 times the Cessna value for the same angle. The encounter simulations were repeated for a range of values of β. Additionally, the turn rates and pilot delay times (time between detection and initiating evasive



maneuver) were varied, as shown in Table 16. Three different intruders (Bell 206, Cessna 172, Microcub) were simulated, and the ownship was a Cessna 172, with the appropriate cross-section values for each aircraft being calculated in real-time when updating Equation 3 during the simulations.

At each time step, Equation 4 is evaluated for the relative geometry and range at that moment, with a time increment of 1/100 of a second. The input encounter geometry data (which are logged in seconds) are interpolated between datapoints to increase the rate of the simulation to 100 Hz. The probability of detection is compared to a random "Monte-Carlo" variable that varies [0,1], and if the probability of detection exceeds the test variable, a detection is flagged for that test, and the ownship begins an avoidance maneuver after the specified delay time. If the intruder/ownship is not detected, the vehicles follow the input encounter trajectories exactly. Once an avoidance maneuver begins, the kinematic model is used to calculate an updated trajectory. Because there is a degree of randomness to these simulations, each encounter geometry was repeated 10 times to compile statistics for calculating the risk ratios.

When the ownship detected an intruder in the simulation, a 12-second delay was implemented before a standard rate turn was executed. Additional simulations were run where the intruder was also executing see and avoid. The horizontal and vertical distances in each encounter were used to determine if there was loss of well clear or near mid-air collision for the encounter. In addition to the standard turn rate and 12 second delay, turn rates of 1.5, 2, and 3 times the standard were simulated and delay times of 3, 6, and 9 seconds. The total number of configurations was therefore 4 delays [3, 6, 9, 12] times 4 turn rates [1, 1.5, 2, 3], 2 avoidance combinations (ownship only, intruder and ownship) and 7 values of  $\beta$ , [1831, 2592, 2859, 4081, 5617, 8500, 17000].

The risk ratio was calculated using the following formula:  $RR = \frac{P(NMAC \text{ or } LoWC \mid encounter, with mitigation|)}{P(NMAC \text{ or } LoWC \mid encounter, without mitigation|)}$ 

The denominator in this equation is determined by the encounter set geometry. Two encounter datasets were used – the #25 MIT-LL with 100 encounters, and the full #25 set with 10,000 encounters. This set is the Airspace Encounter Models for uncorrelated manned (https://github.com/Airspace-Encounter-Models/em-model-manned-bayes (A. Weinert, 2019)). The model is derived from Bayesian inference of manned encounters at low altitude for a variety of conventional and unconventional aircraft, allowing a variety of different encounter sets to be derived. The encounter set used in this work contained a variety of crossing, overtake, and other encounter geometries. For the 100encounter set, there were a total of 78 LoWC and 32 NMAC, while for the 10,000-encounter set, there were 7,123 LoWC and 2,709 NMAC. This gives denominators (without mitigation) for the risk ratio equation of 0.78, 0.32, 0.7123, and 0.2709, respectively. To calculate the numerators, each encounter geometry in the set was run 10 times with mitigation (detect and avoid), and the total number of LoWC and NMAC was tracked for the encounter set.

Each different configuration was run for every encounter in the #25 MIT-LL encounter set with 1000 encounters, and each configuration and encounter were completed 10 times, for a total of  $(4 \times 4 \times 2 \times 7 \times 10,000 \times 10) = 224,000$  simulated encounters. These full results are tabulated in the appendix. In addition, Table 16 shows the results of the risk ratio for  $\beta$ =2859 run on the 10,000-encounter set. In the "both" columns, both the ownship and intruder could perform detect and avoid maneuvers. Overall, the risk ratio for loss of well-clear was about 25-27% lower in the "both" scenario, versus only the ownship avoiding. The risk ratio for the near mid-air collision was 13-15% lower for the "both" scenario, versus only the ownship. Figure 69 shows the risk ratios versus  $\beta$  for the standard rate turn and a standard 12 second delay between detection and avoidance maneuver.



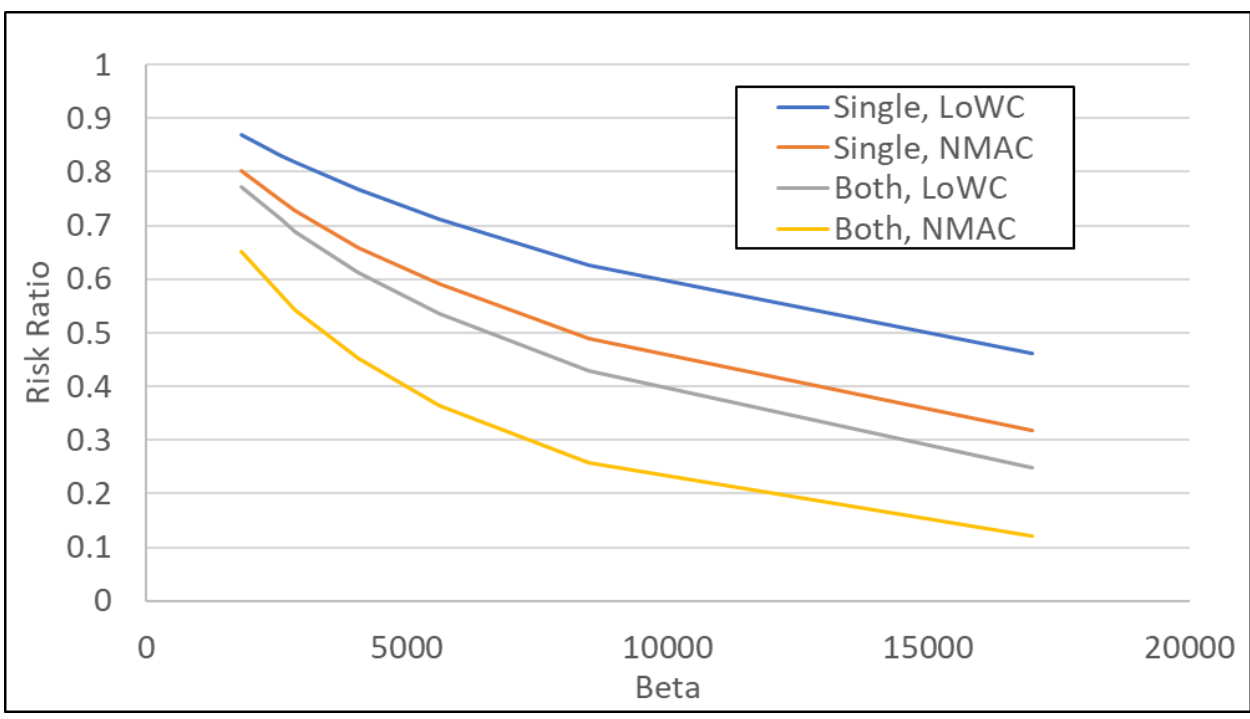


Figure 69. Risk Ratio vs  $\beta$  for one and two Cessna aircraft maneuvering after a detection in the "Standard" case (Turn Rate = standard turn, delay = 12 sec).

Risk ratios were calculated for three different intruder aircraft: a Cessna 172, a Bell 206 helicopter, and the Microcub drone. The apparent cross-sectional area of the intruder is different for each of these intruder aircraft (the "A" term in Equation 2). The ownship aircraft in the simulations was always the Cessna 172. Figure 69 shows the "standard" case for unalerted visual acquisition with two Cessna 172 aircraft using standard rate turns and 12 second delay times between detection and turning. Table 16 lists risk ratios calculated for cases where turns are more aggressive, and delays are less. Table 16 shows the results for  $\beta$ =2859; simulations were run for a variety of values of  $\beta$ , with additional data tabulated in the appendix.

Table 16. Encounter simulation results for  $\beta$ =2859.

Turn Rate(x standard)	Delay (s)	Risk Ratio, Well- Clear (Own Only)	Risk Ratio, NMAC (Own Only)	Risk Ratio, Well- Clear (Both)	Risk Ratio, NMAC (Both)
	Cessna Intru	ıder			
1	3	0.746	0.625	0.596	0.331
1	6	0.800	0.678	0.617	0.444
1	9	0.837	0.781	0.650	0.500
1	12	0.817	0.775	0.650	0.584
1.5	3	0.732	0.575	0.529	0.281
1.5	6	0.771	0.675	0.549	0.400
1.5	9	0.777	0.697	0.594	0.444
1.5	12	0.814	0.756	0.649	0.500





2	3	0.723	0.613	0.464	0.300
2	6	0.745	0.672	0.545	0.369
2	9	0.733	0.669	0.583	0.444
2	12	0.779	0.719	0.617	0.500
3	3	0.631	0.503	0.396	0.247
3	6	0.729	0.619	0.481	0.297
3	9	0.745	0.663	0.518	0.359
3	12	0.754	0.675	0.560	0.466
	Bell 206 Intr		0.070	0.000	000
1	3	0.885	0.797	0.674	0.488
1	6	0.886	0.819	0.709	0.563
1	9	0.915	0.844	0.710	0.569
1	12	0.901	0.838	0.754	0.625
1.5	3	0.855	0.778	0.621	0.413
1.5	6	0.874	0.806	0.638	0.488
1.5	9	0.888	0.856	0.708	0.531
1.5	12	0.886	0.806	0.694	0.581
2	3	0.826	0.738	0.569	0.350
2	6	0.859	0.809	0.613	0.456
2	9	0.882	0.838	0.655	0.528
2	12	0.894	0.866	0.688	0.538
3	3	0.804	0.697	0.522	0.338
3	6	0.837	0.788	0.574	0.413
3	9	0.856	0.809	0.628	0.488
3	12	0.885	0.869	0.644	0.563
	Microcub Int	ruder			
1	3	0.899	0.831	0.677	0.459
1	6	0.909	0.875	0.704	0.581
1	9	0.921	0.838	0.721	0.566
1	12	0.921	0.931	0.756	0.566
1.5	3	0.865	0.791	0.637	0.384
1.5	6	0.878	0.822	0.672	0.516
1.5	9	0.921	0.850	0.687	0.538
1.5	12	0.912	0.906	0.732	0.594
2	3	0.858	0.769	0.606	0.391
2	6	0.883	0.822	0.636	0.447
2	9	0.886	0.888	0.682	0.534
2	12	0.897	0.841	0.722	0.597
3	3	0.833	0.763	0.526	0.338
3	6	0.872	0.838	0.592	0.394
3	9	0.894	0.853	0.641	0.469



3 12 0.900 0.859 0.690 0.5
----------------------------

Simulations were conducted for only the ownship performing detect and avoid and for both the intruder and ownship performing detect and avoid. This made it possible to compare the relationship between the risk ratios for these scenarios. In general, we find that  $RR_{hoth} = a(RR_{one})^b$ .

We find that the values of a and b depend on the turn rate, delay time, and relative cross-sectional area of the aircraft. For the "standard" case, we find that a~0.98 and b~1.8, as shown in the Figure 69, if both the ownship and intruder are Cessna aircraft. This confirms the general rule of thumb that the risk ratio is squared when both aircraft perform detect and avoid. However, the value of the coefficient and exponent change when deviating from the standard turn rate and delay time. Additionally, the values change when the ownship and intruder are not the same aircraft, as may be expected. In general, "a" may have values from 0.65-1.0 and "b" may have values from 1.4-2.6, depending on the different aircraft, delay times, and turn rates used.

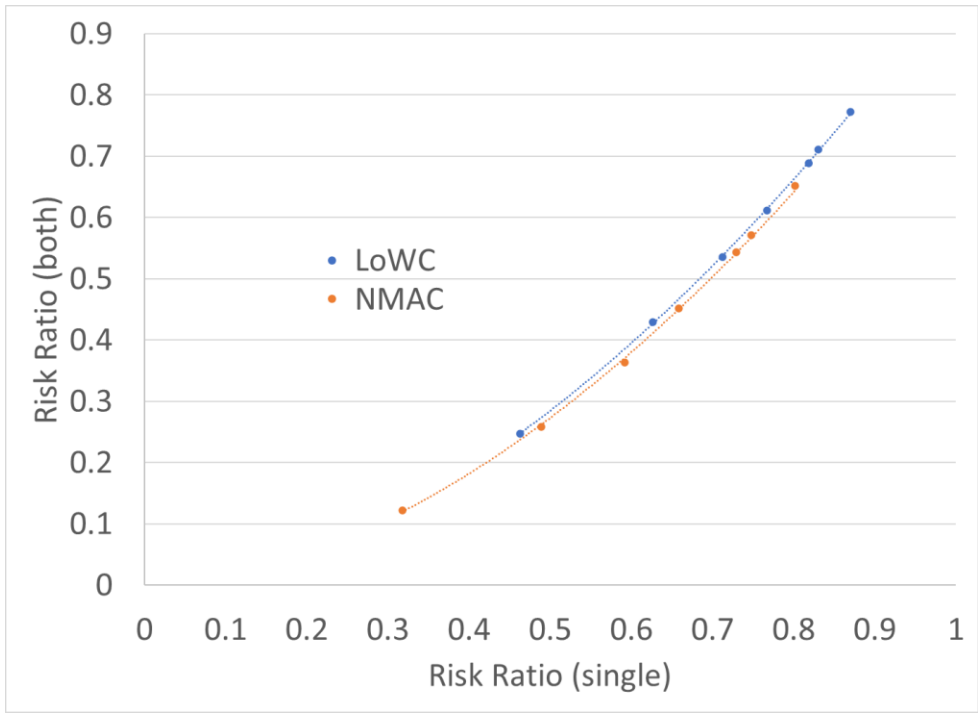


Figure 70. Risk ratio for both aircraft performing detect and avoid, versus only one aircraft, for a range of values of beta

When determining the appropriate risk ratio values to use for DAA systems it is important to consider the safety implications of using a specific set of values, the ASTM standard should err on the side of increased safety but not be so restrictive that the requirement becomes unfeasible. The research provided in this document shows that pilots are not able to see smaller aircraft as well as they are able to see full-sized crewed aircraft. A DAA system on a UAS should not increase the likelihood of LoWC or NMAC compared to encounters between two GA pilots relying on see-and-avoid techniques to avoid each other so the combined see-and-avoid effectiveness of two pilots avoiding one another serves as the baseline for evaluating the ASTM DAA performance standard. The Cessna 172 intruder is used as the example because



the flight testing showed that it was the easiest intruder to see which leads to the most conservative risk ratios erring on the side of increased safety. Consider the RR values for a Cessna 172 intruder with a  $\beta$  value of 2859, 3 times standard turn rate, and a 6 second delay for both aircraft avoiding scenario, the LoWC RR is 0.481 and the NMAC RR is 0.297. Compared to the Cessna intruder with the  $\beta$  of 4081, standard turn rate, and 6 second delay for the both aircraft avoiding scenario, the LoWC RR is 0.529 and NMAC RR is 0.309. The first scenario requires 3 times the standard turn rate which can be excessive for normal see-and-avoid behavior to remain well-clear and would only typically be used in an actual collision avoidance maneuver. The second scenario with better visual performance has a similar effect in see-and-avoid effectiveness shown by the RR values. Both of these examples can be considered conservative in different aspects, such as a larger turn rate or higher visual performance, and both scenarios support the current ASTM DAA RR values for LoWC of 0.5 and NMAC of 0.30.

## **Hardware in the Loop Simulation Development**

In an effort to develop an open-source simulation toolset as part of the Simulation and Analysis Planning, the team began the development of an Unreal Engine (UE) enabled physics-based simulation for encounter modeling. The development of this simulation was conducted using UE version 5.3, which excels in simulating ultra-realistic physics interactions. UE offers extensive utility for numerous use-cases, customization options to tailor the minute details of any simulation, and a wide array of pre-built Application Programming Interface plugins. As a physics-based simulation platform, UE can simulate precise flight dynamics via the JSBSim plugin. JSBSim is an object-oriented (C++), non-linear 6-DOF Flight Dynamics Model (FDM) that provides the capability to fully configure and edit an aircraft's flight control system.



Figure 71. Simulation development setup.

Cesium is utilized as a JavaScript library designed for the visualization of 3D geospatial data, which is integrated into the UE model as shown in Figure 56 (a). This plugin is optimized for dynamic data to be used in web browsers or through UE and has the ability to stream global 3D content from cloud sources. The geospatial data provided by Cesium is sourced from Bing Aerial maps as a comprehensive WGS84 globe, so users can derive their simulation at any location on earth via the input of specific latitude and longitude coordinates. This dataset includes various geospatial components such as terrain imagery, atmospheric effects, and detailed 3D OpenStreetMap features, forming the foundation for rapid development of location-specific simulations. For the hardware components, an aeronautical yoke and throttle quadrant were employed, as shown in Figure 56 (b), (c), and (d). The yoke is constructed from a robust steel shaft with dual linear ball bearings and 180° rotation, while the throttle quadrant includes six aviation levers, seven two-way programmable switches, and 14 warning lights. This hardware setup, combined with the JSBSim FDM and Cesium ion 3D geospatial data, was essential for validating this Hardware-in-the-Loop (HITL) simulator.



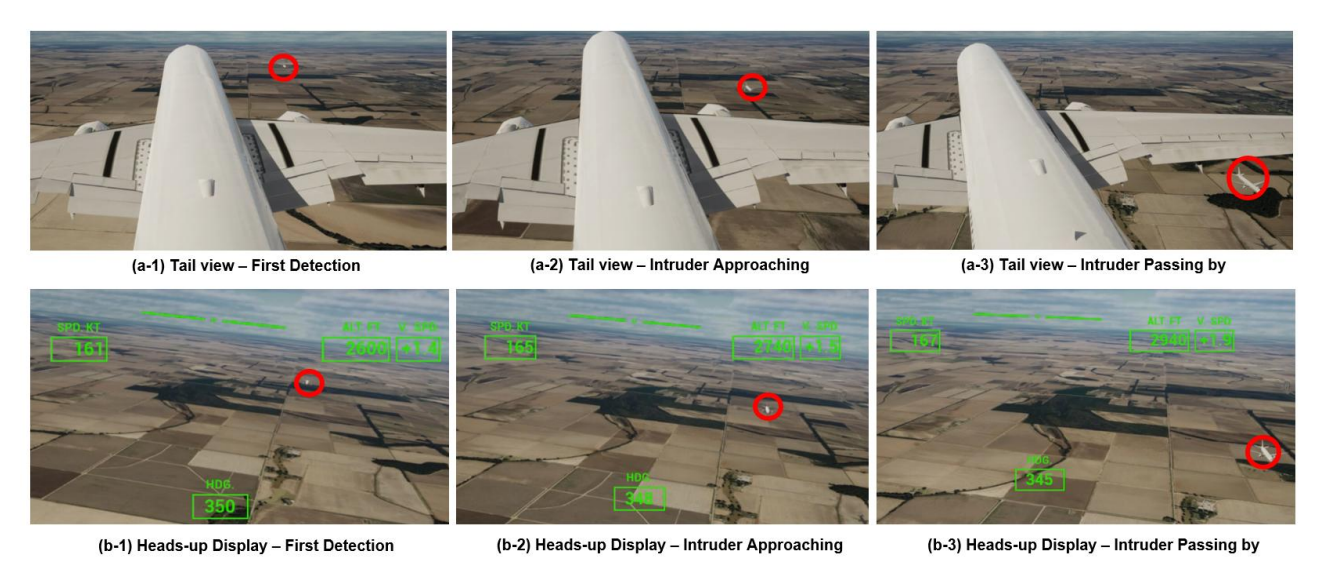


Figure 72. Simulated head-on encounter (front and tail views with HUD).

The figure illustrates how the researchers' physics-based simulator operates under UAS head-on scenarios, showcasing both tail views and Heads-Up Displays (HUD) at various stages of an encounter with an intruding aircraft. In the top row of Figure 72, images (a-1), (a-2), and (a-3) depict the tail view from the simulated aircraft during the encounter with the intruding UAS. Image(a-1) shows the initial detection of the intruding UAS in the distance, highlighted by a red circle. As the scenario progresses, image (a-2) displays the UAS visibly closer to the researchers' aircraft, with the red circle highlighting the approaching UAS and demonstrating the progressive increase in its size as it nears. Finally, image (a-3) shows the UAS passing by the researchers' aircraft, where it is much closer and more prominent, indicating it has come near and then passed alongside the researchers' aircraft.

The bottom row of Figure 72, consisting of images (b-1), (b-2), and (b-3), presents the perspective from the HUD during the same head-on encounter. Image (b-1) shows the initial detection of the intruding UAS on the HUD. The HUD provides critical flight information such as speed, altitude, and heading, with the intruding UAS circled in red, barely visible on the horizon. In the second HUD image, image (b-2), the UAS is closer and more discernible, highlighted by the red circle, illustrating the approaching UAS as it nears the researchers' aircraft, with the HUD still displaying real-time flight data. The final HUD image, image (b-3), shows the UAS passing by the researchers' aircraft, now much closer and more noticeable within the red circle, with the HUD continuing to display crucial flight metrics, indicating how the researchers' system maintains situational awareness throughout the encounter.

Figure 72 effectively demonstrates the capabilities of the physics-based simulator in handling UAS head-on scenarios. The simulator, powered by Unreal Engine UE, JSBSim plugin, and Cesium ion, is a precision tool that accurately replicates real-world flight dynamics and environments. Its ability to depict both external tail views and internal HUD perspectives allows for comprehensive situational awareness. The simulator's providing pilots with real-time information crucial for making informed decisions during such encounters is a testament to its robust functionality. This precision enhances training and preparedness for UAS encounters, instilling confidence in its capabilities.

Further development of this open-source HITL simulator is planned to be continued through other ASSURE efforts such as A81 DAA Human Factors Requirements project. Due to the open-source nature of this developer system, it can be modified to suite the needs of a variety of applications. Future developments



could give researchers a platform to create and perform flight encounters in a virtual environment and tune parameters that impact the test such as weather or aircraft conspicuity.

#### 6 Areas for Future Research

This project, while yielding a number of interesting results, has also exposed the need for more research in several areas. First, additional flight testing could be conducted with the goal of identifying the role of encounter geometry (overtake versus head-on versus crossing) on the pilot factor,  $\beta$ , in visual acquisition. Second, with the eye-tracking system, an even wider range of factors influencing pilot eye motion could be investigated, to potentially include factors like differences in pilot experience, weather factors, if the pilot has been alerted, and instrument rating. Initial results indicate that these factors do influence eye patterns. However, a focused study on eye movements is needed for definitive measurements.

In addition to further encounter testing, the fast-time simulator developed for this project can be used to support a range of future research. In particular, the eye-tracking data collected so far could be used to develop a continuous time Markov chain model (CTMC) of eye movements that could be incorporated into the fast time simulation. The CTMC-based scanning patterns are expected to estimate the pilot's expected number and duration of gaze points at specific locations in the cockpit, which may quantify the pilot's cognitive workload over time. This could be used to improve the current visual acquisition model, which assumes the pilots' focus is uniform across the viewing window. Additionally, incorporating this effort into the fast time simulations could improve the prediction of risk ratios for encounters, while supporting pilot training programs with the guidance on reducing excessive reliance on external visual cues and enhancing pilots' cognitive efficiency

Finally, the fast-time simulator could be modified to include "detect-and-avoid" by unmanned systems, using realistic sensing and perception simulations. This would improve the prediction for the "both" avoiding scenario used to calculate risk ratios when one aircraft is unmanned. In this case, rather than a visual acquisition model, we could implement a realistic sensing model for the unmanned aircraft, which is expected to be different than human visual acquisition.

## 7 Conclusion

MSU researchers successfully identified areas of needed improvement from less modern and recent efforts to establish pilot visual acquisition performance. Researchers updated and modernized the data collection approaches, as well as increased the variability of the intruder aircraft's size, type, and geometry. This included the first academic series of flight testing overtake geometries between two manned aircraft. As a result of this effort, 78 pilots were taken through the flight test procedures and survey process. The running total of pilots tested by MSU, through A23 and A65, for analysis increased to 137. Additionally, researchers explored overtake encounters with a UAS intruder and determined that the probability of visual acquisition is lower than manned fixed wing overtake encounters, and the range of detection was greatly reduced due to the smaller visual footprint of the UAS that was used in this flight-testing campaign.

New techniques to correlate physiological eye movement with cognitive workload and scanning effectiveness were presented. The eye tracking datasets yielded empirical evidence for various hypotheses such as eye movement and pilot focus changing during different stages of flight, and experience playing a role in pilot scanning behavior during flight by exhibiting that a more experienced pilot will be more likely to scan their environment. A pilot with lower experience may not scan their environment as much and will have a much narrower view pattern that does not account for wider angles around the cockpit. As a result of this effort, the traditional J.W. Andrews' visual acquisition model was updated with the much larger dataset. Researchers made suggestions, based on combinations of datasets, for a possible new acceptable Beta value for pilot search effectiveness. These new models were applied to encounter sets in fast-time



simulation to generate statistical analysis of the single pilot See-and-Avoid performance as well as combined two pilot See-and-Be-Seen performance. The range in LoWC and NMAC RR values are typically higher than those found in A23, where encounters against fixed wing crewed aircraft were primarily explored. Overall, the performance of the pilots examined in this effort was lower, resulting in worse risk ratios. The analysis suggests that industry standards for DAA performance requirements are adequate based on the current performance of combined two pilot visual acquisition and avoidance. However, industry should note the applicability of the test results, as tests were designed for cruise flight at low altitudes in Class G airspace.

Last, a live encounter simulation capability has been presented and will be improved upon in the future. This capability will be open-sourced and made available to ASSURE partners as a common consortium-wide capability for future research. Other future work efforts could include the continued development of the fast time simulation to incorporate parameters from real sense and avoid technology that can yield even more insight into the potential impacts of the increasing UAS presence in the NAS.



## 8 Appendix

## **Subject Pilot Briefing Script**

Prior to each flight, the Human Factors Researcher was required to read the following briefing script to the Subject Pilot.

"Hello, my name is [state name]. I'm here to tell you about a research study that is being funded by the FAA and conducted by researchers at Mississippi State University. Ultimately, this research will be used by the FAA to create rules and policies that continue to ensure safe operations in the National Airspace System (NAS) as the presence of unmanned aircraft systems (UAS) increases. The focus is the pilot workload in the cockpit under normal flight conditions.

There will be little to no risk associated with this study, other than the normal risks associated with any flight. There will be no incentive to participate in this study, other than potentially helping you improve your overall performance as a pilot. If you choose to participate, we will not share your information with others, and there will be no penalty or loss of benefits to you should you choose not to participate or discontinue your participation.

You will be asked to fill out a short demographic questionnaire after the flight(s). During the flight, a researcher will accompany you and collect data based on observations they make regarding cockpit activity. The researcher does not intend to be any more of a distraction than any other passenger and will limit their interactions to comply with pre-flight guidance from the Pilot In Command (PIC). After the flight, you will be asked to fill out a perceived workload survey and a very brief survey about certain aspects of the flight and complete an informed consent document. If you are interested in participating or would like additional information, please contact Dr. Kari Babski-Reeves at [email address].



# Demographics and Situational Awareness Survey / Semi-Structured Interview <u>Survey & Workload Questionnaire / Semi-Structured Interview</u>

Participant Number: Date:
Personal Information:
Age:
Years of experience as a pilot:
Ratings held:
Have you participated in this research before? Yes No
Aircraft Experience:
Single-engine: hours Complex: hours
Multi-engine: hours
How much cross-country time in the last 6 months? hours
What aircraft have you had the most time in over the last 6 months (make/model?)
Have you flown ain the last 6 months? Yes No
Pilot Workload Questions:
How familiar were you with the airplane during flight?
Not at all / slightly / moderately / heavily
How heavily did you rely upon visual landmarks to navigate?
Not at all / slightly / moderately / heavily
What percentage of the flight do you think you spent scanning outside the cockpit? %
Did you search in directions other than 12 o'clock? (i.e. directly left or right)
Never / rarely / occasionally / regularly
Did you wear sunglasses? Yes/No
Was your overall flight technique normal given your experience and background level?
No / fairly / <u>Yes</u>
If no, please explain.
Prior to coming to the airfield, did you discuss this flight test with any previous subject pilot?
Yes / No
How much did unfamiliarity with the aircraft increase your workload while flying?
Not at all / Slightly / Significantly



Did the addition of the Tobii eyetracking glasses affect your performance? Not at all / Slightly / Significantly If so, please elaborate:

During the flight, did you give more less attention that you normally would to any of the following aspects of flight? Please give thoughtful and honest consideration to artificial factors such as your knowledge that you were in a test, presence of the safety pilot, it may not have been your normal aircraft, etc.:

	Somewhat	About the	Somewhat
	1ess	same	more
fuel management			
navigation			
visual search for traffic			
holding altitude			
holding course			
weather			

## Researcher Interview Questions

For each positive visual acquisition, answer the following questions:

- What were the characteristics of the aircraft that made it easy/difficult to spot?
- What were the environmental conditions that made it easy/difficult to spot?
- Was there anything else that made detecting the aircraft easy/difficult?

Repeat for each encounter.



## **A65 Encounter Data**

The visual acquisition data in the following tables has been divided by intruder type. General metrics about each encounter can be found in the tables. For Detection Distance (nmi), a value of -1.00 is a missed detection by the subject pilot for that individual encounter.

Table A 1. Fixed wing encounter metrics.

	Table A 1. Fixed wing encounter metrics.					
Encounter Number	Detection Distance (nmi)	Closing Rate (kts)	Intruder Aircraft	Intruder Alt	Encounter Type	CPA (nmi)
1	0.65	22.4	Cessna 172	Below	Overtake	0.04
2	1.61	53.1	Cessna 172	Below	Overtake	0.73
3	2.49	60.0	Cessna 172	Below	Overtake	0.48
4	2.31	49.5	Cessna 172	Below	Overtake	0.34
5	2.22	40.3	Cessna 172	Below	Overtake	0.59
6	0.49	40.4	Cessna 172	Below	Overtake	0.40
7	0.91	47.1	Cessna 172	Below	Overtake	0.70
8	0.70	49.7	Cessna 172	Below	Overtake	0.21
9	0.68	44.5	Cessna 172	Below	Overtake	0.14
10	1.85	53.8	Cessna 172	Below	Overtake	0.19
11	1.20	41.5	Cessna 172	Below	Overtake	0.08
12	1.63	37.6	Cessna 172	Below	Overtake	0.29
13	0.59	41.2	Cessna 172	Below	Overtake	0.19
14	3.71	43.5	Cessna 172	Below	Overtake	0.25
15	2.55	44.7	Cessna 172	Below	Overtake	0.05
16	0.61	49.4	Cessna 172	Below	Overtake	0.12
17	1.52	37.4	Cessna 172	Below	Overtake	0.05
18	0.93	39.8	Cessna 172	Below	Overtake	0.18
19	0.64	37.8	Cessna 172	Below	Overtake	0.01
20	1.72	34.8	Cessna 172	Below	Overtake	0.33
21	1.52	39.5	Cessna 172	Below	Overtake	0.04
22	0.66	50.3	Cessna 172	Below	Overtake	0.21
23	2.39	41.9	Cessna 172	Below	Overtake	0.46
24	1.36	42.8	Cessna 172	Below	Overtake	0.27
25	0.89	37.8	Cessna 172	Below	Overtake	0.02
26	2.05	42.3	Cessna 172	Below	Overtake	0.08
27	0.62	38.4	Cessna 172	Below	Overtake	0.08
28	1.13	41.6	Cessna 172	Below	Overtake	0.13
29	0.73	35.7	Cessna 172	Below	Overtake	0.03
30	1.94	36.0	Cessna 172	Below	Overtake	0.03
31	1.83	24.1	Cessna 172	Below	Overtake	0.83
32	1.73	55.7	Cessna 172	Below	Overtake	0.35
33	-1.00	49.7	Cessna 172	Below	Overtake	0.52
34	0.59	37.0	Cessna 172	Below	Overtake	0.10
35	0.93	46.0	Cessna 172	Below	Overtake	0.21
36	0.68	51.9	Cessna 172	Below	Overtake	0.02
37	2.28	42.2	Cessna 172	Below	Overtake	0.02





38	1.20	42.0	Cessna 172	Below	Overtake	0.08
39	-1.00	40.3	Cessna 172	Below	Overtake	0.04
40	-1.00	35.5	Cessna 172	Below	Overtake	0.10
41	-1.00	34.7	Cessna 172	Below	Overtake	0.10
42	1.89	40.3	Cessna 172	Below	Overtake	0.03
43	0.66	42.3	Cessna 172	Below	Overtake	0.02
44	2.80	47.3	Cessna 172	Below	Overtake	0.09
45	2.44	47.2	Cessna 172	Below	Overtake	0.03
46	1.96	45.0	Cessna 172	Below	Overtake	0.02
47	3.56	58.0	Cessna 172	Below	Overtake	0.51
48	1.94	46.1	Cessna 172	Below	Overtake	0.19
49	2.75	49.5	Cessna 172	Below	Overtake	0.12
50	-1.00	44.8	Cessna 172	Above	Overtake	0.22
51	2.27	47.4	Cessna 172	Above	Overtake	0.02
52	1.45	46.2	Cessna 172	Above	Overtake	0.06
53	1.50	47.3	Cessna 172	Above	Overtake	0.07
54	1.76	50.0	Cessna 172	Above	Overtake	0.18
55	1.05	44.6	Cessna 172	Below	Overtake	0.07
56	0.77	46.1	Cessna 172	Below	Overtake	0.05
57	2.05	40.6	Cessna 172	Below	Overtake	0.16
58	2.07	37.2	Cessna 172	Below	Overtake	0.36
59	1.55	43.5	Cessna 172	Below	Overtake	0.34
60	1.83	47.2	Cessna 172	Below	Overtake	0.10
	l.	1				

Table A 2. Rotorcraft encounter metrics.

Encounter Number	Detection Distance (nmi)	Closing Rate (kts)	Intruder Aircraft	Intruder Alt	Encounter Type	CPA (nmi)
1	0.59	188.2	Bell 206	Below	Head-on	0.03
2	0.93	90.9	Bell 206	Below	Right Crossing	0.39
3	0.12	136.7	Bell 206	Below	Head-on	0.05
4	-1.00	117.3	Bell 206	Below	Head-on	0.07
5	0.89	165.8	Bell 206	Below	Head-on	0.09
6	1.49	70.8	Bell 206	Below	Left Crossing	0.16
7	-1.00	155.0	Bell 206	Below	Head-on	0.36
8	1.21	101.9	Bell 206	Below	Right Crossing	0.28
9	-1.00	142.4	Bell 206	Below	Head-on	0.04
10	0.75	85.4	Bell 206	Below	Left Crossing	0.12
11	-1.00	163.4	Bell 206	Below	Head-on	0.05
12	-1.00	83.7	Bell 206	Below	Right Crossing	0.18
13	0.18	109.8	Bell 206	Below	Head-on	0.17





14							
16	14	-1.00	75.1	Bell 206	Below		0.17
16	15	-1.00	141.1	Bell 206	Below	Head-on	0.03
18	16	-1.00	91.4	Bell 206	Below	•	0.03
18	17	-1.00	134.4	Bell 206	Below	Head-on	0.12
20         -1.00         55.3         Bell 206         Below Crossing         0.67           21         -1.00         124.2         Bell 206         Below Head-on         0.22           22         0.70         66.5         Bell 206         Below Crossing         0.45           23         -1.00         131.5         Bell 206         Below Head-on         0.07           24         1.04         64.7         Bell 206         Below Head-on         0.23           25         -1.00         109.1         Bell 206         Below Head-on         0.23           26         0.16         68.9         Bell 206         Below Head-on         0.03           27         -1.00         166.1         Bell 206         Below Head-on         0.03           28         0.91         52.4         Bell 206         Below Head-on         0.13           29         0.37         119.0         Bell 206         Below Head-on         0.13           30         0.99         74.9         Bell 206         Below Head-on         0.05           32         -1.00         69.4         Bell 206         Below Head-on         0.05           32         -1.00         69.4         B	18	0.21	79.7	Bell 206	Below		0.07
20	19	-1.00	168.0	Bell 206	Below	Head-on	0.04
22         0.70         66.5         Bell 206         Below         Left Crossing Crossing Crossing         0.45           23         -1.00         131.5         Bell 206         Below         Head-on Head-on Head-on O.07           24         1.04         64.7         Bell 206         Below Crossing Crossing Crossing O.94         0.94           25         -1.00         109.1         Bell 206         Below Head-on O.23         0.23           26         0.16         68.9         Bell 206         Below Head-on O.03         0.23           27         -1.00         166.1         Bell 206         Below Head-on O.03         0.03           28         0.91         52.4         Bell 206         Below Head-on O.13         0.86           29         0.37         119.0         Bell 206         Below Head-on O.13         0.28           31         -1.00         144.9         Bell 206         Below Head-on O.05         0.28           32         -1.00         69.4         Bell 206         Below Head-on O.16         0.16           34         1.07         74.4         Bell 206         Below Head-on O.01         0.16           35         -1.00         144.3         Bell 206         Below Head-on O.01	20	-1.00	55.3	Bell 206	Below	_	0.67
22         0.70         66.5         Belt 206         Below         Crossing         0.4s           23         -1.00         131.5         Belt 206         Below         Head-on         0.07           24         1.04         64.7         Belt 206         Below         Right Crossing         0.94           25         -1.00         109.1         Belt 206         Below         Head-on         0.23           26         0.16         68.9         Belt 206         Below         Head-on         0.03           27         -1.00         166.1         Belt 206         Below         Head-on         0.03           28         0.91         52.4         Belt 206         Below         Head-on         0.03           28         0.91         52.4         Belt 206         Below         Head-on         0.13           30         0.99         74.9         Belt 206         Below         Left Crossing         0.28           31         -1.00         144.9         Belt 206         Below         Head-on         0.05           32         -1.00         69.4         Belt 206         Below         Head-on         0.16           34         1.07	21	-1.00	124.2	Bell 206	Below	Head-on	0.22
24         1.04         64.7         Bell 206         Below         Right Crossing         0.94           25         -1.00         109.1         Bell 206         Below         Head-on         0.23           26         0.16         68.9         Bell 206         Below         Left Crossing         0.11           27         -1.00         166.1         Bell 206         Below         Head-on         0.03           28         0.91         52.4         Bell 206         Below         Crossing         0.86           29         0.37         119.0         Bell 206         Below         Left Crossing         0.28           30         0.99         74.9         Bell 206         Below         Head-on         0.13           31         -1.00         144.9         Bell 206         Below         Head-on         0.05           32         -1.00         69.4         Bell 206         Below         Head-on         0.16           34         1.07         74.4         Bell 206         Below         Head-on         0.16           35         -1.00         144.3         Bell 206         Below         Head-on         0.01           36         -1.0	22	0.70	66.5	Bell 206	Below		0.45
24	23	-1.00	131.5	Bell 206	Below	Head-on	0.07
26         0.16         68.9         Bell 206         Below         Left Crossing         0.11           27         -1.00         166.1         Bell 206         Below         Head-on         0.03           28         0.91         52.4         Bell 206         Below         Right Crossing         0.86           29         0.37         119.0         Bell 206         Below         Head-on         0.13           30         0.99         74.9         Bell 206         Below         Left Crossing         0.28           31         -1.00         144.9         Bell 206         Below         Head-on         0.05           32         -1.00         69.4         Bell 206         Below         Head-on         0.16           34         1.07         74.4         Bell 206         Below         Left Crossing         0.03           35         -1.00         144.3         Bell 206         Below         Head-on         0.01           36         -1.00         68.4         Bell 206         Below         Head-on         0.02           37         -1.00         134.9         Bell 206         Below         Head-on         0.02           38 <t< td=""><td>24</td><td>1.04</td><td>64.7</td><td>Bell 206</td><td>Below</td><td>-</td><td>0.94</td></t<>	24	1.04	64.7	Bell 206	Below	-	0.94
26	25	-1.00	109.1	Bell 206	Below	Head-on	0.23
28         0.91         52.4         Bell 206         Below Crossing         0.86           29         0.37         119.0         Bell 206         Below         Head-on         0.13           30         0.99         74.9         Bell 206         Below         Left Crossing         0.28           31         -1.00         144.9         Bell 206         Below         Head-on         0.05           32         -1.00         69.4         Bell 206         Below         Head-on         0.16           34         1.07         74.4         Bell 206         Below         Head-on         0.16           34         1.07         74.4         Bell 206         Below         Head-on         0.01           35         -1.00         144.3         Bell 206         Below         Head-on         0.01           36         -1.00         68.4         Bell 206         Below         Head-on         0.02           37         -1.00         134.9         Bell 206         Below         Head-on         0.02           38         -1.00         81.2         Bell 206         Below         Head-on         0.16           39         -1.00         62.5	26	0.16	68.9	Bell 206	Below		0.11
28         0.91         52.4         Bett 206         Betow Crossing         0.86           29         0.37         119.0         Belt 206         Below         Head-on         0.13           30         0.99         74.9         Belt 206         Below         Left Crossing         0.28           31         -1.00         144.9         Belt 206         Below         Head-on         0.05           32         -1.00         69.4         Belt 206         Below         Right Crossing         0.22           33         0.55         144.4         Belt 206         Below         Head-on         0.16           34         1.07         74.4         Belt 206         Below         Head-on         0.01           35         -1.00         144.3         Belt 206         Below         Head-on         0.01           36         -1.00         68.4         Belt 206         Below         Head-on         0.02           37         -1.00         134.9         Belt 206         Below         Head-on         0.02           38         -1.00         81.2         Belt 206         Below         Head-on         0.11           40         -1.00         62.	27	-1.00	166.1	Bell 206	Below	Head-on	0.03
30         0.99         74.9         Bell 206         Below Crossing         Left Crossing         0.28           31         -1.00         144.9         Bell 206         Below         Head-on         0.05           32         -1.00         69.4         Bell 206         Below         Right Crossing         0.22           33         0.55         144.4         Bell 206         Below         Head-on         0.16           34         1.07         74.4         Bell 206         Below         Left Crossing         0.03           35         -1.00         144.3         Bell 206         Below         Head-on         0.01           36         -1.00         68.4         Bell 206         Below         Right Crossing         0.52           37         -1.00         134.9         Bell 206         Below         Head-on         0.02           38         -1.00         81.2         Bell 206         Below         Head-on         0.16           39         -1.00         62.5         Bell 206         Below         Head-on         0.11           40         -1.00         62.5         Bell 206         Below         Head-on         0.18           41	28	0.91	52.4	Bell 206	Below	_	0.86
30   0.99   74.9   Bell 206   Below   Crossing   0.28	29	0.37	119.0	Bell 206	Below	Head-on	0.13
32         -1.00         69.4         Bell 206         Below         Right Crossing         0.22           33         0.55         144.4         Bell 206         Below         Head-on         0.16           34         1.07         74.4         Bell 206         Below         Left Crossing         0.03           35         -1.00         144.3         Bell 206         Below         Head-on         0.01           36         -1.00         68.4         Bell 206         Below         Right Crossing         0.52           37         -1.00         134.9         Bell 206         Below         Head-on         0.02           38         -1.00         81.2         Bell 206         Below         Head-on         0.16           39         -1.00         149.7         Bell 206         Below         Head-on         0.11           40         -1.00         62.5         Bell 206         Below         Head-on         0.18           41         -1.00         134.1         Bell 206         Below         Head-on         0.05           42         -1.00         87.8         Bell 206         Below         Left Crossing         0.08	30	0.99	74.9	Bell 206	Below		0.28
32	31	-1.00	144.9	Bell 206	Below	Head-on	0.05
34         1.07         74.4         Bell 206         Below         Left Crossing         0.03           35         -1.00         144.3         Bell 206         Below         Head-on         0.01           36         -1.00         68.4         Bell 206         Below         Right Crossing         0.52           37         -1.00         134.9         Bell 206         Below         Head-on         0.02           38         -1.00         81.2         Bell 206         Below         Left Crossing         0.16           39         -1.00         149.7         Bell 206         Below         Head-on         0.11           40         -1.00         62.5         Bell 206         Below         Right Crossing         0.18           41         -1.00         134.1         Bell 206         Below         Head-on         0.05           42         -1.00         87.8         Bell 206         Below         Left Crossing         0.08	32	-1.00	69.4	Bell 206	Below	_	0.22
34	33	0.55	144.4	Bell 206	Below	Head-on	0.16
36         -1.00         68.4         Bell 206         Below         Right Crossing         0.52           37         -1.00         134.9         Bell 206         Below         Head-on         0.02           38         -1.00         81.2         Bell 206         Below         Left Crossing         0.16           39         -1.00         149.7         Bell 206         Below         Head-on         0.11           40         -1.00         62.5         Bell 206         Below         Right Crossing         0.18           41         -1.00         134.1         Bell 206         Below         Head-on         0.05           42         -1.00         87.8         Bell 206         Below         Left Crossing         0.08	34	1.07	74.4	Bell 206	Below		0.03
36	35	-1.00	144.3	Bell 206	Below	Head-on	0.01
38         -1.00         81.2         Bell 206         Below         Left Crossing         0.16           39         -1.00         149.7         Bell 206         Below         Head-on         0.11           40         -1.00         62.5         Bell 206         Below         Right Crossing         0.18           41         -1.00         134.1         Bell 206         Below         Head-on         0.05           42         -1.00         87.8         Bell 206         Below         Left Crossing         0.08	36	-1.00	68.4	Bell 206	Below	_	0.52
38         -1.00         81.2         Bell 206         Below         Crossing         0.16           39         -1.00         149.7         Bell 206         Below         Head-on         0.11           40         -1.00         62.5         Bell 206         Below         Right Crossing         0.18           41         -1.00         134.1         Bell 206         Below         Head-on         0.05           42         -1.00         87.8         Bell 206         Below         Left Crossing         0.08	37	-1.00	134.9	Bell 206	Below		0.02
40       -1.00       62.5       Bell 206       Below       Right Crossing       0.18         41       -1.00       134.1       Bell 206       Below       Head-on       0.05         42       -1.00       87.8       Bell 206       Below       Left Crossing       0.08	38	-1.00	81.2	Bell 206	Below		0.16
40 -1.00 62.5 Bell 206 Below Crossing 0.18 41 -1.00 134.1 Bell 206 Below Head-on 0.05 42 -1.00 87.8 Bell 206 Below Left Crossing 0.08	39	-1.00	149.7	Bell 206	Below	Head-on	0.11
42 -1.00 87.8 Bell 206 Below Left Crossing 0.08	40	-1.00	62.5	Bell 206	Below	_	0.18
42 -1.00 87.8 Bell 206 Below Crossing 0.08	41	-1.00	134.1	Bell 206	Below	Head-on	0.05
43 -1.00 111.4 Bell 206 Below Head-on 0.57	42	-1.00	87.8	Bell 206	Below		0.08
.5   1.00   1.00   50.07	43	-1.00	111.4	Bell 206	Below	Head-on	0.57



1		1		1		
44	-1.00	65.1	Bell 206	Below	Right Crossing	0.25
45	-1.00	132.3	Bell 206	Below	Head-on	0.04
46	0.46	78.6	Bell 206	Below	Left Crossing	0.07
47	-1.00	49.1	Bell 206	Below	Overtake	0.04
48	0.32	32.4	Bell 206	Below	Overtake	0.13
49	1.62	40.4	Bell 206	Below	Overtake	0.04
50	1.07	46.7	Bell 206	Below	Overtake	0.04
51	1.74	49.9	Bell 206	Below	Overtake	0.02
52	1.11	47.1	Bell 206	Below	Overtake	0.02
53	0.17	46.7	Bell 206	Below	Overtake	0.17
54	-1.00	29.9	Bell 206	Below	Overtake	0.00
55	-1.00	39.1	Bell 206	Below	Overtake	0.02
56	-1.00	31.8	Bell 206	Below	Overtake	0.78
57	-1.00	45.7	Bell 206	Below	Overtake	0.06
58	-1.00	36.8	Bell 206	Below	Overtake	0.16
59	0.62	32.5	Bell 206	Below	Overtake	0.26
60	-1.00	30.6	Bell 206	Below	Overtake	0.04
61	0.20	35.4	Bell 206	Below	Overtake	0.19
62	0.47	34.7	Bell 206	Below	Overtake	0.21
63	0.50	59.2	Bell 206	Below	Overtake	0.22
64	-1.00	43.3	Bell 206	Below	Overtake	0.01
65	-1.00	31.8	Bell 206	Below	Overtake	0.01
66	-1.00	29.3	Bell 206	Below	Overtake	0.01
67	-1.00	38.7	Bell 206	Below	Overtake	0.05
68	-1.00	39.0	Bell 206	Below	Overtake	0.03
69	0.29	27.1	Bell 206	Below	Overtake	0.27
70	0.23	40.3	Bell 206	Below	Overtake	0.04
71	-1.00	34.2	Bell 206	Below	Overtake	0.08
72	-1.00	42.4	Bell 206	Below	Overtake	0.15
73	1.05	45.8	Bell 206	Below	Overtake	0.08
74	1.60	39.0	Bell 206	Below	Overtake	0.37
75	0.58	40.7	Bell 206	Below	Overtake	0.29
76	-1.00	27.7	Bell 206	Below	Overtake	0.07
77	-1.00	27.8	Bell 206	Below	Overtake	0.01
78	-1.00	30.4	Bell 206	Below	Overtake	0.01
79	-1.00	44.0	Bell 206	Below	Overtake	0.31

Encounter	Visual Acquisition	Closing rate	Intruder	Intruder	Encounter	CPA (nmi)
	(nmi)	(knots)	Aircraft	Altitude	Type	
1	-1.000	63.1	60% Scale Cub	Below	Overtake	0.012





4	0.390	62.4	60% Scale	Below	Overtake	0.011
4	0.390	02.4	Cub	Detow	Overtake	0.011
12	-1.000	52.7	60% Scale	Below	Overtake	0.007
			Cub			
15	0.264	48.6	60% Scale Cub	Below	Overtake	0.018
16	0.257	49.6	60% Scale	Below	Overtake	0.009
			Cub			
17	-1.000	56.2	60% Scale	Below	Overtake	0.006
			Cub			
18	-1.000	52.1	60% Scale	Below	Overtake	0.004
			Cub			
19	-1.000	52.8	60% Scale	Below	Overtake	0.002
			Cub			
21	-1.000	59.4	60% Scale	Below	Overtake	0.067
			Cub			
29	0.200	57.7	60% Scale	Below	Overtake	0.006
			Cub			
30	0.218	48.9	60% Scale	Below	Overtake	0.003
			Cub			
36	0.418	61.2	60% Scale	Below	Overtake	0.027
			Cub			
38	0.420	65.2	60% Scale	Below	Overtake	0.112
			Cub			
42	0.326	52.7	60% Scale	Below	Overtake	0.022
			Cub			
47	0.215	47.2	60% Scale	Below	Overtake	0.013
			Cub			
51	-1.000	59.0	60% Scale	Below	Overtake	0.007
			Cub			
52	-1.000	45.5	60% Scale	Below	Overtake	0.012
	1.000	45.0	Cub	D 1		0.000
53	-1.000	45.0	60% Scale	Below	Overtake	0.032
F0	1.000	FO 1	Cub	Dalavi	Overstele	0.000
59	-1.000	53.1	60% Scale	Below	Overtake	0.088
C 4	0.000	F0.2	Cub	Dolous	Overtales	0.014
64	0.262	58.3	60% Scale	Below	Overtake	0.014
67	0.070	CO F	Cub	Dolous	Overtales	0.005
67	0.273	60.5	60% Scale	Below	Overtake	0.005
60	1 000	E0.0	Cub	Polow	Overtalia	0.010
68	-1.000	58.8	60% Scale	Below	Overtake	0.012
90	1 000	E2.0	Cub	Polow	Overtalia	0.005
80	-1.000	52.0	60% Scale	Below	Overtake	0.005
00	0.126	E4.0	Cub	Polow	Overtalia	0.026
88	0.136	54.9	60% Scale	Below	Overtake	0.036
			Cub			





00	0.007	F 4 7	C00/ Caala	Dalaw	Oversteles	0.000
89	0.237	54.7	60% Scale Cub	Below	Overtake	0.008
90	-1.000	52.4	60% Scale Cub	Below	Overtake	0.010
91	-1.000	56.0	60% Scale	Below	Overtake	0.015
92	-1.000	58.0	60% Scale Cub	Below	Overtake	0.010
93	0.452	53.7	60% Scale Cub	Below	Overtake	0.008
94	0.301	52.3	60% Scale Cub	Below	Overtake	0.045
96	-1.000	145.5	60% Scale Cub	Below	Overtake	0.020
104	-1.000	59.8	60% Scale Cub	Below	Overtake	0.018
106	-1.000	51.3	60% Scale Cub	Below	Overtake	0.027
107	-1.000	158.3	60% Scale Cub	Below	Overtake	0.029
108	0.985	53.9	60% Scale Cub	Below	Overtake	0.090
111	0.199	52.8	60% Scale Cub	Below	Overtake	0.008
113	-1.000	48.6	60% Scale Cub	Below	Overtake	0.017
114	-1.000	52.7	60% Scale Cub	Below	Overtake	0.004
115	-1.000	44.1	60% Scale Cub	Below	Overtake	0.009
120	-1.000	49.2	60% Scale Cub	Below	Overtake	0.008
121	-1.000	46.4	60% Scale Cub	Below	Overtake	0.013
122	-1.000	46.1	60% Scale Cub	Below	Overtake	0.006
123	0.264	55.7	60% Scale Cub	Below	Overtake	0.024
124	0.565	55.1	60% Scale Cub	Below	Overtake	0.009
125	0.248	51.0	60% Scale Cub	Below	Overtake	0.020
126	-1.000	56.0	60% Scale Cub	Below	Overtake	0.025
127	-1.000	53.4	60% Scale Cub	Below	Overtake	0.023





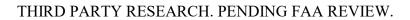
128	-1.000	52.0	60% Scale	Below	Overtake	0.008
			Cub			
130	0.321	52.0	60% Scale	Below	Overtake	0.072
			Cub			
131	0.554	47.4	60% Scale	Below	Overtake	0.025
			Cub			



## **A23** Encounter Data

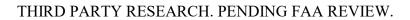
Table A 3. A23 Encounter data for each visual acquisition made by a pilot with a fixed wing intruder

Encounter Number	CPA (nmi)	<b>Encounter Type</b>	Intruder Relative Altitude	Detection Distance (nmi)	Avg. Closing Speed (kts)
1	1.59	'right crossing'	'High'	1.88	12.4
2	0.34	'head on'	'High'	0.31	153.9
3	0.82	'left crossing'	'Low'	1.05	30.5
4	0.19	'head on'	'High'	0.00	229.3
5	0.76	'right crossing'	'High'	0.00	25.8
6	0.16	'head on'	'Low'	0.00	233.4
7	0.14	'right crossing'	'Low'	0.61	235.4
8	1.59	'left crossing'	'Low'	0.00	11.7
9	0.34	'head on'	'Low'	0.00	156.5
10	0.82	'right crossing'	'High'	0.00	32.9
11	0.19	'head on'	'Low'	0.00	215.6
12	0.76	'left crossing'	'Low'	0.00	25.9
13	0.16	'head on'	'High'	0.00	238.6
14	0.14	'left crossing'	'High'	0.00	229.5
15	1.50	'left crossing'	'High'	0.00	12.7
16	0.12	'head on'	'High'	0.29	249.7
17	1.97	'right crossing'	'Low'	0.00	6.6
18	0.23	'head on'	'High'	0.53	213.1
19	1.54	'left crossing'	'High'	0.00	13.1
20	0.10	'head on'	'Low'	0.89	292.6
21	0.28	'right crossing'	'Low'	0.00	74.0
22	0.19	'head on'	'Low'	0.54	227.8
23	1.50	'right crossing'	'Low'	0.00	13.4
24	0.12	'head on'	'Low'	0.00	250.9
25	1.97	'left crossing'	'High'	0.00	7.8
26	0.23	'head on'	'Low'	0.00	200.2
27	1.54	'right crossing'	'Low'	0.00	13.5
28	0.10	'head on'	'High'	0.00	297.6
29	0.28	'left crossing'	'High'	0.00	73.8
30	0.19	'head on'	'High'	0.00	233.6
31	1.23	'left crossing'	'Low'	0.00	14.2
32	0.23	'head on'	'High'	0.00	251.1
33	0.19	'right crossing'	'High'	0.00	82.0
34	0.14	'right crossing'	'High'	0.00	308.4
35	0.48	'left crossing'	'High'	0.00	55.5
36	0.12	'head on'	'High'	0.00	308.1
37	0.45	'right crossing'	'Low'	0.00	30.2
38	0.12	'head on'	'High'	0.00	306.4
39	1.23	'right crossing'	'High'	0.00	15.2



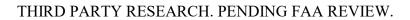


40	0.23	'head on'	'Low'	0.00	281.8
41	0.19	'left crossing'	'Low'	0.00	72.3
42	0.14	'left crossing'	'Low'	0.00	301.2
43	0.48	'right crossing'	'Low'	0.86	64.0
44	0.12	'head on'	'Low'	0.00	303.5
45	0.45	'left crossing'	'High'	0.00	30.8
46	0.12	'head on'	'Low'	0.00	290.6
47	0.09	'left crossing'	'High'	2.60	126.8
48	0.14	'head on'	'High'	0.00	240.2
49	0.77	'right crossing'	'High'	2.05	16.3
50	0.08	'head on'	'Low'	1.88	287.5
51	0.26	'left crossing'	'Low'	2.64	72.5
52	0.17	'head on'	'Low'	0.36	247.9
53	0.79	'right crossing'	'Low'	0.00	16.9
54	0.12	'head on'	'Low'	0.78	255.4
55	0.09	'right crossing'	'Low'	0.00	125.4
56	0.14	'head on'	'Low'	0.00	250.9
57	0.77	'left crossing'	'Low'	0.00	14.7
58	0.08	'head on'	'High'	0.00	281.3
59	0.26	'right crossing'	'High'	0.00	65.9
60	0.17	'head on'	'High'	0.00	247.6
61	0.79	'left crossing'	'High'	0.00	18.2
62	0.12	'head on'	'High'	0.00	263.5
63	0.25	'left crossing'	'High'	0.20	70.7
64	0.09	'head on'	'Low'	0.10	277.4
65	0.16	'right crossing'	'Low'	1.78	53.5
66	0.10	'head on'	'Low'	0.66	287.7
67	0.31	'left crossing'	'High'	0.73	44.0
68	0.09	'head on'	'Low'	1.17	295.7
69	0.39	'right crossing'	'Low'	2.07	24.6
70	0.09	'head on'	'High'	1.55	301.0
71	0.25	'right crossing'	'Low'	0.00	71.8
72	0.09	'head on'	'High'	0.00	282.0
73	0.16	'left crossing'	'High'	0.14	54.7
74	0.10	'head on'	'High'	0.00	309.3
75	0.31	'right crossing'	'Low'	0.00	47.2
76	0.09	'head on'	'High'	0.00	295.9
77	0.39	'left crossing'	'High'	1.70	28.9
78	0.09	'head on'	'Low'	0.00	281.9
79	0.45	'left crossing'	'Low'	0.00	103.3
80	0.08	'head on'	'Low'	0.76	344.8
81	0.17	'right crossing'	'High'	0.24	140.2
82	0.22	'head on'	'High'	0.00	238.5



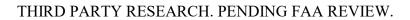


83	0.36	'left crossing'	'Low'	0.00	118.0
84	0.18	'head on'	'High'	0.42	253.9
85	0.09	'right crossing'	'High'	0.59	210.6
86	0.34	'head on'	'High'	1.10	208.8
87	0.14	'head on'	'Low'	0.47	281.0
88	0.62	'left crossing'	'High'	0.00	68.4
89	0.08	'head on'	'High'	0.12	317.8
90	1.77	'right crossing'	'Low'	0.00	24.1
91	0.20	'head on'	'Low'	0.31	232.1
92	0.36	'left crossing'	'Low'	0.61	101.9
93	0.08	'head on'	'Low'	2.18	271.3
94	0.13	'head on'	'High'	2.23	269.0
95	0.62	'right crossing'	'Low'	1.04	72.0
96	0.08	'head on'	'Low'	0.00	300.9
97	0.20	'head on'	'High'	0.00	227.6
98	0.36	'right crossing'	'High'	0.00	107.5
99	0.08	'head on'	'High'	1.51	263.5
100	0.17	'right crossing'	'High'	0.32	148.0
101	0.09	'head on'	'Low'	1.57	264.6
102	0.17	'left crossing'	'Low'	1.51	129.2
103	0.18	'head on'	'Low'	0.75	216.4
104	0.46	'right crossing'	'Low'	0.00	69.7
105	0.08	'head on'	'High'	0.85	299.8
106	0.35	'left crossing'	'Low'	0.56	109.0
107	0.10	'head on'	'High'	0.22	283.5
108	0.17	'left crossing'	'Low'	1.94	156.8
109	0.09	'head on'	'High'	0.00	278.1
110	0.17	'right crossing'	'High'	0.39	143.4
111	0.18	'head on'	'Low'	0.00	219.9
112	0.46	'left crossing'	'High'	1.26	90.7
113	0.08	'head on'	'Low'	2.13	321.8
114	0.35	'right crossing'	'High'	1.10	111.6
115	0.10	'head on'	'Low'	2.01	275.3
116	0.13	'right crossing'	'High'	1.38	179.2
117	0.09	'head on'	'High'	0.41	337.6
118	0.17	'left crossing'	'High'	0.75	151.9
119	0.19	'head on'	'Low'	0.75	254.3
120	0.47	'right crossing'	'High'	1.17	90.4
121	0.12	'head on'	'Low'	0.38	271.6
122	0.23	'left crossing'	'High'	1.64	134.6
123	0.19	'head on'	'High'	0.39	240.0
124	0.13	'left crossing'	'Low'	0.00	185.1
125	0.09	'head on'	'Low'	0.00	317.7



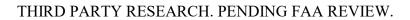


126	0.17	'right crossing'	'Low'	0.00	155.4
127	0.19	'head on'	'High'	0.00	259.1
128	0.47	'left crossing'	'Low'	0.00	117.1
129	0.12	'head on'	'Low'	0.00	298.7
130	0.23	'right crossing'	'Low'	0.00	138.6
131	0.19	'head on'	'Low'	0.18	227.0
132	0.09	'right crossing'	'High'	0.00	341.9
133	0.94	'left crossing'	'High'	0.00	45.6
134	0.22	'left crossing'	'Low'	0.00	269.9
135	0.82	'right crossing'	'Low'	0.00	55.6
136	0.08	'head on'	'Low'	0.00	323.5
137	0.66	'left crossing'	'High'	0.00	87.7
138	0.30	'head on'	'Low'	0.00	184.1
139	1.51	'left crossing'	'Low'	1.90	30.1
140	0.10	'left crossing'	'High'	0.00	345.5
141	0.94	'right crossing'	'Low'	1.78	42.3
142	0.22	'right crossing'	'High'	0.00	273.3
143	0.82	'left crossing'	'High'	1.13	53.2
144	0.08	'head on'	'High'	0.00	312.6
145	0.66	'right crossing'	'Low'	0.00	101.1
146	0.30	'head on'	'High'	0.00	194.5
147	0.15	'left crossing'	'Low'	0.56	153.3
148	0.15	'head on'	'Low'	0.64	249.0
149	0.11	'head on'	'High'	0.00	301.7
150	0.14	'left crossing'	'Low'	0.24	114.5
151	0.11	'head on'	'Low'	0.00	316.7
152	0.09	'head on'	'High'	0.43	316.7
153	0.35	'right crossing'	'High'	0.00	111.9
154	0.11	'head on'	'Low'	1.37	300.8
155	0.15	'left crossing'	'High'	1.41	140.1
156	0.10	'head on'	'Low'	0.00	284.4
157	0.25	'right crossing'	'High'	0.00	159.6
158	0.08	'head on'	'High'	1.05	290.2
159	0.50	'left crossing'	'High'	0.00	72.7
160	0.21	'head on'	'High'	0.23	206.4
161	0.31	'left crossing'	'Low'	0.21	48.6
162	0.10	'head on'	'High'	0.34	290.9
163	0.09	'head on'	'Low'	0.00	317.2
164	0.17	'left crossing'	'Low'	0.00	98.5
165	0.15	'head on'	'Low'	0.25	270.5
166	0.10	'head on'	'High'	0.00	325.7
167	0.10	'left crossing'	'Low'	0.51	162.0
168	0.11	'head on'	'High'	0.00	290.6



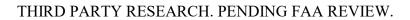


169	0.10	'head on'	'High'	0.00	336.6
170	0.67	'right crossing'	'Low'	0.00	96.2
171	0.59	'left crossing'	'High'	0.00	55.5
172	1.04	'head on'	'Low'	1.41	73.0
173	0.24	'head on'	'High'	1.01	183.5
174	0.36	'right crossing'	'Low'	0.00	136.7
175	0.23	'left crossing'	'High'	0.00	110.9
176	0.10	'head on'	'High'	0.46	315.6
177	0.12	'head on'	'Low'	0.88	286.1
178	1.15	'left crossing'	'Low'	1.48	75.5
179	0.25	'head on'	'High'	0.00	274.2
180	0.12	'head on'	'Low'	0.29	298.0
181	1.56	'left crossing'	'High'	1.61	9.9
182	0.40	'right crossing'	'Low'	0.60	113.0
183	1.07	'left crossing'	'High'	0.00	82.7
184	0.82	'right crossing'	'Low'	0.00	71.0
185	0.14	'head on'	'High'	1.12	287.9
186	1.56	'right crossing'	'Low'	0.00	10.3
187	0.40	'left crossing'	'High'	0.40	122.6
188	1.07	'right crossing'	'Low'	1.09	71.6
189	0.82	'left crossing'	'High'	1.18	76.3
190	0.14	'head on'	'Low'	0.38	301.4
191	1.56	'left crossing'	'Low'	2.28	37.4
192	0.36	'right crossing'	'High'	1.47	107.0
193	0.15	'left crossing'	'Low'	0.17	234.5
194	0.54	'right crossing'	'Low'	2.00	114.0
195	0.88	'head on'	'Low'	0.89	92.0
196	1.56	'right crossing'	'High'	0.00	27.8
197	0.36	'left crossing'	'Low'	0.00	94.5
198	0.15	'right crossing'	'High'	0.00	219.5
199	0.54	'left crossing'	'High'	1.15	113.6
200	0.88	'head on'	'High'	0.00	102.7
201	0.11	'head on'	'Low'	0.00	326.2
202	0.75	'head on'	'High'	0.81	121.2
203	1.03	'right crossing'	'Low'	2.50	22.1
204	0.69	'left crossing'	'Low'	1.27	74.2
205	0.49	'right crossing'	'Low'	2.50	145.6
206	0.52	'left crossing'	'Low'	1.01	138.4
207	0.10	'head on'	'High'	0.00	350.9
208	1.03	'left crossing'	'High'	0.00	24.0
209	0.69	'right crossing'	'High'	0.00	78.4
210	0.49	'left crossing'	'High'	0.00	147.8
211	0.52	'right crossing'	'High'	0.68	131.5





212	0.10	'head on'	'Low'	0.84	350.7
213	0.17	'right crossing'	'Low'	0.30	165.0
214	0.74	'left crossing'	'Low'	1.20	59.8
215	0.18	'right crossing'	'High'	0.21	157.8
216	0.60	'left crossing'	'Low'	1.03	111.3
217	0.17	'left crossing'	'High'	0.00	172.6
218	0.74	'right crossing'	'High'	0.96	76.0
219	0.18	'left crossing'	'Low'	0.00	157.8
220	0.60	'right crossing'	'High'	1.83	111.4
221	0.90	'right crossing'	'Low'	1.46	44.2
222	0.64	'left crossing'	'High'	0.00	62.1
223	0.55	'right crossing'	'Low'	0.95	130.0
224	0.56	'left crossing'	'Low'	1.74	79.9
225	0.44	'head on'	'Low'	0.57	183.1
226	0.90	'left crossing'	'High'	0.00	59.8
227	0.64	'right crossing'	'Low'	0.00	76.2
228	0.55	'left crossing'	'High'	0.77	133.6
229	0.56	'right crossing'	'High'	0.00	78.2
230	0.44	'head on'	'High'	0.00	187.0
231	1.46	'right crossing'	'Low'	2.03	15.7
232	0.40	'left crossing'	'High'	1.79	173.0
233	0.41	'right crossing'	'Low'	0.94	146.7
234	0.53	'left crossing'	'Low'	1.03	94.3
235	0.69	'head on'	'High'	0.00	105.0
236	1.46	'left crossing'	'High'	0.00	19.8
237	0.40	'right crossing'	'Low'	0.00	145.9
238	0.41	'left crossing'	'High'	0.00	139.1
239	0.53	'right crossing'	'High'	0.00	106.8
240	0.69	'head on'	'Low'	0.00	110.1
241	0.23	'right crossing'	'High'	2.28	117.4
242	1.07	'left crossing'	'High'	0.00	43.8
243	0.55	'right crossing'	'Low'	0.00	75.8
244	0.54	'left crossing'	'Low'	0.00	127.6
245	0.13	'head on'	'Low'	0.00	257.0
246	0.23	'left crossing'	'Low'	0.00	137.7
247	1.07	'right crossing'	'Low'	0.00	37.3
248	0.55	'left crossing'	'Low'	0.00	97.7
249	0.54	'right crossing'	'High'	0.00	118.2
250	0.13	'head on'	'High'	0.00	271.5
251	1.18	'overtake'	'Low'	1.26	2.2
252	1.46	'head on'	'Low'	0.00	109.8
253	0.37	'overtake'	'High'	0.00	15.4
254	0.23	'right crossing'	'High'	0.00	36.2





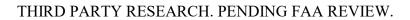
255	0.27	'overtake'	'Low'	0.00	46.1
256	0.26	'right crossing'	'Low'	0.74	12.5
257	0.34	'right crossing'	'Low'	0.00	45.9
258	0.44	'overtake'	'Low'	0.00	10.6
259	0.29	'overtake'	'Low'	0.29	19.6
260	0.25	'overtake'	'Low'	0.58	44.1
261	0.18	'overtake'	'High'	0.00	63.6
262	0.10	'overtake'	'Low'	1.52	56.9
263	0.11	'overtake'	'Low'	0.13	13.3
264	0.13	'overtake'	'Low'	0.00	27.6
265	0.16	'right crossing'	'High'	2.52	14.1
266	1.43	'right crossing'	'High'	0.00	27.3
267	0.09	'head on'	'Low'	0.00	360.2
268	0.09	'left crossing'	'High'	0.00	102.2
269	0.21	'head on'	'High'	0.20	289.7
270	0.16	'right crossing'	нідіі 'High'	0.00	194.9
271		'right crossing'			
272	0.08	'left crossing'	'High'	0.46	295.9
273	0.17	'head on'	'High'	0.68	128.3
274	0.29	'right crossing'	'Low'	0.41	230.4
	1.07	'right crossing'	'High'	2.36	20.7
275 276	0.11	'left crossing'	'High'	1.33	329.1
277	0.42	'head on'	'Low'	0.00	92.3
278	0.14	'right crossing'	'High'	0.00	294.0
	0.15	'head on'	'Low'	2.24	162.3
279	0.17		'Low'	1.63	281.3
280	0.23	'left crossing' 'head on'	'Low'	0.93	114.3
281	0.23		'High'	0.55	238.8
282	0.25	'right crossing' 'head on'	'Low'	0.95	90.7
283	0.12		'Low'	0.00	296.1
284	0.16	'left crossing'	'Low'	0.96	85.1
285	0.62	'right crossing'	'Low'	0.00	199.0
286	0.13	'right crossing'	'Low'	0.62	151.8
287	0.36	'head on'	'High'	0.00	215.0
288	0.22	'left crossing'	'Low'	0.00	106.8
289	0.26	'head on'	'Low'	0.92	290.9
290	0.08	'overtake'	'Low'	0.00	60.8
291	0.08	'left crossing'	'High'	1.57	48.8
292	0.98	'overtake'	'High'	0.00	9.7
293	0.31	'left crossing'	'High'	0.00	105.6
294	0.36	'head on'	'High'	0.00	208.2
295	0.11	'head on'	'High'	0.00	330.2
296	1.29	'left crossing'	'High'	2.29	35.0
297	0.15	'head on'	'Low'	0.63	313.5



298	0.09 'head on'	'Low'	0.65	279.9
-----	----------------	-------	------	-------

Table A 4. A23 Encounter data for each helicopter encounter that occured.

Table A 4. A23 Encounter data for each helicopter encounter that occured.  Encounter CDA (CDA (CDA) Encounter data for each helicopter encounter that occured.  Intruder Detection Distance Av.					Avg. Closing
Number	CPA (nmi)	Encounter Type	Relative Altitude	(nmi)	Rate (kts)
1	0.920	'right crossing'	'Low'	0.000	81.0
2	0.260	'head on'	'Low'	0.063	241.6
3	0.133	'left crossing'	'Low'	0.000	28.5
4	0.126	'left crossing'	'Low'	0.000	111.8
5	0.402	'right crossing'	'High'	1.024	130.0
6	0.211	'head on'	'High'	2.108	179.8
7	0.141	'left crossing'	'High'	0.348	76.0
8	0.251	'head on'	'High'	0.000	61.9
9	0.127	'right crossing'	'High'	0.000	55.2
10	0.227	'right crossing'	'Low'	0.000	195.5
11	0.144	'left crossing'	'Low'	0.000	126.2
12	0.299	'head on'	'High'	0.000	130.8
13	0.269	'right crossing'	'High'	1.440	52.3
14	0.483	'right crossing'	'Low'	1.088	188.1
15	0.151	'left crossing'	'Low'	0.243	71.5
16	0.230	'left crossing'	'High'	0.093	189.2
17	0.364	'right crossing'	'Low'	0.405	36.8
18	0.398	'right crossing'	'High'	0.148	167.8
19	0.130	'left crossing'	'Low'	0.000	49.7
20	0.055	'left crossing'	'Low'	0.555	125.8
21	0.093	'right crossing'	'High'	0.482	40.4
22	0.172	'head on'	'Low'	0.000	167.4
23	0.139	'left crossing'	'Low'	1.090	66.4
24	0.088	'left crossing'	'Low'	0.433	120.5
25	0.085	'left crossing'	'Low'	0.000	52.0
26	0.129	'head on'	'Low'	0.000	195.8
27	0.102	'right crossing'	'High'	0.000	99.8
28	0.134	'head on'	'High'	0.000	203.4
29	0.194	'left crossing'	'High'	0.000	52.8
30	1.365	'head on'	'High'	0.000	168.8
31	0.110	'right crossing'	'High'	0.000	114.2
32	1.455	'head on'	'High'	0.801	192.2
33	0.378	'left crossing'	'Low'	2.254	70.3
34	0.128	'right crossing'	'High'	0.000	211.2
35	0.104	'right crossing'	'Low'	0.000	89.4
36	0.099	'left crossing'	'High'	0.633	184.0
37	0.077	'left crossing'	'Low'	2.142	12.9
38	0.106	'right crossing'	'High'	0.293	199.0
39	0.084	'right crossing'	'Low'	0.000	28.0
40	0.194	'head on'	'High'	0.000	122.9
41	0.113	'left crossing'	'High'	1.001	73.6
42	0.920	'head on'	'High'	0.000	235.3
			-		





43	0.260	'right crossing'	'High'	0.000	100.5
44	0.133	'head on'	'Low'	1.561	231.0
45	0.126	'left crossing'	'High'	2.684	100.0
46	0.402	'head on'	'High'	2.144	218.5
47	0.211	'right crossing'	'High'	2.302	97.5
48	0.141	'head on'	'Low'	1.939	239.5



#### **Additional Hazard Identification Forms**

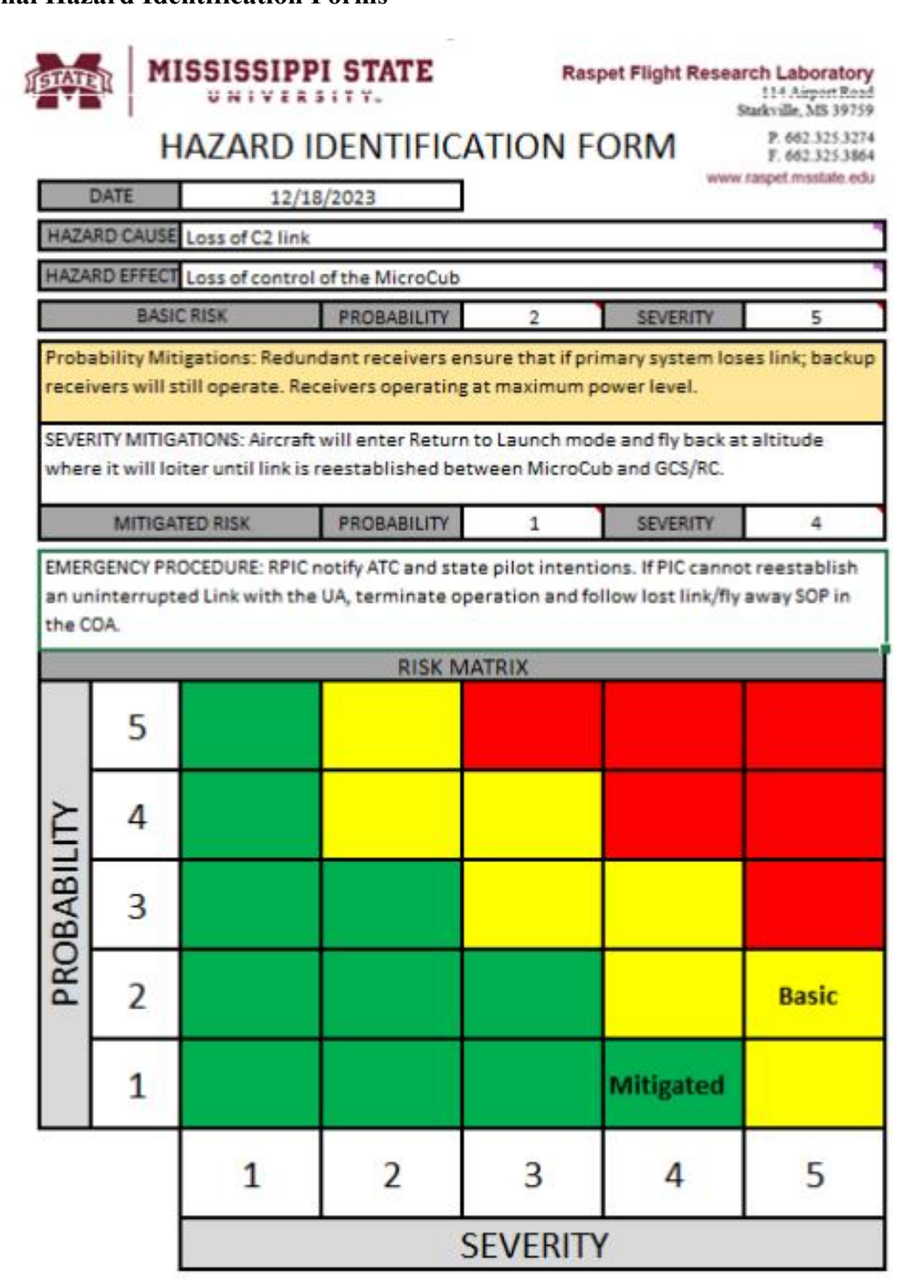


Figure A 1. Loss of C2 hazard ID.



## HAZARD IDENTIFICATION FORM

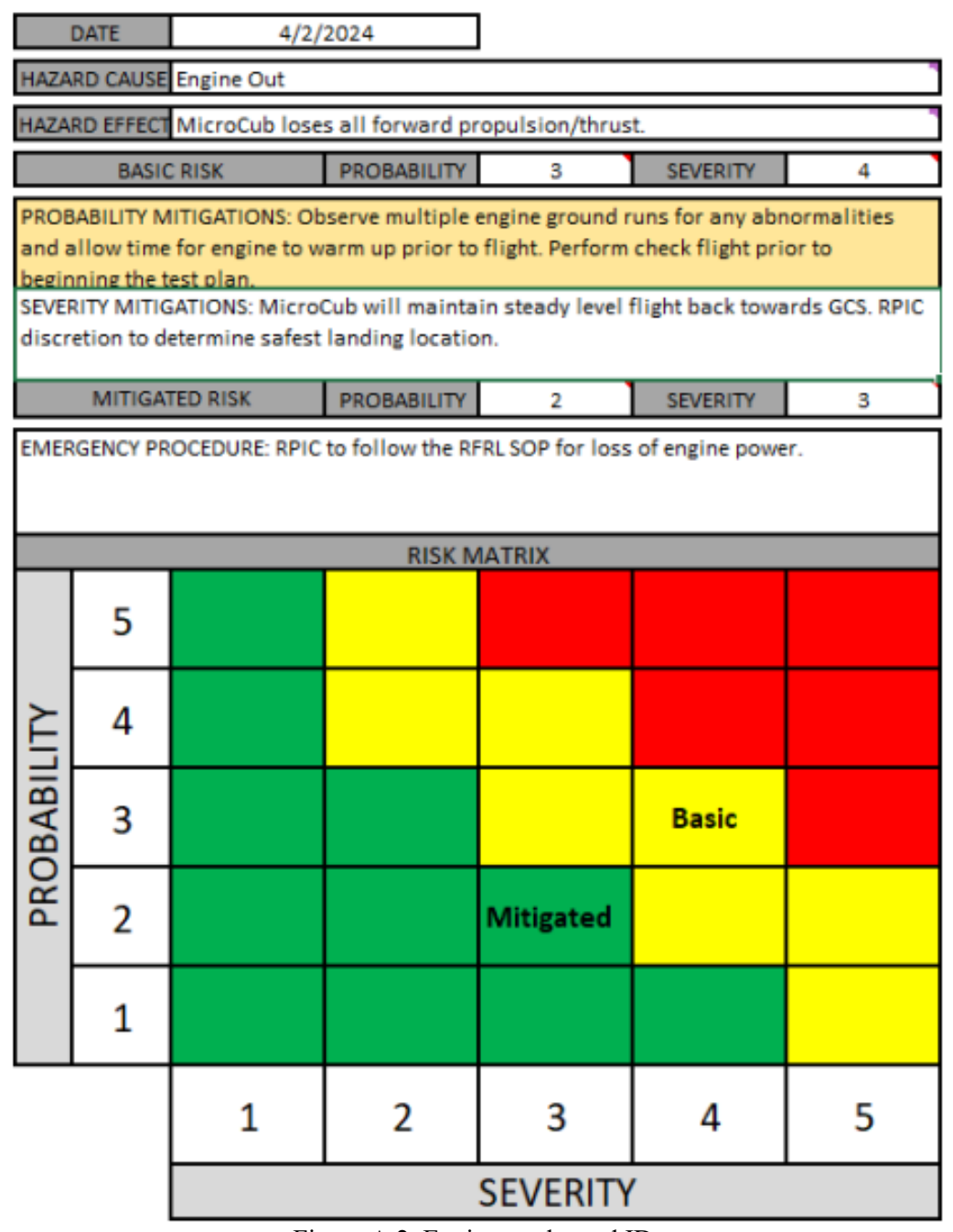


Figure A 2. Engine out hazard ID.





## Raspet Flight Research Laboratory

114 Airport Road Starkville, MS 39759

# Hazard Identification Form

P. 662.325.3274 F. 662.325.3864

	Date	4/2/	2024	www.raspet.msstate.							
Haza	ard Cause	4/2/2024  CROSSFIRE and RFD900x are on the same 902-928 MHz band (config dependent									
Haza	Hazard Effect Radio interference resulting in lost link										
	Basi	c Risk	Probability	5	Severity	2					
	Probability Mitigation:  Severity Mitigations: If interference between the radios occurs, the MicroCub will enter										
		It will return to a									
	Mitigat	ted Risk	Probability	5	Severity	1					
			Risk	Cube							
	5	Mitigated	Basic								
lity	4										
Probability	3										
Pro	2										
	1										
		1	2	3	4	5					
				Severity							

Figure A 3. Radio interference hazard ID.



## **Test Aircraft Characteristics**

Table A 5. Cessna 172P performance.

Parameter	Description	Unit
Aircraft Manufacturer	Cessna	[-]
Aircraft Type	Fixed Wing Single-Engine	[-]
Aircraft Model	172P	[-]
	N6089K	
	N99527	
Aircraft Registration Number	N52100	[-]
	N97789	
	N62098	
Propeller Type	2 Blade Propeller	[-]
Engine Model	Lycoming O-320-D2J	[-]
Engine Performance	160 hp	[-]
Maximum Takeoff Weight	2558	[lbs]
Length	27.16	[ft]
Height	8.9	[ft]
Frontal Area	40	[sq-ft]
Top Surface Area	262	[sq-ft]
Side Area	92	[sq-ft]
Wingspan	36.08	[ft]
Payload Capacity	870	[lbs]
Endurance	4.8	[hrs]
Max Speed	163	[kts]
Cruise Speed	124	[kts]
Number of seats	4	[-]
Aircraft Color	White	[-]



Figure A 4. Cessna 172P.



Table A 6. Cessna 172R performance.

Parameter	Description	Unit
Aircraft Manufacturer	Cessna	[-]
Aircraft Type	Fixed Wing Single-Engine	[-]
Aircraft Model	172R	[-]
	N3506G	
	N24748	
Aircraft Registration Number	N5312K	
	N5314R	
	N53143	
Propeller Type	2 Blade Propeller	[-]
Engine Model	Lycoming IO-360-L2A	[-]
Engine Performance	160 hp @ 2400 RPM	[-]
Maximum Takeoff Weight	2450	[lbs]
Length	27.16	[ft]
Height	8.9	[ft]
Frontal Area	40	[sq-ft]
Top Surface Area	262	[sq-ft]
Side Area	92	[sq-ft]
Wingspan	36.08	[ft]
Payload Capacity	870	[lbs]
Endurance	4.8	[hrs]
Max Speed	123	[kts]
Cruise Speed	122	[kts]
Number of seats	4	[-]
Aircraft Color	White	[-]



Figure A 5. Cessna 172R.



Table A 7. Cirrus SR20 performance.

Parameter	Description	Unit
Aircraft Manufacturer	Cirrus	[-]
Aircraft Type	Fixed Wing Single-Engine	[-]
Aircraft Model	SR20	[-]
Aircraft Registration Number	N589DS-N593DS	[-]
Propeller Type	3 Blade Propeller	[-]
Engine Model	Continental IO 360 Series	[-]
Engine Performance	215	[hp]
Maximum Takeoff Weight	3000	[lbs]
Length	26	[ft]
Height	8.92	[ft]
Wingspan	38	[ft]
Payload Capacity	1028	[lbs]
Endurance	N/A	[hrs]
Max Cruise Speed	155	[kts]
Wing Incidence Angle	-	[deg]
Number of seats	5	[-]
Aircraft Color	White / Green	[-]





Table A 8. Bell 206 performance.

Parameter	Description	Unit
Aircraft Manufacturer	Bell	[-]
Aircraft Type	Turboshaft Rotorcraft	[-]
Aircraft Model	206B	[-]
Aircraft Registration Number	N97PH	[-]
Propeller Type	Rotor – 2 blade	[-]
Engine Model	Allison 250-C20 SER Turboshaft	[-]
Engine Performance	420	[hp]
Maximum Takeoff Weight	3200	[lbs]
Length	31.2	[ft]
Height	9.5	[ft]
Wingspan	6.4	[ft]
Payload Capacity	N/A	[lbs]
Endurance	N/A	[hrs]
Max Speed	118	[kts]
Cruise Speed	105	[kts]
Wing Incidence Angle	-	[deg]
Number of seats	4	[-]
Aircraft Color	Red/White	[-]



Figure A 7. Bell 206.



Table A 9. Hempel 60% clipped wing Cub performance.

Parameter	Description	Unit
Aircraft Manufacturer	Hempel	[-]
Aircraft Type	Fixed Wing - Single Engine	[-]
Aircraft Model	60% Clipped Wing Cub	[-]
Aircraft Registration Number	N455MS	[-]
	N456MS	L J
Propeller Type	2 Blade Propeller	[-]
Engine Model	3W International SP-275	[-]
Engine Deuferman	2-Stroke	r 1
Engine Performance	21 HP	[-]
Maximum Takeoff Weight	96	[lbs]
Length	14	[ft]
Height	4.17	[ft]
Frontal Area	13.32	[sq-ft]
Top Surface Area	82.8	[sq-ft]
Side Area	26.6	[sq-ft]
Wingspan	18	[ft]
Payload Capacity	[-]	[lbs]
Endurance	1	[hrs]
Max Speed	[-]	[kts]
Cruise Speed	50	[kts]
Wing Incidence Angle	N/A	[-]
Aircraft Color	Maroon/White	[-]



Figure A 8. Hempel 60% clipped wing Cub

## **Risk Ratio Values**

Table A 10 Risk Ratio values for various parameters

Beta	Turn Rate	Delay	Single,	Single,	ous parameter <b>Both</b> ,	Both,	Aircraft
Deta	(x Standard)	Time	LoWC	NMAC	LoWC	NMAC	Туре
1831	1	3	0.929	0.888	0.769	0.584	microcub
1831	1.5	3	0.928	0.875	0.726	0.525	microcub
1831	2	3	0.899	0.850	0.703	0.481	microcub
1831	3	3	0.897	0.813	0.669	0.459	microcub
1831	1	6	0.928	0.884	0.768	0.675	microcub
1831	1.5	6	0.915	0.891	0.737	0.588	microcub
1831	2	6	0.899	0.825	0.729	0.597	microcub
1831	3	6	0.897	0.841	0.694	0.550	microcub
1831	1	9	0.954	0.919	0.800	0.666	microcub
1831	1.5	9	0.938	0.897	0.774	0.641	microcub
1831	2	9	0.918	0.891	0.764	0.622	microcub
1831	3	9	0.914	0.878	0.736	0.588	microcub
1831	1	12	0.953	0.906	0.829	0.725	microcub
1831	1.5	12	0.936	0.916	0.792	0.688	microcub
1831	2	12	0.931	0.925	0.800	0.700	microcub
1831	3	12	0.923	0.869	0.754	0.653	microcub
2592	1	3	0.900	0.819	0.681	0.497	microcub
2592	1.5	3	0.887	0.838	0.662	0.478	microcub
2592	2	3	0.862	0.753	0.631	0.384	microcub
2592	3	3	0.855	0.734	0.560	0.350	microcub
2592	1	6	0.919	0.844	0.718	0.563	microcub
2592	1.5	6	0.904	0.800	0.691	0.584	microcub
2592	2	6	0.887	0.828	0.664	0.475	microcub
2592	3	6	0.876	0.800	0.601	0.466	microcub
2592	1	9	0.937	0.906	0.737	0.638	microcub
2592	1.5	9	0.924	0.872	0.724	0.588	microcub
2592	2	9	0.899	0.863	0.695	0.553	microcub
2592	3	9	0.886	0.847	0.644	0.538	microcub
2592	1	12	0.924	0.894	0.751	0.638	microcub
2592	1.5	12	0.922	0.878	0.719	0.619	microcub
2592	2	12	0.905	0.866	0.722	0.581	microcub
2592	3	12	0.905	0.872	0.672	0.534	microcub
2859	1	3	0.899	0.831	0.677	0.459	microcub
2859	1.5	3	0.865	0.791	0.637	0.384	microcub
2859	2	3	0.858	0.769	0.606	0.391	microcub
2859	3	3	0.833	0.763	0.526	0.338	microcub
2859	1	6	0.909	0.875	0.704	0.581	microcub
2859	1.5	6	0.878	0.822	0.672	0.516	microcub



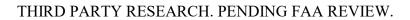


2859	2	6	0.883	0.822	0.636	0.447	microcub
2859	3	6	0.883	0.822	0.592	0.394	microcub
2859	1	9	0.872	0.838	0.392	0.566	microcub
2859	1.5	9	0.921	0.850	0.721	0.538	microcub
2859	2	9	0.886	0.888	0.682	0.534	
	3	9	0.894		0.641	0.334	microcub
2859	ļ	12	0.894	0.853		0.469	microcub
2859 2859	1 1.5	12	0.921	0.931	0.756 0.732	0.594	microcub
							microcub
2859	2	12	0.897	0.841	0.722	0.597	microcub
2859	3	12	0.900	0.859	0.690	0.547	microcub
4081	1	3	0.867	0.781	0.615	0.409	microcub
4081	1.5	3	0.826	0.713	0.533	0.344	microcub
4081	2	3	0.791	0.678	0.499	0.313	microcub
4081	3	3	0.788	0.663	0.441	0.203	microcub
4081	1	6	0.869	0.816	0.608	0.466	microcub
4081	1.5	6	0.853	0.769	0.597	0.394	microcub
4081	2	6	0.835	0.753	0.535	0.394	microcub
4081	3	6	0.837	0.719	0.479	0.350	microcub
4081	1	9	0.892	0.859	0.659	0.506	microcub
4081	1.5	9	0.869	0.794	0.582	0.434	microcub
4081	2	9	0.865	0.825	0.571	0.438	microcub
4081	3	9	0.838	0.800	0.535	0.419	microcub
4081	1	12	0.899	0.822	0.691	0.534	microcub
4081	1.5	12	0.878	0.872	0.659	0.509	microcub
4081	2	12	0.877	0.809	0.624	0.478	microcub
4081	3	12	0.850	0.784	0.617	0.459	microcub
5617	1	3	0.817	0.706	0.503	0.325	microcub
5617	1.5	3	0.776	0.672	0.445	0.222	microcub
5617	2	3	0.771	0.644	0.390	0.213	microcub
5617	3	3	0.735	0.616	0.363	0.194	microcub
5617	1	6	0.828	0.713	0.545	0.353	microcub
5617	1.5	6	0.833	0.731	0.491	0.369	microcub
5617	2	6	0.790	0.706	0.463	0.313	microcub
5617	3	6	0.768	0.688	0.409	0.284	microcub
5617	1	9	0.844	0.791	0.564	0.384	microcub
5617	1.5	9	0.822	0.747	0.537	0.372	microcub
5617	2	9	0.806	0.747	0.478	0.359	microcub
5617	3	9	0.801	0.734	0.458	0.300	microcub
5617	1	12	0.874	0.819	0.604	0.431	microcub
5617	1.5	12	0.846	0.781	0.573	0.488	microcub
5617	2	12	0.824	0.781	0.514	0.400	microcub





5617	3	12	0.823	0.788	0.508	0.372	microcub
8500	1	3	0.823	0.788	0.386	0.191	microcub
8500	1.5	3	0.783	0.581	0.326	0.191	microcub
8500	2	3	0.737	0.503	0.320	0.153	microcub
8500	3	3	0.671	0.503	0.238	0.133	microcub
8500	1	6	0.071	0.675	0.238	0.113	microcub
8500	1.5	6	0.776	0.656	0.417	0.247	microcub
8500	2	6	0.697	0.594	0.400	0.250	microcub
8500	3	6	0.682	0.575	0.285	0.230	microcub
8500	1	9	0.832	0.709	0.283	0.306	microcub
8500	1.5	9	0.832	0.675	0.479	0.266	microcub
8500	2	9	0.782	0.673	0.401	0.200	
		9					microcub
8500	3		0.735	0.603	0.359	0.263	microcub
8500	1	12	0.818	0.750	0.505	0.388	microcub
8500	1.5	12	0.783	0.684	0.469	0.363	microcub
8500	2	12	0.774	0.703	0.453	0.322	microcub
8500	3	12	0.745	0.656	0.382	0.316	microcub
17000	1	3	0.624	0.434	0.208	0.078	microcub
17000	1.5	3	0.571	0.388	0.172	0.066	microcub
17000	2	3	0.531	0.363	0.138	0.066	microcub
17000	3	3	0.451	0.291	0.110	0.013	microcub
17000	1	6	0.667	0.506	0.276	0.122	microcub
17000	1.5	6	0.613	0.484	0.208	0.094	microcub
17000	2	6	0.573	0.406	0.178	0.075	microcub
17000	3	6	0.494	0.394	0.136	0.075	microcub
17000	1	9	0.695	0.578	0.297	0.163	microcub
17000	1.5	9	0.640	0.481	0.254	0.131	microcub
17000	2	9	0.622	0.509	0.214	0.134	microcub
17000	3	9	0.562	0.419	0.182	0.103	microcub
17000	1	12	0.704	0.606	0.362	0.241	microcub
17000	1.5	12	0.649	0.578	0.315	0.209	microcub
17000	2	12	0.613	0.591	0.260	0.159	microcub
17000	3	12	0.609	0.503	0.244	0.166	microcub
1831	1	3	0.923	0.844	0.722	0.569	bell206
1831	1.5	3	0.908	0.844	0.700	0.531	bell206
1831	2	3	0.891	0.819	0.681	0.528	bell206
1831	3	3	0.878	0.809	0.635	0.453	bell206
1831	1	6	0.936	0.894	0.783	0.653	bell206
1831	1.5	6	0.917	0.878	0.759	0.628	bell206
1831	2	6	0.917	0.881	0.722	0.538	bell206
1831	3	6	0.896	0.838	0.664	0.494	bell206





1831	1	9	0.954	0.919	0.808	0.656	bell206
1831	1.5	9	0.921	0.894	0.773	0.619	bell206
1831	2	9	0.912	0.922	0.744	0.647	bell206
1831	3	9	0.900	0.850	0.714	0.619	bell206
1831	1	12	0.940	0.916	0.800	0.722	bell206
1831	1.5	12	0.929	0.884	0.787	0.722	bell206
1831	2	12	0.928	0.869	0.771	0.659	bell206
1831	3	12	0.935	0.891	0.732	0.622	bell206
2592	1	3	0.886	0.797	0.667	0.481	bell206
2592	1.5	3	0.872	0.803	0.619	0.472	bell206
2592	2	3	0.859	0.797	0.588	0.428	bell206
2592	3	3	0.858	0.741	0.562	0.359	bell206
2592	1	6	0.906	0.884	0.721	0.613	bell206
2592	1.5	6	0.874	0.822	0.671	0.519	bell206
2592	2	6	0.887	0.872	0.621	0.428	bell206
2592	3	6	0.847	0.781	0.605	0.466	bell206
2592	1	9	0.922	0.872	0.729	0.600	bell206
2592	1.5	9	0.900	0.847	0.713	0.600	bell206
2592	2	9	0.872	0.856	0.676	0.541	bell206
2592	3	9	0.868	0.816	0.650	0.506	bell206
2592	1	12	0.923	0.853	0.750	0.663	bell206
2592	1.5	12	0.914	0.853	0.701	0.600	bell206
2592	2	12	0.894	0.900	0.710	0.569	bell206
2592	3	12	0.883	0.838	0.682	0.597	bell206
2859	1	3	0.885	0.797	0.674	0.488	bell206
2859	1.5	3	0.855	0.778	0.621	0.413	bell206
2859	2	3	0.826	0.738	0.569	0.350	bell206
2859	3	3	0.804	0.697	0.522	0.338	bell206
2859	1	6	0.886	0.819	0.709	0.563	bell206
2859	1.5	6	0.874	0.806	0.638	0.488	bell206
2859	2	6	0.859	0.809	0.613	0.456	bell206
2859	3	6	0.837	0.788	0.574	0.413	bell206
2859	1	9	0.915	0.844	0.710	0.569	bell206
2859	1.5	9	0.888	0.856	0.708	0.531	bell206
2859	2	9	0.882	0.838	0.655	0.528	bell206
2859	3	9	0.856	0.809	0.628	0.488	bell206
2859	1	12	0.901	0.838	0.754	0.625	bell206
2859	1.5	12	0.886	0.806	0.694	0.581	bell206
2859	2	12	0.894	0.866	0.688	0.538	bell206
2859	3	12	0.885	0.869	0.644	0.563	bell206
4081	1	3	0.838	0.775	0.565	0.372	bell206



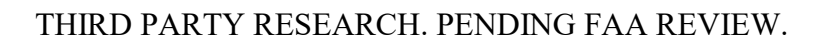


4081	1.5	3	0.822	0.713	0.527	0.353	bell206
4081	2	3	0.803	0.728	0.476	0.272	bell206
4081	3	3	0.759	0.659	0.405	0.209	bell206
4081	1	6	0.864	0.778	0.646	0.444	bell206
4081	1.5	6	0.838	0.725	0.551	0.356	bell206
4081	2	6	0.813	0.728	0.545	0.397	bell206
4081	3	6	0.769	0.706	0.479	0.366	bell206
4081	1	9	0.862	0.781	0.644	0.428	bell206
4081	1.5	9	0.859	0.825	0.617	0.456	bell206
4081	2	9	0.823	0.741	0.549	0.447	bell206
4081	3	9	0.827	0.775	0.527	0.381	bell206
4081	1	12	0.882	0.838	0.671	0.528	bell206
4081	1.5	12	0.844	0.825	0.614	0.472	bell206
4081	2	12	0.860	0.834	0.603	0.472	bell206
4081	3	12	0.835	0.816	0.576	0.441	bell206
5617	1	3	0.813	0.731	0.474	0.244	bell206
5617	1.5	3	0.772	0.647	0.432	0.281	bell206
5617	2	3	0.738	0.591	0.388	0.238	bell206
5617	3	3	0.704	0.588	0.332	0.163	bell206
5617	1	6	0.828	0.728	0.538	0.359	bell206
5617	1.5	6	0.806	0.700	0.477	0.294	bell206
5617	2	6	0.787	0.641	0.458	0.294	bell206
5617	3	6	0.741	0.638	0.397	0.291	bell206
5617	1	9	0.846	0.750	0.562	0.409	bell206
5617	1.5	9	0.832	0.728	0.506	0.422	bell206
5617	2	9	0.797	0.678	0.495	0.328	bell206
5617	3	9	0.769	0.669	0.468	0.316	bell206
5617	1	12	0.856	0.825	0.569	0.463	bell206
5617	1.5	12	0.833	0.775	0.558	0.419	bell206
5617	2	12	0.819	0.753	0.508	0.397	bell206
5617	3	12	0.787	0.744	0.499	0.391	bell206
8500	1	3	0.751	0.603	0.374	0.194	bell206
8500	1.5	3	0.718	0.563	0.322	0.144	bell206
8500	2	3	0.667	0.581	0.262	0.109	bell206
8500	3	3	0.608	0.438	0.214	0.088	bell206
8500	1	6	0.763	0.650	0.442	0.309	bell206
8500	1.5	6	0.731	0.613	0.368	0.238	bell206
8500	2	6	0.722	0.628	0.323	0.184	bell206
8500	3	6	0.696	0.616	0.282	0.138	bell206
8500	1	9	0.790	0.716	0.458	0.309	bell206
8500	1.5	9	0.751	0.666	0.417	0.300	bell206





8500	2	9	0.718	0.659	0.399	0.253	bell206
8500	3	9	0.692	0.631	0.349	0.238	bell206
8500	1	12	0.092	0.706	0.527	0.238	bell206
8500	1.5	12	0.732	0.694	0.327	0.372	bell206
8500	2	12	0.778	0.034	0.404	0.372	bell206
8500	3	12	0.778	0.738	0.417	0.341	bell206
17000	1	3	0.740	0.691	0.336	0.303	bell206
17000	1.5	3	0.560	0.438	0.213	0.084	bell206
17000		3	0.526		0.136		
	3	3		0.369		0.038	bell206
17000			0.447	0.247	0.099	0.034	bell206
17000	1	6	0.658	0.516	0.249	0.109	bell206
17000	1.5	6	0.592	0.459	0.219	0.103	bell206
17000	2	6	0.571	0.391	0.176	0.109	bell206
17000	3	6	0.508	0.344	0.117	0.066	bell206
17000	1	9	0.686	0.541	0.314	0.172	bell206
17000	1.5	9	0.612	0.519	0.258	0.144	bell206
17000	2	9	0.590	0.506	0.231	0.109	bell206
17000	3	9	0.549	0.428	0.169	0.109	bell206
17000	1	12	0.678	0.594	0.324	0.231	bell206
17000	1.5	12	0.656	0.556	0.279	0.194	bell206
17000	2	12	0.667	0.606	0.236	0.147	bell206
17000	3	12	0.604	0.506	0.222	0.153	bell206
1831	1	3	0.831	0.709	0.679	0.459	cessna
1831	1.5	3	0.827	0.663	0.638	0.459	cessna
1831	2	3	0.812	0.706	0.609	0.391	cessna
1831	3	3	0.732	0.578	0.571	0.341	cessna
1831	1	6	0.840	0.756	0.749	0.591	cessna
1831	1.5	6	0.840	0.766	0.692	0.541	cessna
1831	2	6	0.810	0.697	0.650	0.506	cessna
1831	3	6	0.773	0.666	0.601	0.444	cessna
1831	1	9	0.874	0.806	0.760	0.672	cessna
1831	1.5	9	0.847	0.772	0.692	0.575	cessna
1831	2	9	0.823	0.766	0.683	0.544	cessna
1831	3	9	0.818	0.744	0.651	0.544	cessna
1831	1	12	0.882	0.859	0.759	0.625	cessna
1831	1.5	12	0.876	0.831	0.710	0.606	cessna
1831	2	12	0.832	0.800	0.705	0.578	cessna
1831	3	12	0.829	0.775	0.685	0.559	cessna
2592	1	3	0.800	0.669	0.605	0.375	cessna
2592	1.5	3	0.754	0.578	0.546	0.359	cessna
2592	2	3	0.713	0.569	0.469	0.303	cessna





2562	Τ.,		0.665	0.464	0.454	0.000	I
2592	3	3	0.682	0.481	0.451	0.288	cessna
2592	1	6	0.788	0.675	0.641	0.463	cessna
2592	1.5	6	0.783	0.678	0.569	0.397	cessna
2592	2	6	0.742	0.619	0.565	0.363	cessna
2592	3	6	0.695	0.609	0.500	0.381	cessna
2592	1	9	0.837	0.763	0.683	0.538	cessna
2592	1.5	9	0.779	0.678	0.633	0.525	cessna
2592	2	9	0.755	0.666	0.595	0.484	cessna
2592	3	9	0.745	0.694	0.563	0.466	cessna
2592	1	12	0.817	0.688	0.704	0.588	cessna
2592	1.5	12	0.828	0.769	0.664	0.516	cessna
2592	2	12	0.797	0.691	0.632	0.503	cessna
2592	3	12	0.788	0.741	0.585	0.469	cessna
2859	1	3	0.746	0.625	0.596	0.331	cessna
2859	1.5	3	0.732	0.575	0.529	0.281	cessna
2859	2	3	0.723	0.613	0.464	0.300	cessna
2859	3	3	0.631	0.503	0.396	0.247	cessna
2859	1	6	0.800	0.678	0.617	0.444	cessna
2859	1.5	6	0.771	0.675	0.549	0.400	cessna
2859	2	6	0.745	0.672	0.545	0.369	cessna
2859	3	6	0.729	0.619	0.481	0.297	cessna
2859	1	9	0.837	0.781	0.650	0.500	cessna
2859	1.5	9	0.777	0.697	0.594	0.444	cessna
2859	2	9	0.733	0.669	0.583	0.444	cessna
2859	3	9	0.745	0.663	0.518	0.359	cessna
2859	1	12	0.817	0.775	0.650	0.584	cessna
2859	1.5	12	0.814	0.756	0.649	0.500	cessna
2859	2	12	0.779	0.719	0.617	0.500	cessna
2859	3	12	0.754	0.675	0.560	0.466	cessna
4081	1	3	0.706	0.538	0.476	0.269	cessna
4081	1.5	3	0.659	0.466	0.417	0.259	cessna
4081	2	3	0.629	0.472	0.400	0.200	cessna
4081	3	3	0.571	0.400	0.308	0.119	cessna
4081	1	6	0.731	0.625	0.529	0.309	cessna
4081	1.5	6	0.708	0.581	0.487	0.338	cessna
4081	2	6	0.690	0.500	0.423	0.253	cessna
4081	3	6	0.617	0.453	0.359	0.206	cessna
4081	1	9	0.760	0.663	0.562	0.413	cessna
4081	1.5	9	0.715	0.638	0.528	0.334	cessna
4081	2	9	0.701	0.638	0.462	0.331	cessna
4081	3	9	0.645	0.569	0.442	0.313	cessna





4081	1	12	0.768	0.691	0.606	0.463	cessna
4081	1.5	12	0.768	0.663	0.545	0.444	cessna
4081	2	12	0.749	0.675	0.543	0.444	cessna
4081	3	12	0.701	0.616	0.487	0.350	cessna
5617	1	3	0.659	0.428	0.395	0.181	cessna
5617	1.5	3	0.606	0.425	0.333	0.144	cessna
5617	2	3	0.531	0.423	0.327	0.144	cessna
5617	3	3	0.495	0.303	0.227	0.091	cessna
5617	1	6	0.703	0.566	0.414	0.263	cessna
5617	1.5	6	0.631	0.500	0.385	0.203	cessna
5617	2	6	0.583	0.478	0.338	0.194	cessna
5617	3	6	0.549	0.419	0.283	0.153	cessna
5617	1	9	0.712	0.594	0.485	0.328	cessna
5617	1.5	9	0.662	0.506	0.435	0.288	cessna
5617	2	9	0.627	0.497	0.386	0.241	cessna
5617	3	9	0.594	0.500	0.324	0.228	cessna
5617	1	12	0.718	0.622	0.496	0.369	cessna
5617	1.5	12	0.677	0.575	0.460	0.350	cessna
5617	2	12	0.663	0.566	0.431	0.331	cessna
5617	3	12	0.624	0.528	0.387	0.300	cessna
8500	1	3	0.514	0.306	0.253	0.109	cessna
8500	1.5	3	0.486	0.300	0.195	0.081	cessna
8500	2	3	0.422	0.256	0.169	0.088	cessna
8500	3	3	0.363	0.203	0.133	0.028	cessna
8500	1	6	0.568	0.388	0.336	0.169	cessna
8500	1.5	6	0.536	0.378	0.268	0.134	cessna
8500	2	6	0.471	0.325	0.229	0.097	cessna
8500	3	6	0.410	0.250	0.160	0.081	cessna
8500	1	9	0.592	0.491	0.349	0.197	cessna
8500	1.5	9	0.532	0.381	0.296	0.147	cessna
8500	2	9	0.494	0.403	0.279	0.159	cessna
8500	3	9	0.469	0.338	0.236	0.113	cessna
8500	1	12	0.613	0.525	0.391	0.256	cessna
8500	1.5	12	0.596	0.488	0.351	0.231	cessna
8500	2	12	0.538	0.438	0.331	0.184	cessna
8500	3	12	0.527	0.428	0.271	0.184	cessna
17000	1	3	0.373	0.169	0.113	0.038	cessna
17000	1.5	3	0.285	0.128	0.067	0.013	cessna
17000	2	3	0.222	0.122	0.046	0.003	cessna
17000	3	3	0.179	0.094	0.042	0.006	cessna
17000	1	6	0.390	0.209	0.147	0.053	cessna





17000	1.5	6	0.335	0.178	0.113	0.047	cessna
17000	2	6	0.277	0.159	0.100	0.053	cessna
17000	3	6	0.238	0.134	0.054	0.016	cessna
17000	1	9	0.454	0.275	0.192	0.088	cessna
17000	1.5	9	0.383	0.253	0.147	0.053	cessna
17000	2	9	0.338	0.200	0.119	0.072	cessna
17000	3	9	0.278	0.159	0.109	0.038	cessna
17000	1	12	0.467	0.316	0.244	0.122	cessna
17000	1.5	12	0.396	0.250	0.188	0.116	cessna
17000	2	12	0.373	0.291	0.158	0.094	cessna
17000	3	12	0.319	0.219	0.133	0.094	cessna



#### 9 References

- A. Weinert, N. U. (2019). "Developing a Low Altitude Manned Encounter Model Using ADS-B Observations". Big Sky: 2019 IEEE Aerospace Conference.
- Amerson, D., Ryker, K., White, C., Bassou, R., Goodin, C., Dabbiru, L., . . . Dayarantha, V. (2023). ASSURE A23 - Validation of Low Altitude Detect and Avoid Standards FInal Report. Starkville: ASSURE.
- Andrews, J. (1991). *Unalerted Air-to-Air Visual Acquisition*. Lexington, MA: Massachusetts Institute of Technology Lincoln Laboratory.
- ASTM International. (2023). ASTM F3442 Standard Specification for Detect and Avoid System Performance Requirements. *ASTM International*.
- Duff, N. (2023, June 14). Retrieved from Delta State University News and Events: https://www.deltastate.edu/news-and-events/2023/06/dsu-aviation-takes-delivery-of-new-state-of-the-art-aircraft/
- FlightAware. (n.d.). Aircraft Registration. Retrieved from https://www.flightaware.com/
- General Operating & Flight Rules 14 C.F.R § 91. (2022). Retrieved from Code of Federal Regulations: https://www.ecfr.gov/current/title-14/chapter-I/subchapter-F/part-91#p-91.225(i)
- Korchenderfer, M., Espindle, L., Kuchar, J., & Griffith, J. (2008). Correlated encounter model for cooperative aircraft in the national airspace system version 1.0. Project Report ATC-344 MIT Lincoln Laboratory.
- Tobii. (n.d.). *Tobii Pro Glasses 3*. Retrieved from Tobii: https://www.tobii.com/products/eye-trackers/wearables/tobii-pro-glasses-3
- Underhill, N., & al., e. (2023). Estimating See and Be Seen Performance with an Airborne Visual Acquisition Model. arXiv.
- Weitz, L. (2015). Derivation of a point-mass aircraft model used for fast-time simulation. MITRE Corporation.